UNIVERSITY of NEW ORLEANS
Office of Research and Sponsored Programs
CERM Bldg., Room No. 452 · New Orleans, Louisiana 70148
Phone: (504) 280-7489 · Fax: (504) 280-6752 · E-mail: kewalsh@uno.edu

March 27, 2009

Defense Technical Information Center
8725 John J. Kingman Road, Ste., 0944
Fort Belvoir, VA 22060-6218

Dear Defense Technical Information Center Administration:

Herewith is the final technical report for award N00173-06-2-C901 for the project entitled "Ocean and coastal modeling: Nonlinear acoustic propagation" under the direction of principal investigator Dr. George Ioup from the University of New Orleans.

The period of performance for this award was June 27, 2006 through June 30, 2008.

For questions or comments regarding the technical report, please contact Dr. George Ioup at geioup@uno.edu or 504-280-6715.

All inquiries regarding the Final Property Report or Final Financial Status Report should be directed to the Office of Sponsored Programs Accounting, Senior Account Manager, Mr. Bruce Dyer, bhdyer@uno.edu, 504-280-5541

Thank you.

-Kari Walsh
Research Award Administrator
Office of Research and Sponsored Programs (ORSP)
University of New Orleans

Cc: Naval Research Laboratory
Office of Naval Research, ATL Reg Ofc

Final Report Overview

N00173-06-2-C901

Ocean and Coastal Modeling

George E. Ioup, Juliette W. Ioup, Germana Peggion, Department of Physics
Martin J. Guillot, Department of Mechanical Engineering
J. Alex McCorquodale, Department of Civil and Environmental Engineering
Ioannis Y. Georgiou, Pontchartrain Institute for Environmental Sciences
University of New Orleans

This grant consisted of work divided into two parts. The first part, "Ocean Modeling," was performed off-campus. The lead researcher was Dr. Germana Peggion of the Department of Physics at UNO. Her colleagues for this research were employees of the Oceanography Division of the Naval Research Laboratory at Stennis Space Center (NRL-SSC). The main objective of the ocean modeling portion of this grant was to collaborate with and assist NRL-SSC in implementing, evaluating, and applying ocean forecasting systems in support of naval applications.

The second part of the grant (Coastal Modeling) consisted of calculations concerning storm surge simulations over south Louisiana and was performed on campus. The lead investigator was Dr. Martin Guillot of the Department of Mechanical Engineering at UNO. He was assisted in this work by Dr. Ioannis Georgiou of the Pontchartrain Institute for Environmental Sciences at UNO and Dr. Alex McCorquodale of the Department of Civil and Environmental Engineering at UNO. The objective was to compute water surface elevations over southern Louisiana due to storm surge produced by the updated "Standard Project Hurricane" (SPH). The SPH defines a methodology for producing hurricane path, forward speed and wind field scenarios that are used as design criteria to guide the design heights of the levee system in southeast Louisiana.

Dr. George Ioup and Dr. Juliette Ioup of the Department of Physics at UNO administered the grant.

There are five parts to this report. The first is this overview. The second is a summary of achievements for the Ocean Modeling by Dr. Peggion organized by Task and titled Ocean Modeling. The third is a summary of the achievements for the Coastal Modeling by Dr. Guillot and Dr. Georgiou titled Standard Project

Hurricane Update: ADCIRC Storm Simulations Over Southeast Louisiana. The fourth and fifth are two manuscripts to be published in the Journal of Marine Systems, which summarize some of the work by Dr. Peggion and her colleagues, Super-ensemble Forecasts and Resulting Acoustic Sensitivities in Shallow Waters, and A Note on Ncom Temperature Forecast Error Calibration Using the Ensemble Transform. The latter papers were also supported by a funding from NRL-SSC through NASA-Stennis and the Louisiana Board of Regents to UNO as well as by a follow-on NRL cooperative agreement with UNO, N00173-07-2-C901.

STANDARD PROJECT HURRICANE UPDATE: ADCIRC STORM SIMULATIONS OVER SOUTHEAST LOUISIANA

By
Dr. Martin J. Guillot
Dr. Ioannis Georgiou
University of New Orleans
New Orleans, LA

Objective

The purpose of the current effort is to compute storm surges produced by the standard project hurricane (SPH) using the ADCIRC storm surge model and to compare surges resulting from indices defined in a 1959 National Weather Bureau report with indices defined as part of the SPH reanalysis after the 2005 hurricane season.

Standard Project Hurricane

The SPH is one of the design criteria the U.S. Army Corps of Engineers uses for hurricane protection projects along the east and gulf coasts of the United States. The SPH is a hypothetical hurricane based on historical data and observations of hurricanes that have occurred the Atlantic basin along the east and gulf coasts and was originally defined in 1959 as part of the National Hurricane Research Project in the U.S. Weather Bureau Report No. 33 [1] (subsequently referred to as NHRP 33) using data from storms that occurred during the period 1900-1956. That report defined the SPH as "...the most severe storm that is considered reasonably characteristic of a region in which the basin is located". The U.S. Weather Bureau and the U.S. Army Corps of Engineers (USACE) jointly derived the specifications, criteria and procedures for computing the SPH defined in NHRP 33. The U.S east and gulf coasts were divided into zones of approximately equal area and SPH indices were defined for each zone. The three zones defined on the gulf coast are shown in Figure 1 (taken from NHRP 33). The primary indices used to define the SPH within each zone are: central pressure index (CPI), maximum 30 ft (10 m) over water winds, radius of maximum winds and forward speed. The New Orleans area is located in zone B.

The SPH has undergone reanalysis several times since originally defined in NHRP 33. Reanalysis has included redefining both the SPH indices based on more recent (after 1956) data and refining the methodologies used to compute the wind and pressure fields. In 1979 a reanalysis of the SPH indices based on storms through 1975 was published in NOAA Technical Report 23 [2] (subsequently referred to as NWS 23). That document redefined the SPH as "a steady state hurricane having a severe combination of values of meteorological parameters that will give high sustained wind speeds reasonably characteristic of a given region", and also revised the methodologies used for computing the wind and pressure fields from those used in 1959 NRRP 33 report. In 1996, Thompson and Cardone [5] developed a model for generating tropical cyclones based on the planetary boundary layer approach. This approach was incorporated into the Ocean

Weather, Inc (OWI) meso-scale vortex numerical model for specification of surface wind and pressure fields inside tropical cyclones based on specifying the appropriate indices. After the 2005 hurricane season, the SPH indices were reanalyzed again to include all data from 1851 through the 2005 hurricane season. Levinson [3] presents the results of the SPH reanalysis and compares the 1979 indices defined in NWS 23 with the new indices defined as part of the SPH reanalysis after the 2005 hurricane season.

The current study focuses on comparing storm surges predicted by the ADCIRC storm surge model using the SPH indices defined in NHRS 33 (1959) and the SPH indices defined in the reanalysis after the 2005 hurricane season. For the remainder of this report, the SPH indices as defined in NHRS 33 will be referred to as the "old" SPH and the SPH indices defined as part of the SPH reanalysis after the 2005 hurricane season will be referred to as the "new" SPH. The methodology for computing the wind and pressure fields for the old SPH is based on the methods in the 1979 NWS 23 report and the methodology for computing the wind and pressure fields for the new SPH is based on OWI tropical cyclone model called TC96. Storm surges are computed using the shallow water modeling system ADCIRC

The approximate SPH wind field parameters used in this study are presented in Table 1.

Table 1: SPH indices used to define the new and old SPH.

	Central Pressure Index (mb)	Radius of Maximum Winds (nautical mile)	Max Wind Speed (mph)	Method for computing wind and pressure
New SPH	904.1	11	132.0	OWI TC96 model
Old SPH	934.6	30	104.0	NWS 23

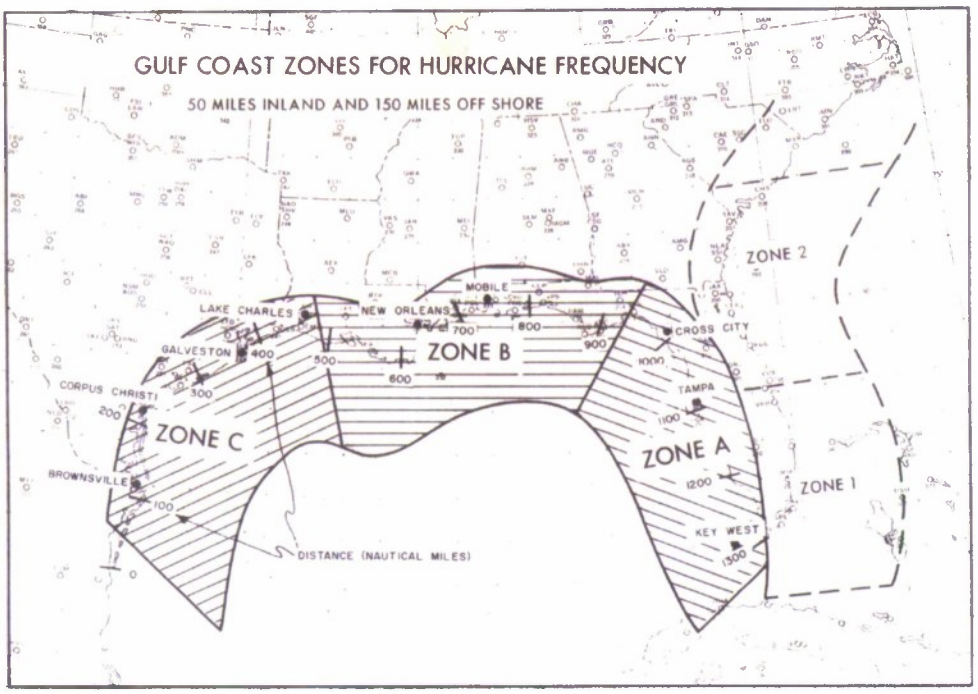

Figure 11.

Figure 1: Gulf coast zones defined in Report 33.

ADCIRC Storm Surge Modeling System

The ADCIRC storm surge model was originally developed by Leuttich and Westerink [4] and since then has undergone extensive development by several researchers and organizations. The model is based on the finite element method and incorporates the generalized wave continuity equation (GWCE) for numerical stability. ADCIRC computes water surface elevations and velocities at nodal points for the 2-D depth averaged shallow water equations. A parallel version of ADCIRC has been developed to run on several parallel architectures, including Linux clusters. For this study the ADCIRC model was run on the 64 node Linux cluster at the University of New Orleans. Version *46.52* is used in conjunction with the southeast Louisiana mesh *sl15v3_2007_r09a*. The code, mesh, control files as well as wind fields were provided by the U.S. Army Corps of Engineers, New Orleans District. The wind fields used to force the ADCIRC model and are discussed in more detail below.

Modifications to Original Mesh

The ADCIRC mesh consists of nodes, elements and boundaries. ADCIRC has the capability to model several types of boundary conditions including, but not limited to, elevation (tidal), inflow (river), outflow and weir. Levees are modeled using weir boundaries. Weirs are specified at the given levee height for each levee using weir node pairs and when the water surface elevation exceeds the elevation specified at the weir node pair, weir equations are used to compute flow over that levee to simulate levee overtopping. For the SPH study, levee overtopping was prevented in the Lake Pontchartrain and vicinity, including the west bank by specifying the elevation of the node weir pairs of the flood protection levees to be 25 m. The purpose is to help determine levee heights that would be required to protect the New Orleans area and west bank from an SPH event. The specific levees raised are shown in Figure 2.

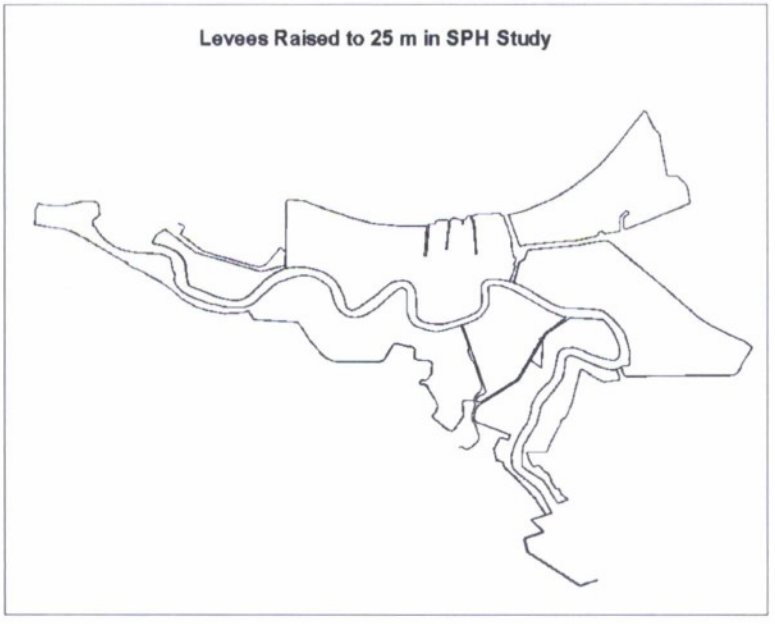

Figure 2; Node weir pairs that simulate flood protection levees in and around New Orleans that were raised to 25 m.

SPH Tracks and Wind Fields

The SPH study consists of three primary tracks labeled A, C and F. The tracks are based on COE experience and historical storm data, and are shown in Figure 3 along with the forward translational speed along each track. The old and new SPH wind field contours are shown Figure 4 and Figure 5, respectively. Several things are noted about the wind fields. While the new SPH is a stronger storm in terms of maximum wind speed, it is also a much smaller storm, with radius of maximum winds almost one third of the old SPH. Additionally, as can be seen from comparing the two figures, the wind field extends farther for the old SPH than the new SPH. For example, for the storm positions shown, the wind speed in the Mississippi sound near the entrance to Lake Borgne

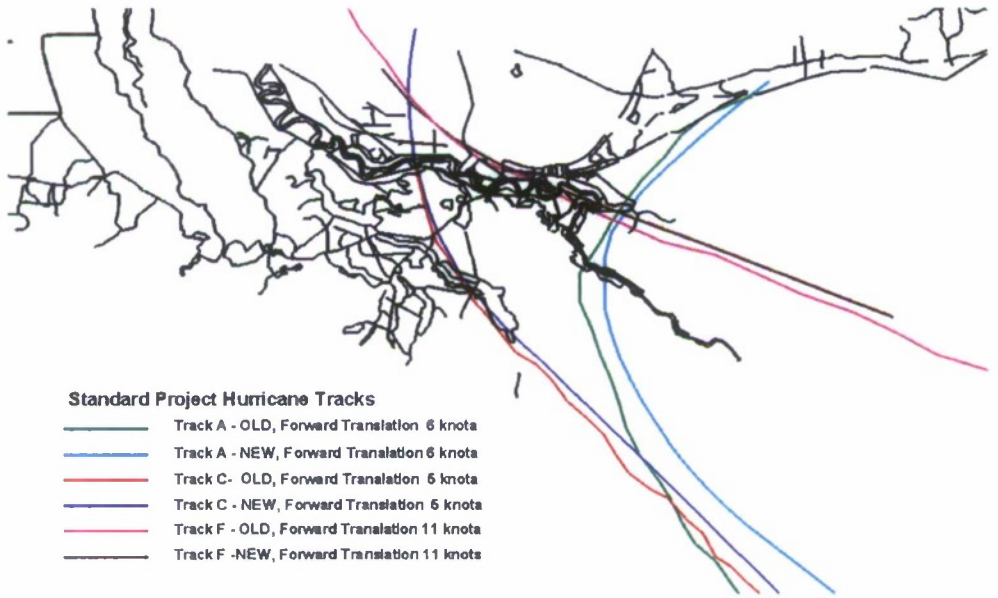

Figure 3: SPH Storm Tracks and forward translational speed.

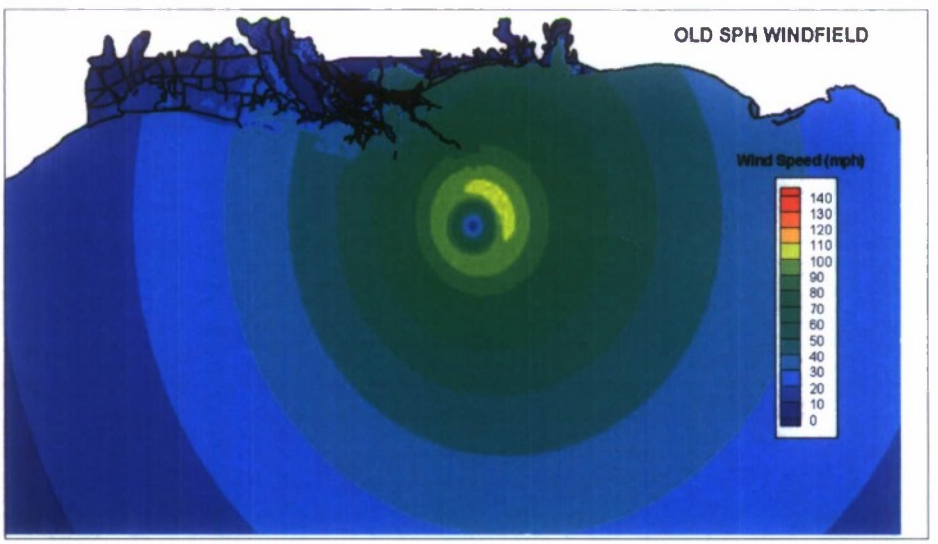

Figure 4: Old SPH wind field

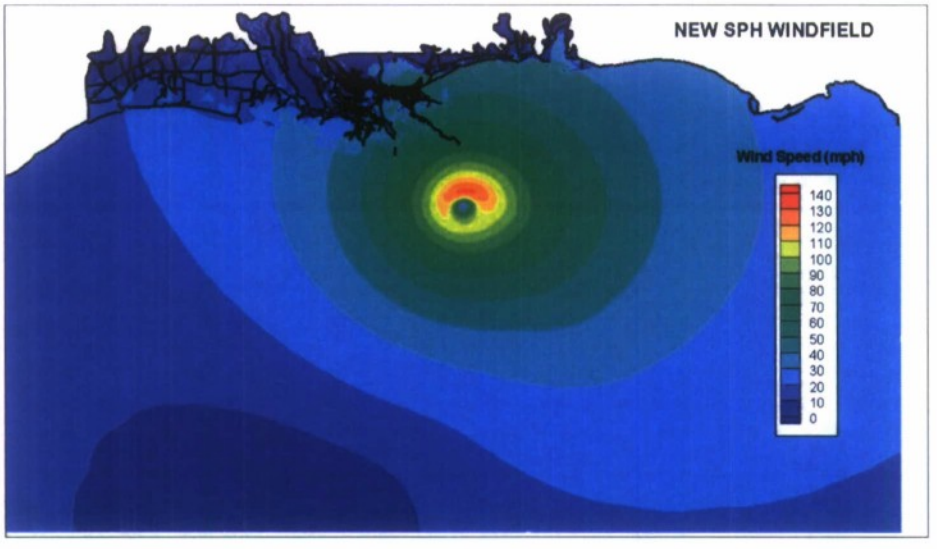

Figure 5: New SPH wind field

is on the order of 70-80 mph for the old SPH, whereas for the new SPH, the wind speed has dropped to 40-50 mph. The larger size of the old SPH can have a significant effect on the computed storm surge, as will be shown in the results section.

Results

The results of the study are presented in a series of contour plots of maximum water surface elevation, elevation difference and water surface elevation histories at selected locations within the Lake Pontchartrain and vicinity study area.

All simulations were begun 30 hours before land fall with wind ramping to full strength during the first 6 hours, so that full force winds began 24 hours prior land fall. Prior to performing the SPH simulations, ADCIRC was run without winds for a 2 day simulation with inflow boundary conditions specified on the Atchafalaya and Mississippi rivers to provide correct initial water surface elevations for the SPH simulations These results were saved and the SPH simulations were hot started from these initial conditions. No tidal dynamics were included in this study.

The maximum water surface elevation contours for tracks A, C and F are shown in Figure 6 through Figure 8 for the (a) old and (b) new SPH respectively. Figure 6 shows that for track A, the surge produced along the south shore of Lake Pontchartrain is higher for the old SPH than for the new SPH. This is due to the larger area of the wind field for the old SPH. Near the MRGO and Plaquemines Parish on the east side of the Mississippi river, the storm surges for the old and new SPH are comparable. However, the higher surge extends farther into the Mississippi sound for the new SPH. This is expected, since the eye passes over this area and the maximum winds near the eye wall are higher for the new SPH. For track C it is clearly seen by comparing

Figure 7 (a) and (b) that the old SPH produces a higher storm surge for most of the area of interest, except on the south shore of lake Pontchartrain around New Orleans east. Figure 8 (a) and (b) show that the storm surge produced by track F is substantially lower than for track A and C. Figure 9 (a) and (b) shows the maximum water surface elevations

produced by considering all tracks for the old and new SPH, respectively. Figure 10 through Figure 13 show the differences in computed water surface elevation (new – old) for tracks A, C, F and considering the maximum of all tracks, respectively. The difference contour plots more clearly demonstrate the differences in computed water surface elevation between the old and new SPH.

Next, water surface elevation histories were computed at selected points in the flood protection system in the New Orleans and surrounding areas. The elevation recording stations are shown in Figure 14 and are grouped for plotting purposes into four sections along the flood protection system. The maximum water surface elevations for at each of the 22 stations are shown in Table () for each storm and the maximum of all storms.

Figure 15 shows that along the south shore of Lake Pontchartrain, the old SPH produces a maximum storm surge of approximately 5.5 meters whereas the new SPH produces a maximum storm surge between 4 and 5 meters. For both storms the storm surge is relatively constant at stations 2, 3 an 4, but is higher at stations 1 and 5. Also, the storm surge peaks approximately 2 hours later for the old SPH. Figure 16 indicates that the maximum storm surge in the New Orleans east section occurs at station 10 and is approximately 7 meters. In the MRGO/IHNC section, Figure 17 indicates that a maximum storm surge of 8 meters occurs at stations 13-16 and is approximately equal for both storms. No appreciable flooding occurred at the west bank stations for track A and so those stations are not plotted.

Figure 18 shows that track C produces significantly lower peak surge along the south shore of Lake Pontchartrain than track A, with a maximum surge occurring at station 1 of approximately 4.5 meters for the old SPH and just under 4 meters for the new SPH. In New Orleans east, Figure 19 shows that the maximum storm surge occurs at station 10 and is 6.4 meters for the old SPH and 4.4 meters for the new SPH. Figure 20 shows maximum surge occurring at station 11 of approximately 8 meters for the old SPH and 6.4 meters for the new SPH. Stations 13-16 show a maximum surge of 7.8 meters for the old SPH and 5.8 for the new SPH. On the west bank, Figure 21 indicates that the old SPH produces significantly higher storm surge at stations 18 and 19 with at maximum surge of 7.8 meters for the old SPH and a maximum surge of 5.0 meters for the new SPH. Unfortunately, stations 20-22 indicate that the surge has not yet peaked for the old SPH, indicating that the simulation ended before the maximum surge was captured. The new SPH produces a maximum surge of less than 4 meters at those locations.

Elevation histories produced by Track F are shown in Figure 22 through Figure 25. In contrast to Tracks A and C, the new SPH produces higher storm surges for Track F rather than the old SPH at the selected locations. This is not surprising, since the eye of the storm passes over the city and the new SPH, although smaller has stronger winds near the eye. It is seen from Figure 22 that Track F produces significant storm surge on the south shore of Lake Pontchartrain and, in fact, produces higher storm surges there than tracks A and C. At the other locations the storm surge is still significant, but not as high as Track A or C.

The maximum water surface elevations at each recording station for each storm track are presented in Table 2 as well as the overall maximum for both the old and new SPH.

Conclusions

The study produced some unexpected results. Initially it was thought that the stronger storm defined by the new SPH would produce higher storm surges, but that was not always the case. It is clear from the maximum water surface elevation contours and water surface elevation histories that the larger storm defined by the old SPH indices has significant influence on the resulting peak storm surges at most locations of interest.

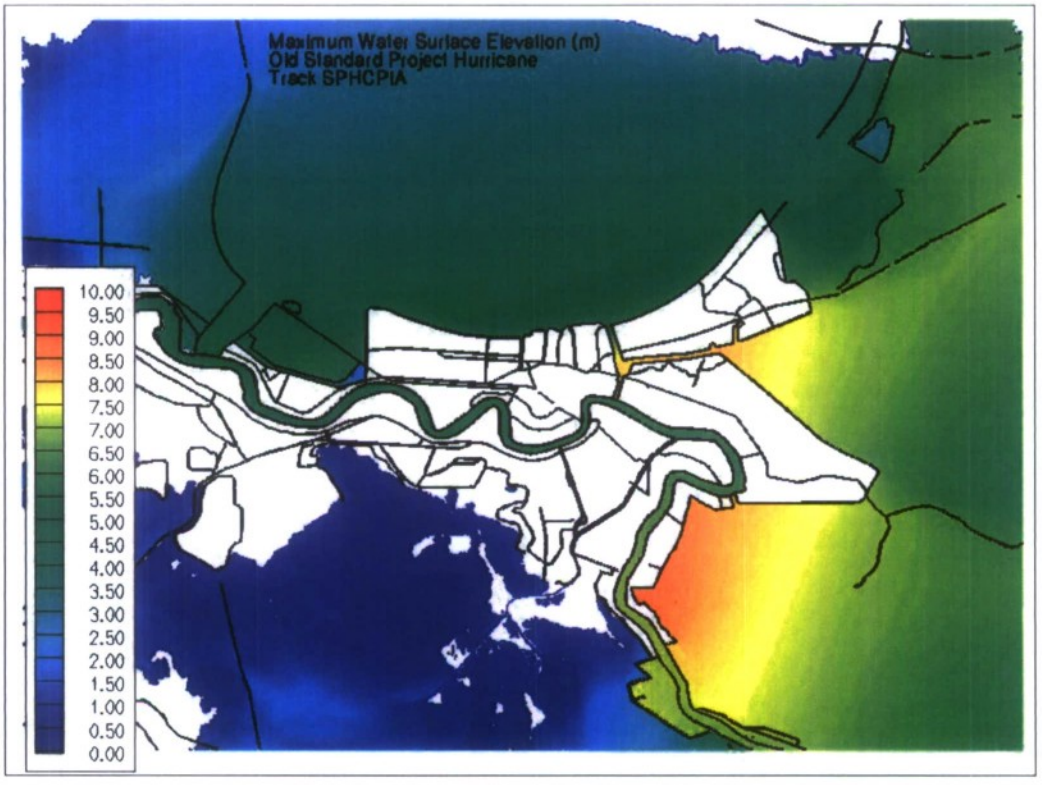

(a)

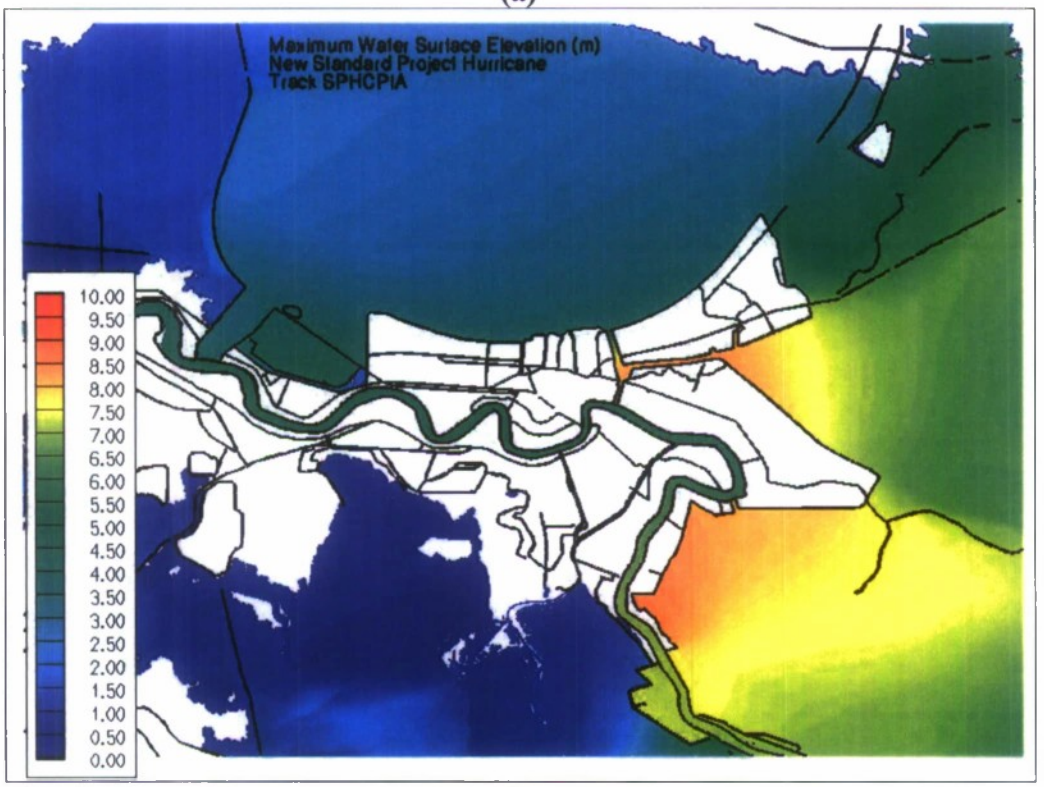

(b)

Figure 6: Computed maximum water surface elevation SPH Track A, (a) old SPH, (b) new SPH

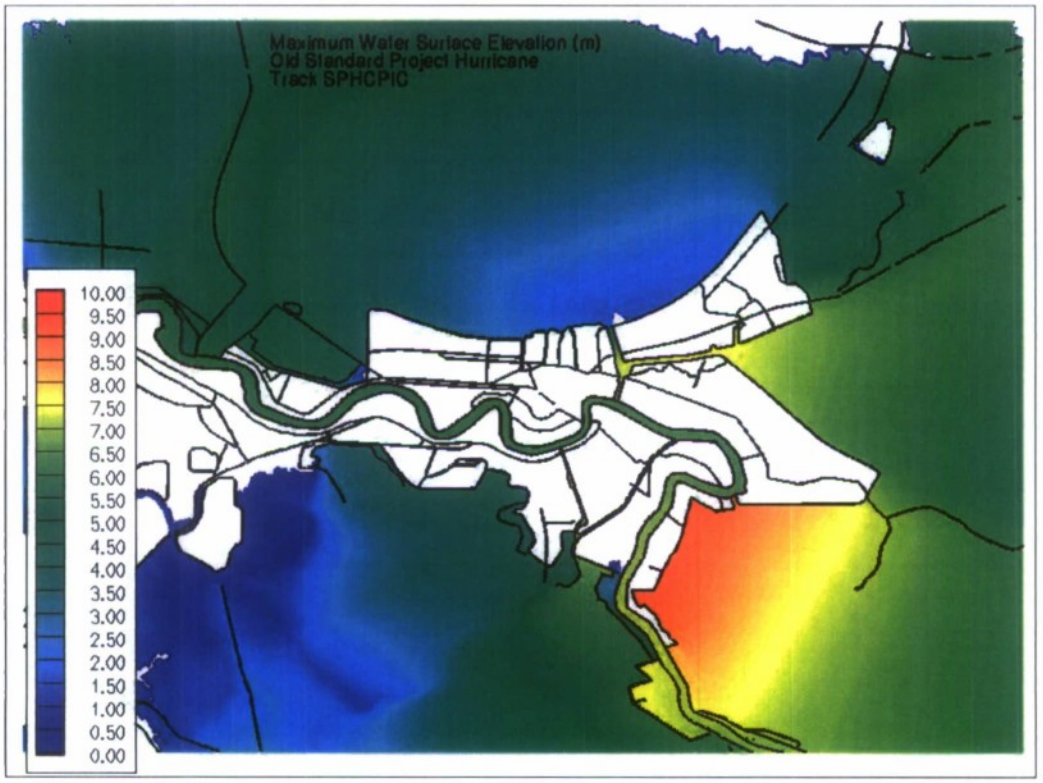

(a)

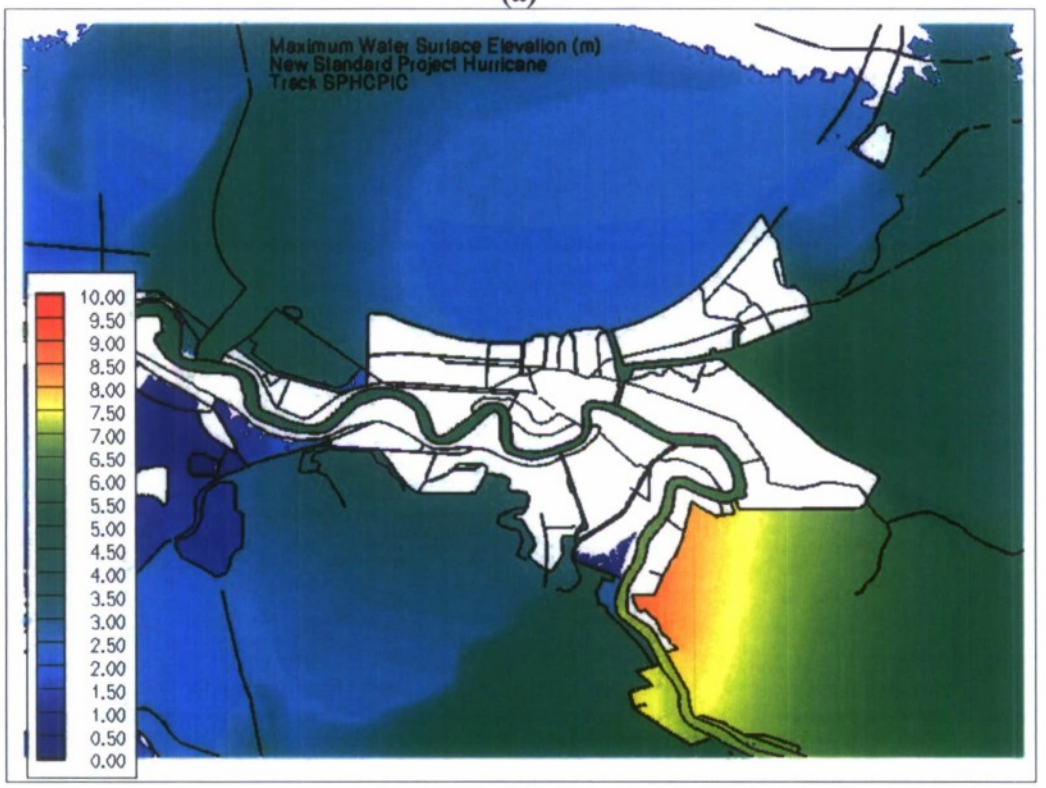

(b)

Figure 7: Computed maximum water surface elevation SPH Track C, (a) old SPH, (b) new SPH

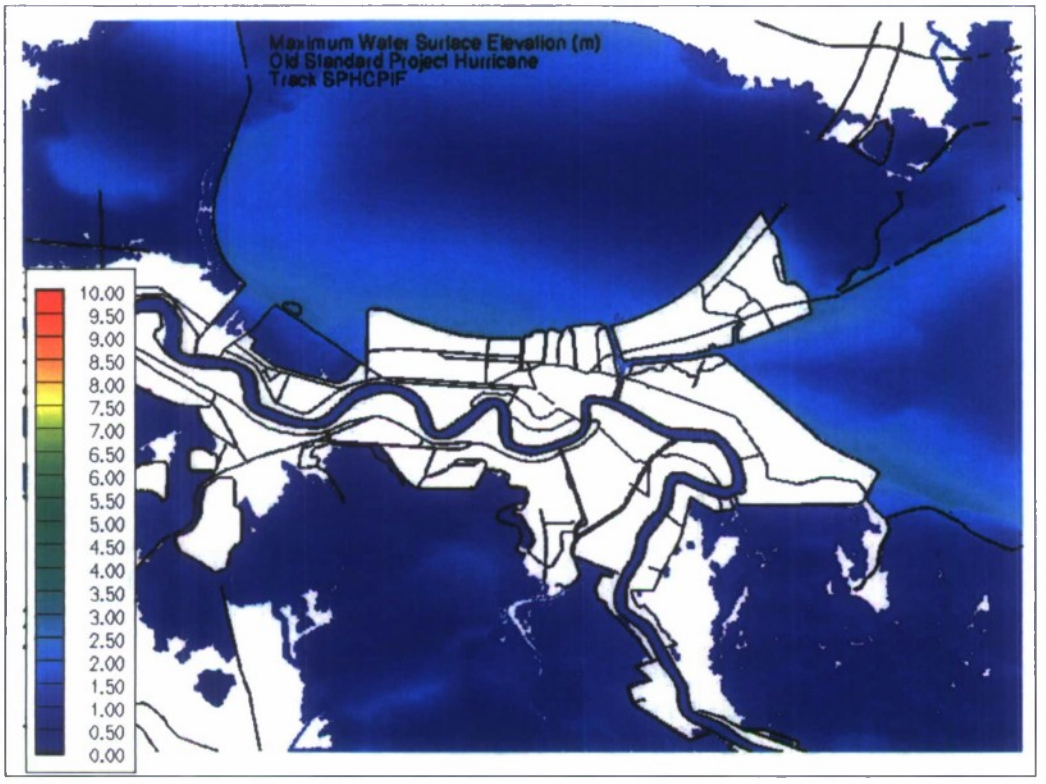

(a)

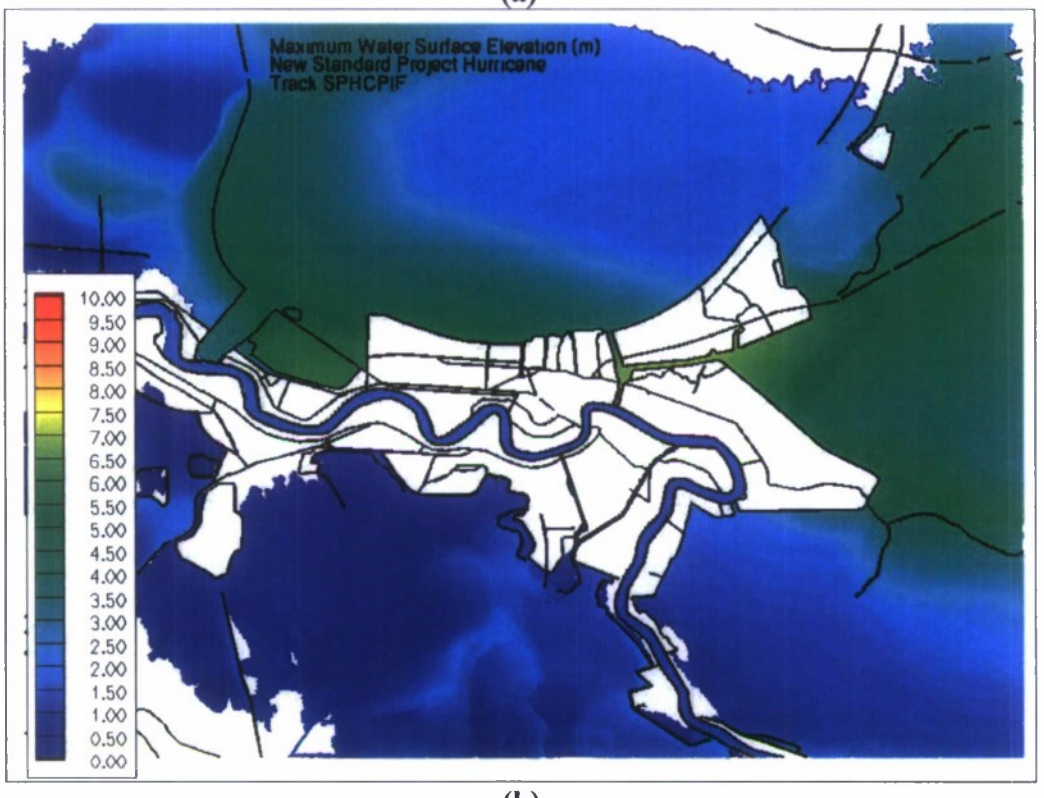

(b)

Figure 8: Computed maximum water surface elevation SPH Track F, (a) old SPH, (b) new SPH

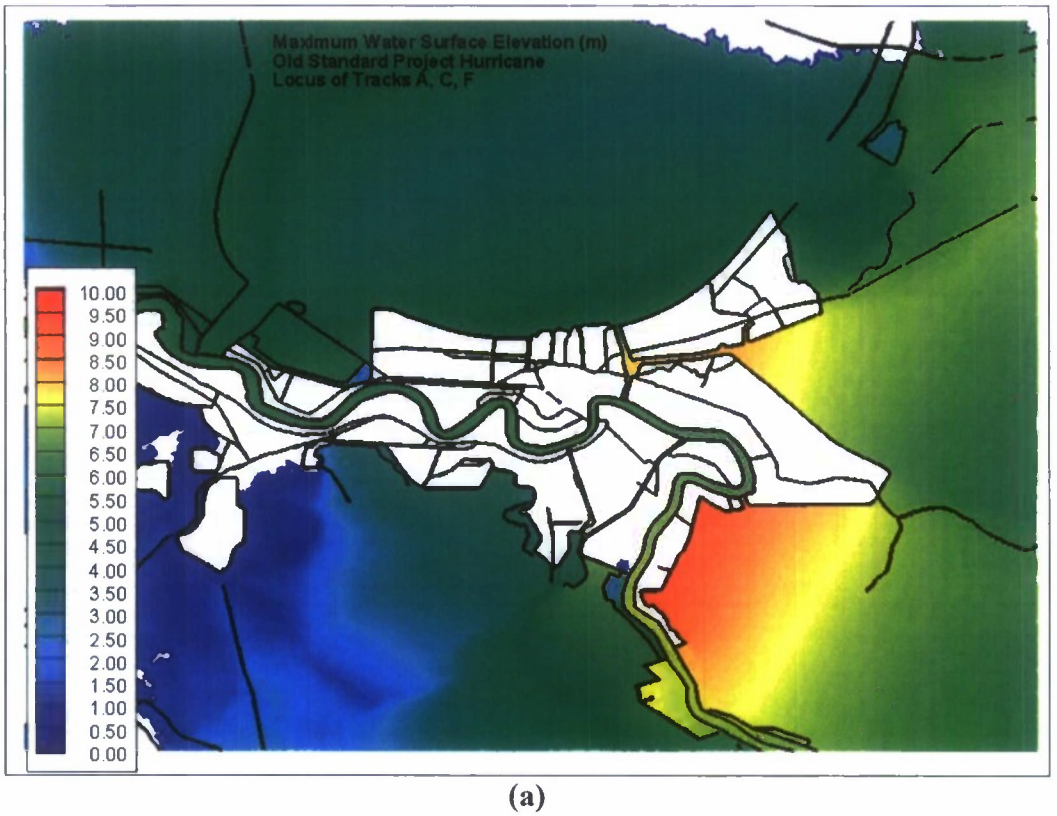

(a)

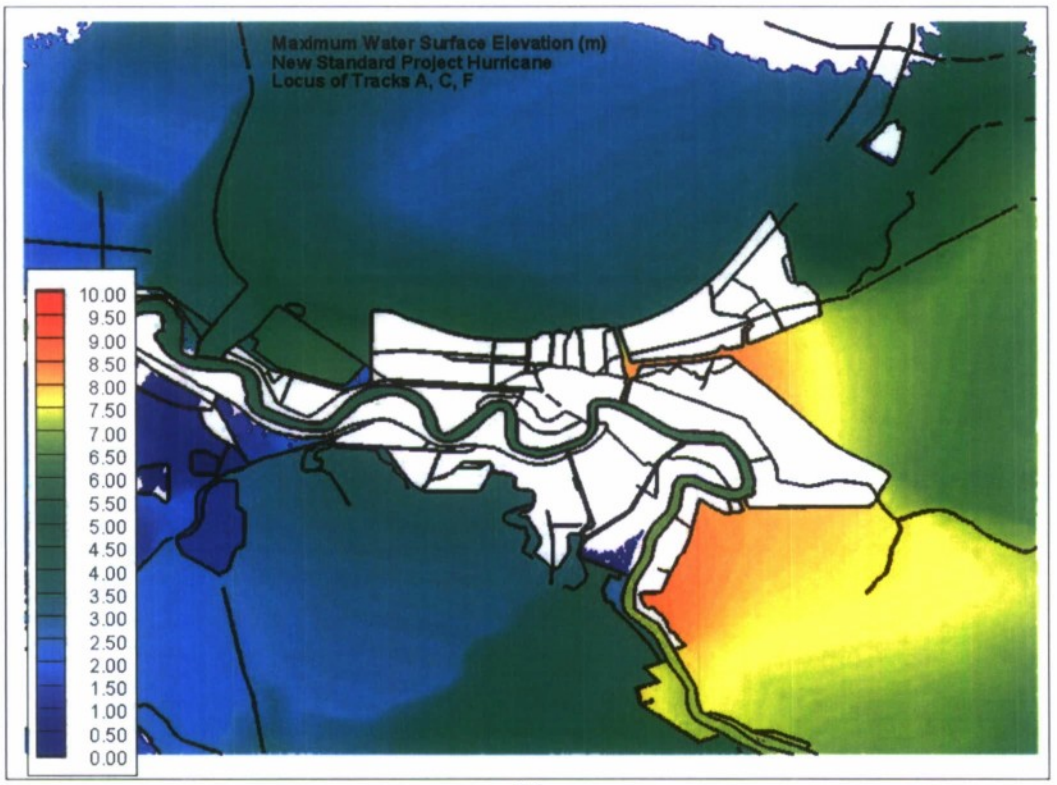

(b)

Figure 9: Computed maximum water surface elevation, locus of Tracks A, C and F, (a) old SPH, (b) new SPH

Figure 10: Difference in computed maximum water surface elevation (new-old), Track A

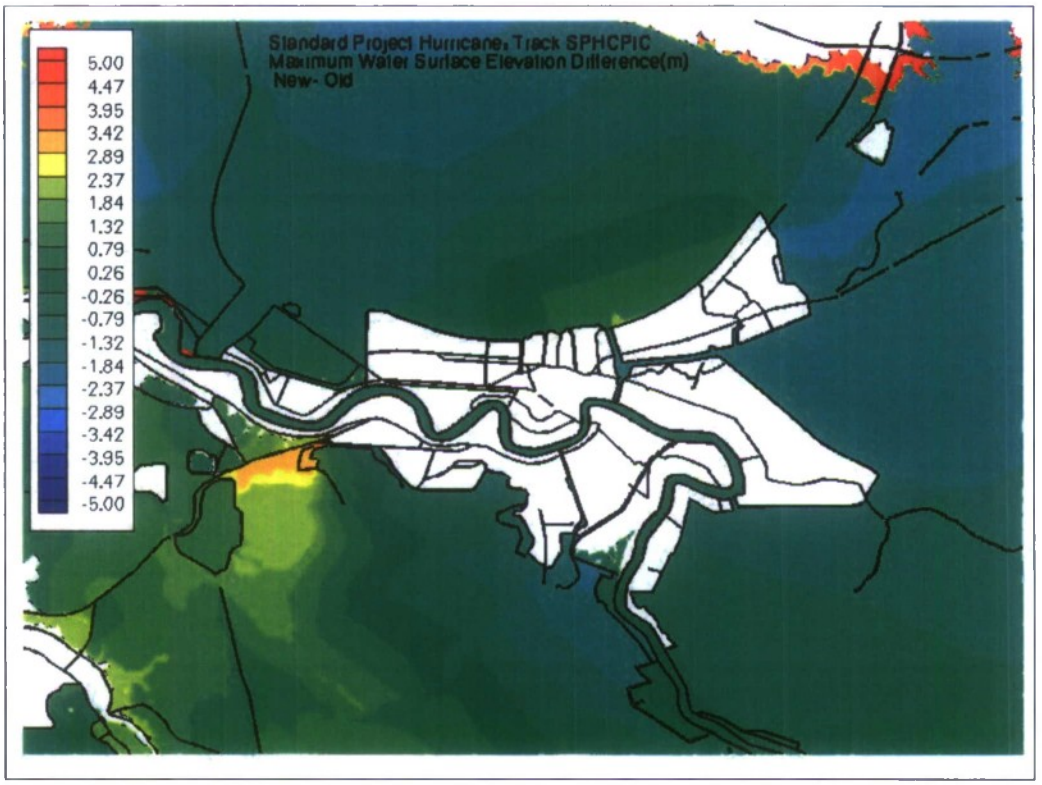

Figure 11: Difference in computed maximum water surface elevation (new-old), Track C.

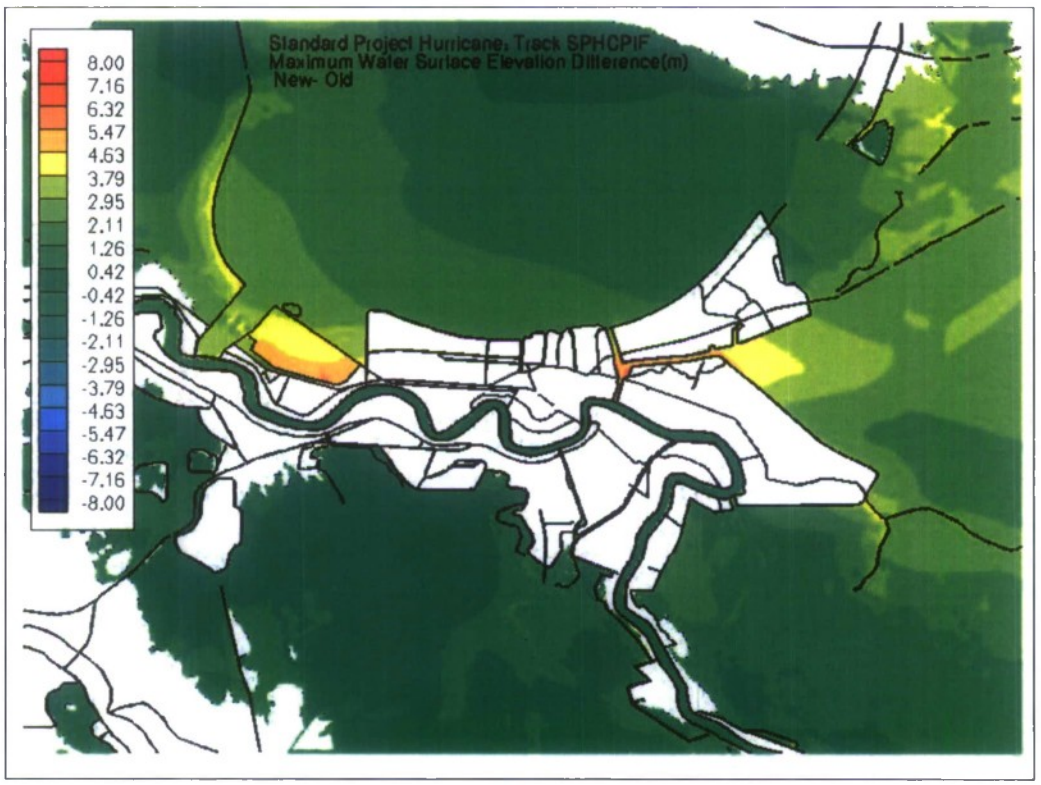

Figure 12: Difference in computed maximum water surface elevation (new-old), Track F.

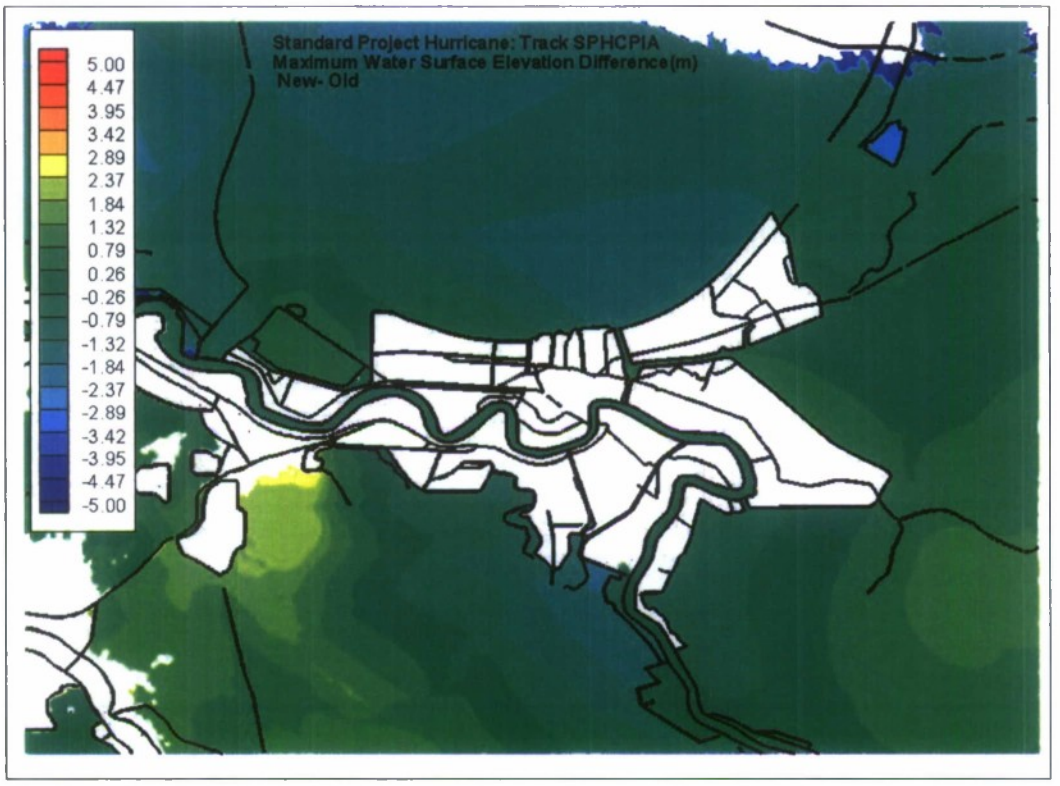

Figure 13: Difference in computed maximum water surface elevation (new-old), locus of tracks A,C and F.

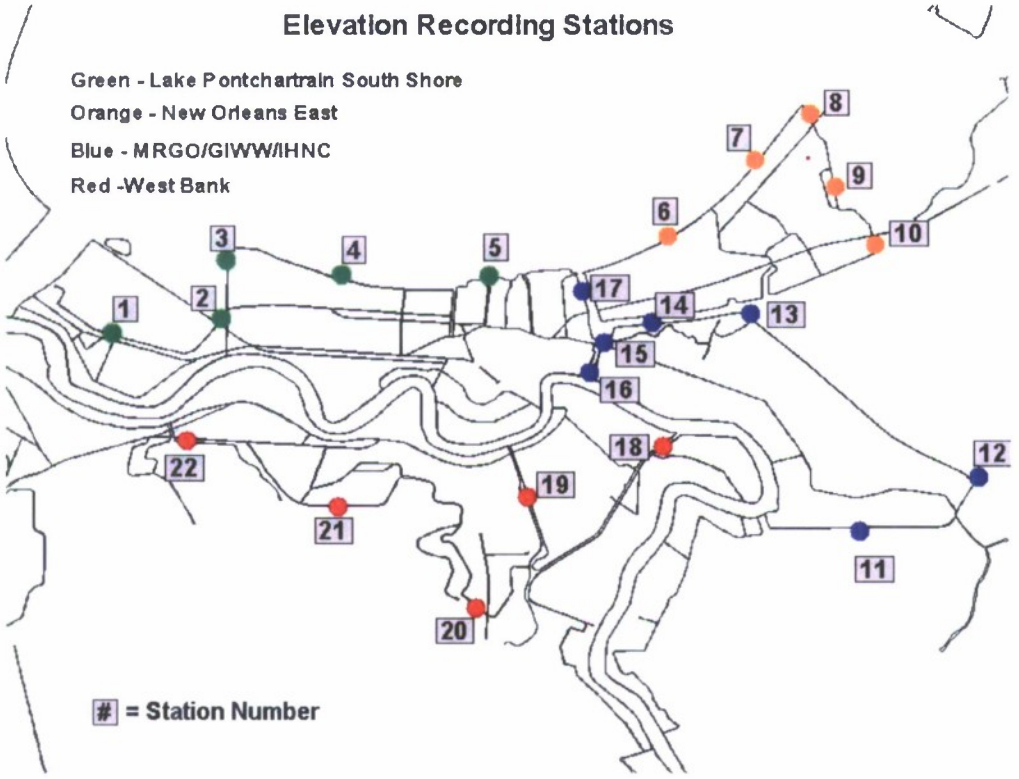

Figure 14: Elevation recording station locations grouped into sections.

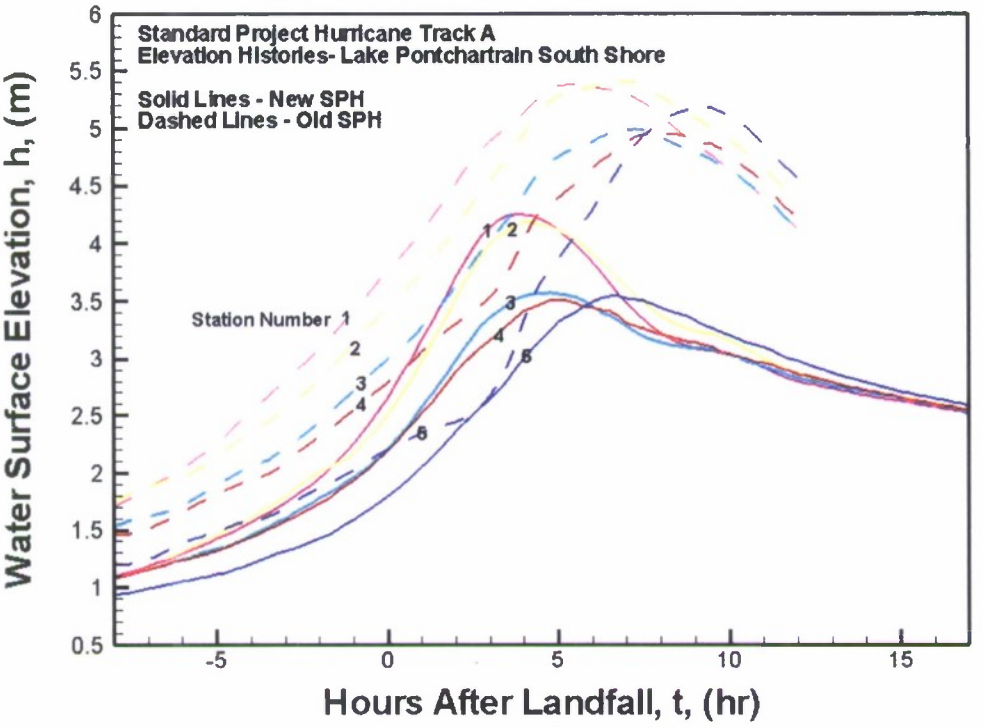

Figure 15: Track A SPH Elevation histories at selected locations along south shore of Lake Pontchartrain in St. Charles and Jefferson Parish and New Orleans Lakefront.

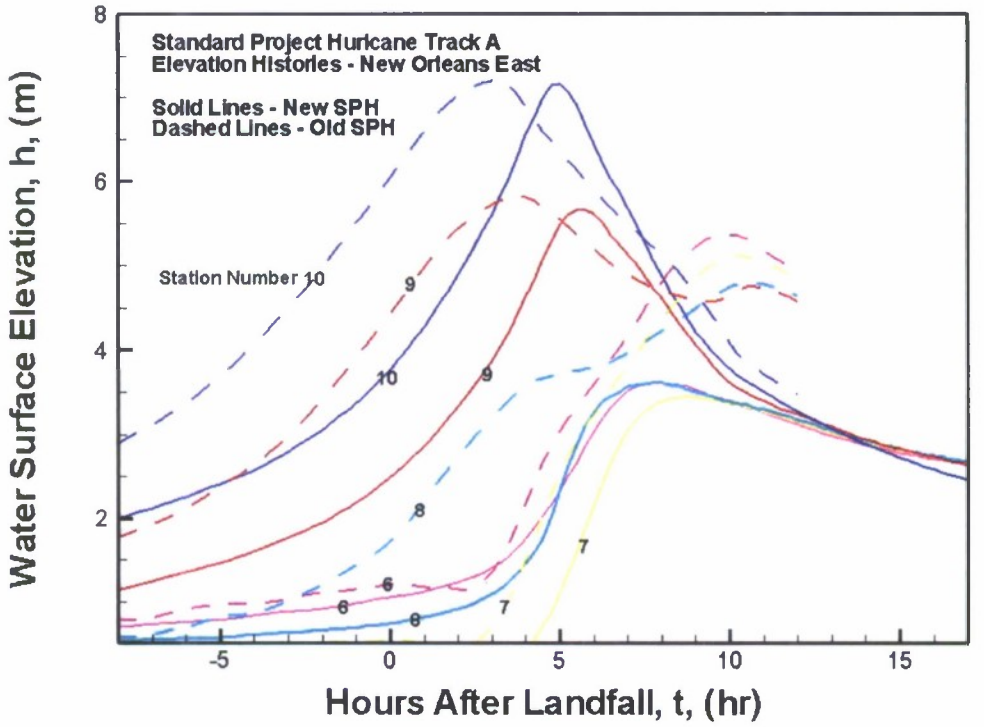

Figure 16: Track A SPH Elevation histories at selected locations along south shore of Lake Pontchartrain in New Orleans East.

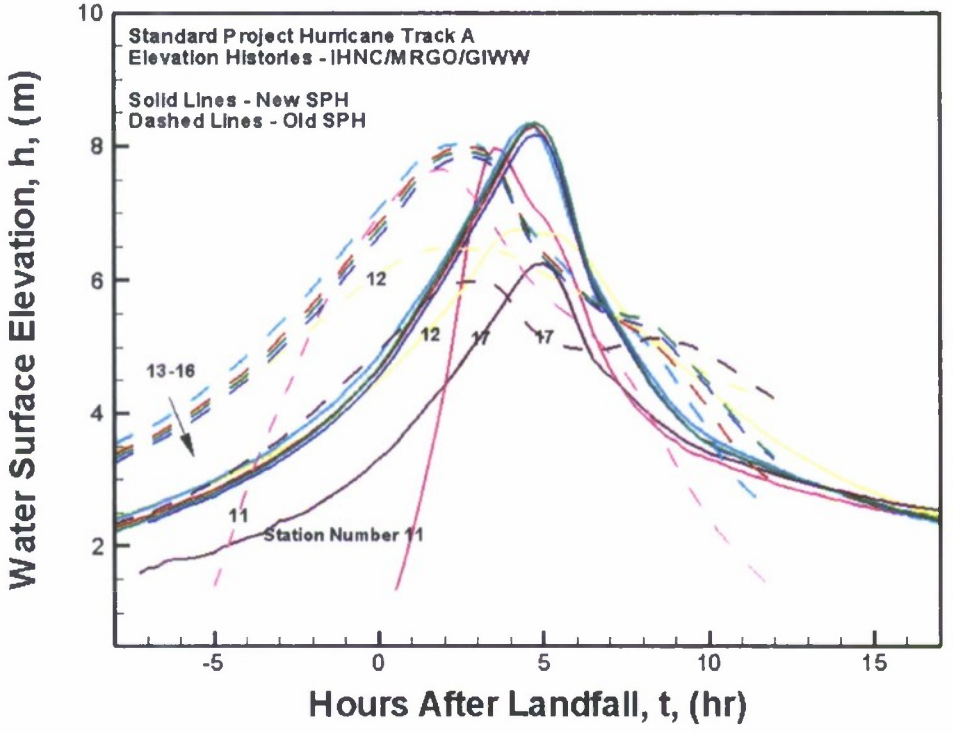

Figure 17: Track A SPH Elevation histories at selected locations along MRGO, industrial canal, and GIWW.

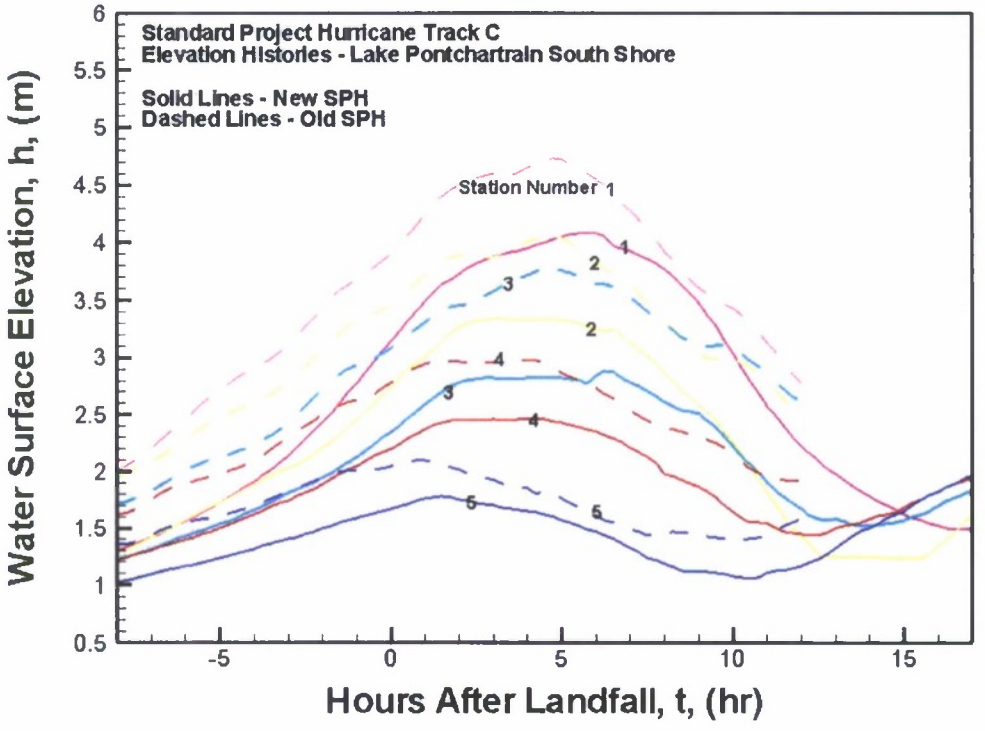

Figure 18: Track C SPH Elevation histories at selected locations along south shore of Lake Pontchartrain in St. Charles and Jefferson Parish and New Orleans Lakefront.

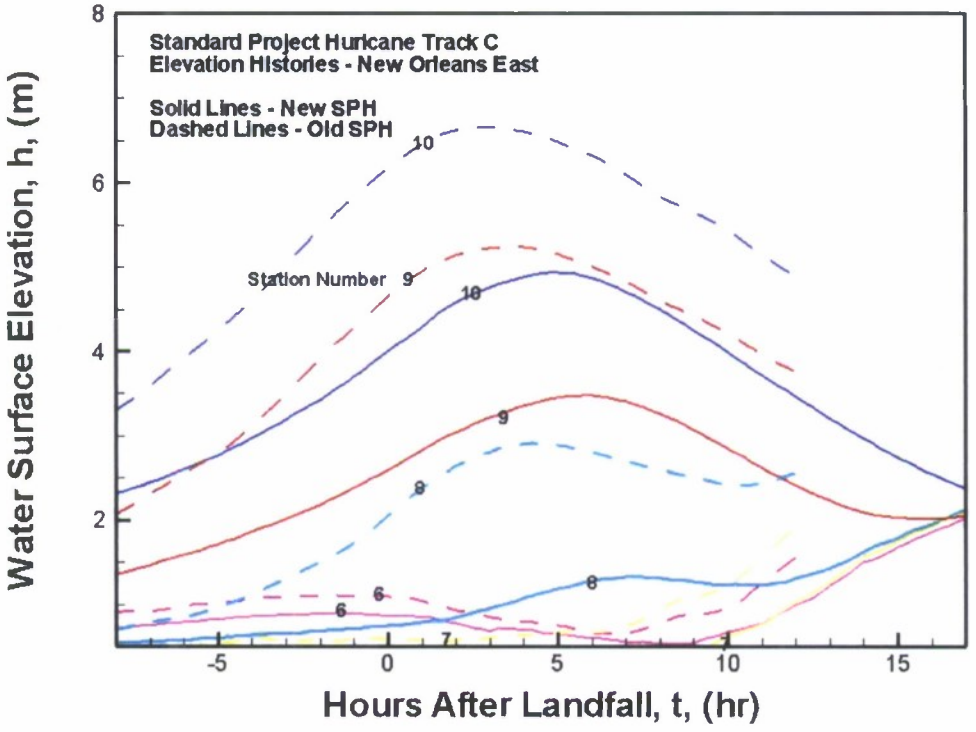

Figure 19: Track C SPH Elevation histories at selected locations along south shore of Lake Pontchartrain in New Orleans East.

Figure 20: Track C SPH Elevation histories at selected locations along MRGO, industrial canal, and GIWW.

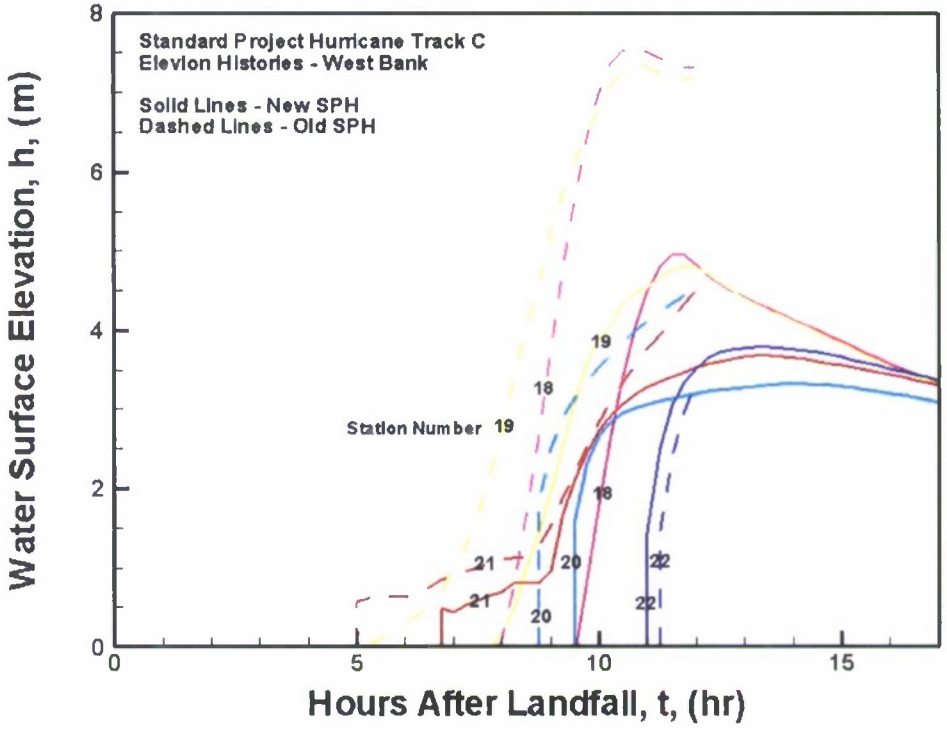

Figure 21: Track C SPH Elevation histories at selected locations on West Bank.

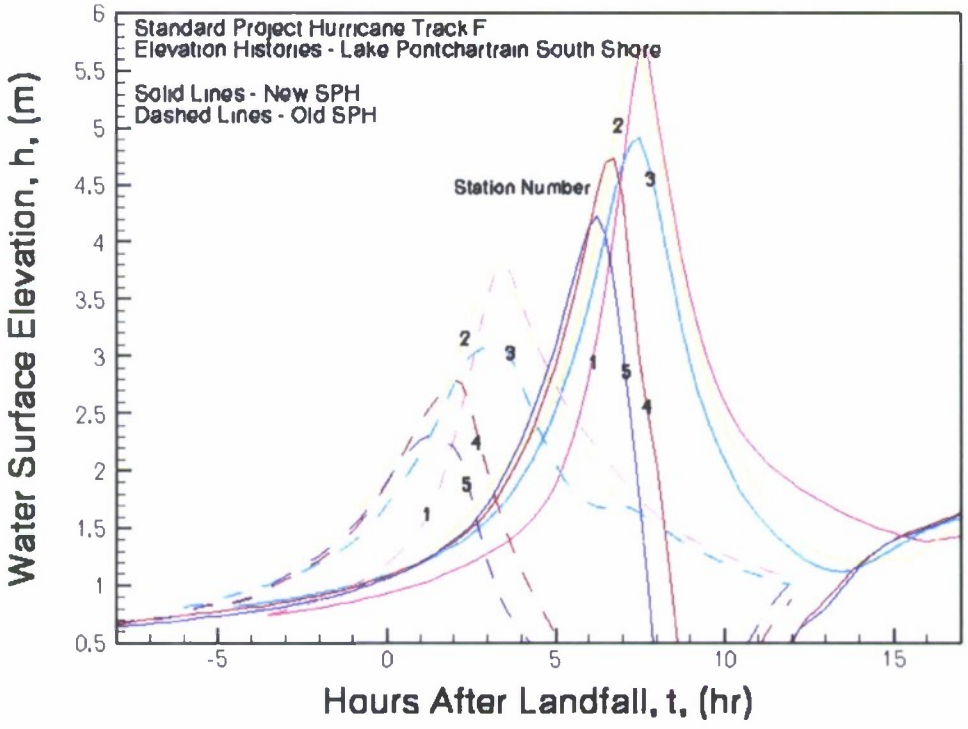

Figure 22: Track F SPH Elevation histories at selected locations along south shore of Lake Pontchartrain in St. Charles and Jefferson Parish and New Orleans Lakefront.

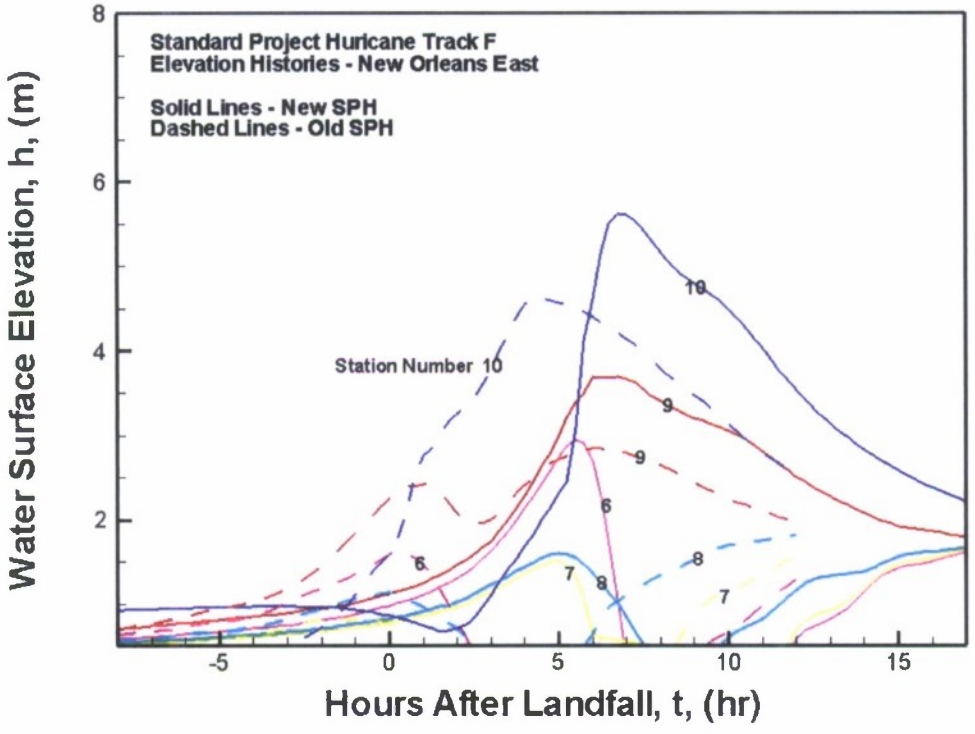

Figure 23: Track F SPH Elevation histories at selected locations along south shore of Lake Pontchartrain in New Orleans East.

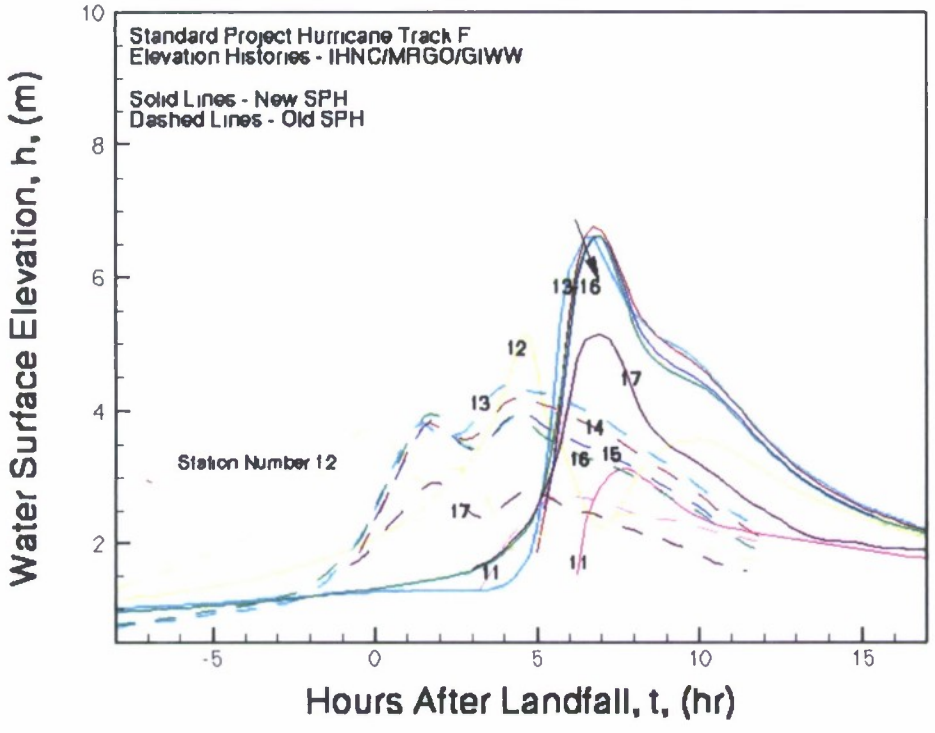

Figure 24: Track F SPH Elevation histories at selected locations along MRGO, industrial canal, and GIWW.

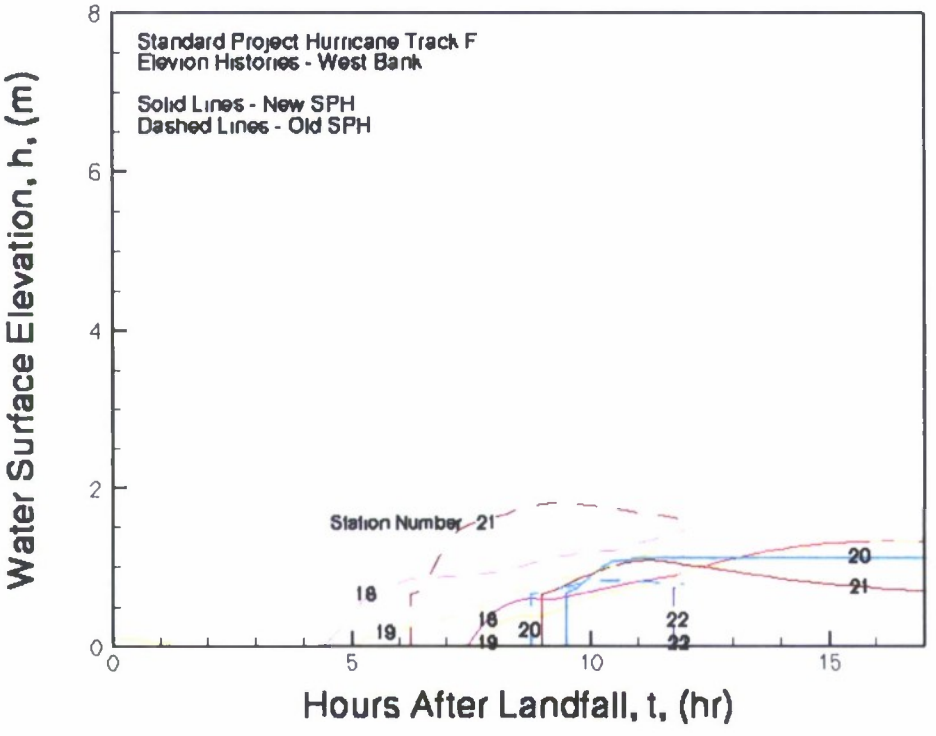

Figure 25: Track F SPH Elevation histories at selected locations on West Bank.

Table 2: Maximum recorded water surface elevations at selected recording stations.

Maximum Water Surface Elevation at Recording Stations								
	Track A		Track C		Track F		Maximum	
Station	Old	New	Old	New	Old	New	Old	New
1	5.4	4.3	4.7	4.1	3.7	5.7	5.4	5.7
2	5.5	4.2	4.1	3.7	3.7	5.7	5.5	5.7
3	4.8	3.5	3.7	2.9	3.0	4.9	4.8	4.9
4	4.8	3.4	3.0	2.4	2.7	4.7	4.8	4.7
5	5.2	3.5	2.1	1.7	1.7	4.1	5.2	4.1
6	5.3	3.5	1.0	0.8	1.6	2.8	5.3	3.5
7	5.0	3.3	2.0	2.0	1.5	1.5	5.0	3.3
8	4.7	3.5	2.6	2.0	1.8	1.7	4.7	3.5
9	6.8	6.7	5.3	3.5	2.9	3.7	6.8	6.8
10	9.1	9.1	6.8	5.0	4.6	5.2	9.1	9.1
11	8.0	8.0	8.0	7.0	2.7	3.2	8.0	8.0
12	6.5	6.7	6.1	4.8	3.7	5.1	6.5	6.7
13	8.0	8.5	7.5	5.5	4.4	6.5	8.0	8.5
14	7.9	8.2	7.4	5.5	4.1	6.7	7.9	8.2
15	7.8	8.1	7.2	5.4	4.0	6.5	7.8	8.1

16	7.7	8.0	7.1	5.4	3.9	6.5	7.7	8.0
17	6.0	6.2	5.5	4.3	2.7	5.0	6.0	6.2
18	0.0	0.0	7.5	5.0	1.8	1.8	7.5	5.0
19	0.0	0.0	7.3	4.8	1.2	1.2	7.3	4.8
20	0.0	0.0	4.5	3.3	0.7	1.1	4.5	3.3
21	0.0	0.0	4.5	3.6	1.7	1.5	4.5	3.6
22	0.0	0.0	3.0	3.6	0.0	0.0	3.0	3.6

References

[1] Graham, H.E., Nunn, D.E., "Meteorological Considerations Pertinent to the Standard Project Hurricane, Atlantic and Gulf Coasts of the United States", National Weather Bureau, Report 33, November 1959.

[2] "Meteorological Criteria for Standard Project Hurricane and Probable Maximum Hurricane Wind Fields, Gulf and East Coasts of the United States", National Oceanic and Atmospheric Administration (NOAA), Technical Report NWS 23, Washington, D.C., September 1979.

[3] Levinson, D.H. "Update to the Standard Project Hurricane Indices", Preliminary Technical Report, National Oceanic and Atmospheric Administration, Climate Monitoring Branch, National Climatic Data Center, Asheville, NC, May 15, 2006.

[4] Luettich, R.A., Westerink, J.J., Sheffner, N.W., "ADCIRC An Advanced Three-dimensional Circulation Model for Shelves, Coasts and Estuaries. Report 1: Theory and Methodology of ADCIRC-2DDI and ADCIRC-3DL", U.S. Army Corps of Engineers Waterways Experiment Station Technical Report DRP-92-6, Vicksburg, MS, 1992.

[5] Thompson, E.F, Cardone, V.J. "Practical modeling of hurricane surface wind fields", *Journal of Waterway, Port and Coastal Engineering*, ASCE, **122, 4,** 195-105, 1996.

Ocean Modeling

Task 1. Model Hindcasting in Smart Climatology

Collaboration with: James Dykes[1], Lucy Fitzgerald Smedstad[1]

Research Objectives: This project aims to develop concepts and techniques that clearly define smart climatology for strategic planning for ASW, SPECOPS and MIW, enabling superior analysis of environmental variability to support tactical decision planning. Ultimately, smart climatology is to take into account the effects on strategic planning of tactical extremes in ocean and atmospheric conditions caused by the large-scale climatic variations. A demonstration of this project is planned to provide the guidance for future potential transition of an end-to-end capability to the war fighter. The portion of this project requiring HPC resources involves running (MetOc) models for long historical periods with the goal of providing quick-turn-around results on demand.

Methodology: MSRC resources were utilized in generating the data and information based on running atmospheric and oceanographic models over a long period of time in the past, also known as hindcasts. A high resolution tactical scale climatology dataset required for knowledge extraction was generated by an air/ocean/wave coupled system, which has been constrained by relevant large-scale climatic variations. The system components include COAMPS®, WAVEWATCH III, NCOM, and SWAN for creating strategic and tactical climatologies in data-sparse and data-void areas, creating a three-dimensional depiction of the atmosphere and the ocean over a three-year period (1997 through 1999). This period is limited in time to cover the anomalous events of an extreme El Niño and La Niña for demonstration, and is expected to expand in later work. Certain parameters are extracted depending on the mission scenario. Ultimately, all the models will be closely coupled under ESMF, but for now they were run separately. The ocean models used forcing provided by either NCEP/NCAR Reanalysis or COAMPS® run at NRL Monterey. Global NCOM output provided the boundary conditions for the regional NCOM.

UNO contribution: NCOM in a 2 coupled nest configuration were run from midway in 1997 through 1999. All the resulting model output files including the complete atmospheric model outputs were stored on the Sun-Fire-15000 (vincent) at NAVO MRSC server occupying about 15 terabytes total. This server provided a convenient means for data sharing amongst team members. The processed output was passed on to NRL-7440 to be used in pattern analysis procedures resulting in information that will allow to examine and validate the types of data and statistics that may impact strategic planning.

Task 2. Relocatable NCOM

Collaboration with: C. Rowley, R. Allard, E. Coelho

Research Objectives: The main purpose of this project is to develop and evaluate a real time ocean prediction system developed at the Naval Research Laboratory (NRL) in support of naval operations. The system is portable on several computer platforms and operating systems, and

rapidly relocatable. Analysis and prediction are available for any part of the world usually within a few hours from the request, making it a particularly useful system in emergency situations. The major challenge is to offer a default set of parameters that can provide accurate solutions for any given configuration, yet allowing the flexibility of tuning and calibrating for a given domain configuration. Since is it unrealistic to assume data are available at the spatial and temporal resolutions necessary for specification of the boundary conditions, the system has the capability of multiple 1-way nesting from basin-scale to regional to high-resolution coastal domains.

Methodology: The relocatable system was evaluated in several realtime configurations in support of NAVO operations and other research joint program. While the exercises at NAVO have the support of allocated computer resources, other realtime applications are sensibly constrained by the computational requirement and a timely deliver of the solution

UNO contributions: in FY 2006-2007, the relocatable system was evaluated in 2 major realtime exercises:

1. **SW_06** (Shallow Water 2006) a joint experiment with NRL and other academic institutions (Rutgers University being the leader organization) off the New Jersey coast. Relo_NCOM was configured in 3 nest domains with a horizontal resolution ranging from 2.5 to .6 km. the inner nest was designed to capture the internal wave activity at the shelf break and provide accurate forecast to the acoustic group.
2. **MREA_07** (Marine Rapid Environmental Assessment 2007). One of the NRL contributions to the exercise was to provide, in realtime, ocean forecasts in support of the operations at sea. The NRL prediction system, was configured with 3 nesting domains at resolutions of 4, 2, and 0.6 km. Two separate inner nests were configured for the BP_07 (Elba) and LASIE (LaSpezia) areas of operations, respectively. For this application, no data were assimilated in realtime. However, a small (10 members) ensemble of free-runs was used for water column temperature forecast Root Mean Square (RMS) error prediction. Ocean forecast are usually the final component of a long string of products developed at several different centers: a delay in acquiring one of the input data, the classic computer breakdowns (just to mention a few issues) may create a domino effect and ultimately a late delivery of the forecast. Preliminary model/data comparison and new simulations in a pseudo forecast mode, but with different model parameters (such as increased vertical resolution) highlight the skills and limits of the default configuration.

Presentations:

G. Peggion: How to develop a relocatable prediction system. OGS Trieste, May 19 2006
G. Peggion: A Rapidly Relocatable Ocean Prediction System: *Congress SIMAI 2006*. Baia S. Samuele, Italy,May, 25,2006
G. Peggion: A realtime Ocean Prediction System: Rapid Environment Assessment Conference, Lerici, Italy. Sept 25-27, 2007

Publications:

Rixen, M. et. al.; 2007: Super-ensemble forecasts and resulting acoustic sensitivities in shallow waters. Presented at the Rapid Environment Assessment Conference, Septt 25-27, Lerici, Italy. Paper to be published on a special issue in the Journal of Marine Systems focused on *'Coastal processes :challenges for monitoring and prediction'.* (in press)

Coelho, E et al.; 2007: A note on NCOM temeprature forecast error calibration using the ensemble transform. Presented at the Rapid Environment Assessment Conference, Septt 25-27, Lerici, Italy. Paper to be published on a special issue in the Journal of Marine Systems focused on *'Coastal processes :challenges for monitoring and prediction'.* (in press)

Coelho, E., G. Peggion, C. Rowley, and G. Jacobs: 2007: Forecast error analysis of limited data assimilation schemes using perturbed and multi-model ensembles. *Geophysical Research Abstracts*, **9**, 04122,

G. Peggion, 2006: A rapidly relocatable coastal ocean prediction system. *Proceeding of Congress SIMAI 2006*. Baia S. Samuele, Italy,May, 22-26, 2006. DOI: 10.1685/CSC06126

A Note On Ncom Temperature Forecast Error Calibration Using The Ensemble Transform

Emanuel F. Coelho, Germana Peggion, Clark Rowley, Gregg Jacobs, Richard Allard, Elaina Rodriguez

PII: S0924-7963(09)00155-9
DOI: doi: 10.1016/j.jmarsys.2009.01.028
Reference: MARSYS 1825

To appear in: *Journal of Marine Systems*

Received date: 12 June 2008
Revised date: 24 July 2008
Accepted date: 22 January 2009

Please cite this article as: Coelho, Emanuel F., Peggion, Germana, Rowley, Clark, Jacobs, Gregg, Allard, Richard, Rodriguez, Elaina, A Note On Ncom Temperature Forecast Error Calibration Using The Ensemble Transform, *Journal of Marine Systems* (2009), doi: 10.1016/j.jmarsys.2009.01.028

A NOTE ON NCOM TEMPERATURE FORECAST ERROR CALIBRATION USING THE ENSEMBLE TRANSFORM

Emanuel F. Coelho[1,2*], Germana Peggion[1,3], Clark Rowley[1], Gregg Jacobs[1], Richard Allard[1] and Elaina Rodriguez[3]

[1]Naval Research Laboratory, Stennis Space Center, MS-USA

[2]University of Southern Mississippi, MS-USA

[3]University of New Orleans, Louisiana, LA-USA

Abstract:

During the MREA07 trial, off the NW coast of Italy in the late spring and summer of 2007, Navy Coastal Ocean Modeling (NCOM) multiple nests free run ensembles were made available in real-time for the LASIE07 and BP07 events and a fairly complete set of observations were collected inside the inner nests domains. This note addresses the problem of predicting NCOM local unbiased 0-24 hours forecast errors by perturbing a limited number of possible error sources through Monte-Carlo simulations, without local data assimilation. It discusses preliminary results using the Ensemble Transform (Bishop and Toth, 1999) to calibrate the ensemble spread by adjusting its characteristics (spread-skill relationship and magnitude) to an observed or pre-estimated error field. A small (10 members) ensemble of free-runs was used for water column temperature forecast Root Mean Square (RMS) error prediction. After being post-processed they were compared with observed errors and those estimated using time variability as an error proxy. The ensemble runs were generated through atmospheric forcing perturbations using the space-time deformation method as proposed by Xiandong, et al., (2007), keeping independent initial

---

* Corresponding author. Naval Research Laboratory, Stennis Space Center, MS39529
Tel: + 01 228 688 5710 ; *E-mail address*: emanuel.coelho.ctr.po@nrlssc.navy.mil

conditions. Because at the starting time all runs shared the same IC, the ensemble was run for roughly two weeks for spinning up and then used during the following 10 days for data comparisons, during which the ensemble spread did not diverge and was consistent with the observed dynamics. Comparisons of ensemble spread of temperature profiles with local observed errors and time variability (assumed as an error proxy) showed they were consistent through this 10 days analysis period, with performances above the non-calibrated ensemble estimates and time-variability used as error proxy.

Key words: Ocean Ensembles, Forecasting, Ocean Models, Forecasting Errors, Environmental Assessment (43-45N, 9-10.5E)

-

---

1. Introduction

When considering numerical prediction of ocean dynamic states using nested domains, several sources of error can contribute to cascading uncertainty into state variable estimation (Coelho and Rixen, 2008). These sources of error include the errors of the initial and lateral boundary conditions, local forcing, bathymetry errors, numerical approximations and filtering, errors due to approximations when assimilating observations, errors in the forcing terms and un-resolved scales (sub-grid variability). To address this problem, local unbiased (correlation) and persistent errors (bias) of the Navy Coastal Ocean Modeling (NCOM) System nested in global ocean domains, are typically reduced and monitored by assimilating dynamical balanced analysis fields of state variables, derived from observation networks, using the Navy Coupled Ocean Data Assimilation (NCODA) system (e.g., Cummings 2005). This system also provides an error estimate of these analysis fields at an analysis time.

In recent implementations (Coelho et al., 2008; Fabre et al., 2008), ensemble based stochastic methods have been used to track these NCOM analysis multi-scale ocean errors by running the model several times using different forcing and starting from different initial conditions. The resultant ensemble spread was constrained at each new analysis time by the new estimate of the analysis errors using a technique named Ensemble Transform (ET) (Bishop and Tott, 1999). In order to be accurate, the perturbed ensemble members should be taken from a fairly large number of independent runs to resolve state variables error covariances and should include all significant sources of error and uncertainty (Judd, et al., 2007, Lermusiaux, et al., 2006). Since this is not easy to obtain in operational timeframes, and once a smaller number of runs are selected, one can expect the ensemble to perform differently inside the simulation domain and through time depending on the number of the dominant error modes. This limitation motivates on-going work in developing dedicated metrics to diagnose and prognoses ensemble performances through the overall domains and forecasting lead times.

In any case, it is anticipated that a small number of runs may still provide useful information under certain conditions (e.g. when there are no strong non-linearity and bias errors are on the same order of magnitude of the correlations errors). Furthermore, if the ensemble estimates define a domain that contain the most relevant features and scales of the physical system, then they can be improved in their consistency through calibration and post-processing by adjusting their spread and bias to some training sequence. These methods have been successfully used for meteorological ensemble calibration (e.g.Doblas-Reyes, 2005; Hammil, 2007) and for multi-model ocean ensembles applications (e.g. Rixen and Coelho, 2007; Coelho, 2008).

It should be noted that with a small number of independent runs we should not expect to resolve the full ocean state covariances with the original model grid resolution, but one can expect a

small number of runs between 10-15 may still bc adequate to track single variable forecast errors on a re-sampled spatial domain as long as the number of indcpendent variables can be kept within the order of $O(10^3)$, following the estimates of Judd (2007). This note will discuss the limitations of a small ensemble size used during the MREA07 trial and proposes a method to improve forecast error prediction consistency for specific target variables, applicable also for non-statc variables estimates when there are not many observations or prior to use observations into the assimilation process.

Several methods have been used to perturb the initial conditions fields based on the observed errors. In particular Bishop and Toth (1999) proposed a technique named Ensemble Transform that allows computing dynamically balanced initial conditions perturbations that are consistent with a best estimate of the error covariance. On the other hand, ensemble calibration can also be sought through post-processing using Bayesian methods (e.g. Gneiting, 2004, Coelho, 2005 and Rixen and Coelho, 2005), within the limits of the known cross-correlations among the observed and modeled variables. This work combine both techniques as a post-processing method, applied to local single variable ensemble spread calibration. The methodology uses the perturbed model statistics re-scaled through an estimate of the error variance, to obtain short term estimates of posterior normal probability distributions envelopes of a selected ensemble variable.

The MREA07 (BP07 and LASIE trials), took place off La Spezia, Italy in the spring and summer of 2007 (e.g., LeGac and Hermand, 2007). During the trial, mesoscale relocatable NCOM implementations using the RELO system were made available in real-time without performing local data assimilation, though remote sensing and global data was assimilated on the outer nests used for boundary conditions and initialization. In standard implementations the RELO system runs together with the Navy Coupled Ocean Data Assimilation (NCODA) system that performs observations quality control and produce local analysis for assimilation that in the present version

are based on a Multi-Variate Optimum Interpolation technique (e.g. Cummings, 2005). NCODA also provides the analysis error fields that are used to re-set the ensemble spread of the initial fields in operational ensemble runs using the same ET technique (e.g. Fabre et al., 2008). This present solution does not provide reliable analysis error covariances but it is planned the NCODA system will evolve in the near future into using hybrid Monte-Carlo ensembles (e.g. Lermusiaux et al., 2006) and Variational analysis (e.g. Nogodock, et al., 2007). This will improve error covariance estimates and produce analysis fields consistent with the boundary conditions and other forcing fields. For this specific implementation, the NCODA assisted assimilation process in the inner nests was turned off to allow a fully independent analysis of the model results and observations, simulating a scenario where no local data would be available in useful timeframes).

During this trial the free-run error fields of the RELO system were estimated using an ensemble of 10 independent runs with independent initial conditions starting from a common field far back in time and perturbed through atmospheric forcing using space-time deformation of the surface forcing fields (Xiandong, 2007). The ensemble spread of the free runs was then re-scaled in post-processing through an Ensemble Transform (Bishop and Toth, 1999) using the temporal variability as an error proxy. These preliminary error estimates were then used for model benchmarking and aiming specific ocean-acoustic applications (e.g. Carriere et.al, this volume) and to estimate the relative impact of different observational strategies (Coelho et al., 2007).

2. RELO-NCOM Setup

The Relocatable Navy Coastal Ocean Model (RELO-NCOM) is a scalable, portable, and user-friendly system for nowcasting and short-term (2-3 day) forecasting simulations (Rowley, 2007). There are two major components: 1) NCOM (Martin, 2000) and 2) the Navy Coupled Ocean Data Assimilation (NCODA) (Cummings, 2005) for data analysis and model initialization. For a rapid configuration, the system relies on a set of data and products available on a global scale

(bathymetry, winds, analysis of the remote sensing data). These products are generally on a low resolution and it is possible to substitute them with local and high-resolution databases. RELO-NCOM meets the naval requirements to generate real-time description of the environmental variables and it is operational at the US Naval Oceanographic Office (NAVO).

There is a fundamental difference between assessing an ocean model configuration in a research and an operational mode. Both need to be designed, calibrated, and evaluated to encompass the dominant dynamics of a given region. The goal is to provide the best possible representation of the dynamical features of a specific area. However, a predictive system that supports operational applications must be rapidly relocatable anywhere in the ocean (oil-spill response and naval operations are the most relevant applications), and easily reconfigured. The principal goal is to provide good representations everywhere with the available data (i.e., in spite of the absence of complete sets of observations), motivating the need to associate with the system a reliable error diagnostics and prediction tool, to allow tracking consistently the error dynamics.

For the MREA07 trial the RELO-NCOM was deliberately set on its default mode as for a generic application with little or no tuning of the physical and numerical parameters. Furthermore, no MREA07 or other data were assimilated into the inner nests. The goal of this implementation was to test the modeling skills of these free runs and estimate the relevance of the atmospheric forcing as a single source of error.

The daily predictive cycle during MREA07 is described as follows:

- NCOM is started from the previous day's nowcast (-24 hr) and forced by the available operational winds. Open Boundary Conditions (OBC) are extracted from the simulation of the parent domain. The OBC for the outer most nest are extracted from NCOM configured on a global scale at a 1/8° resolution (NCOM-GL) which is operational the

Naval Oceanographic Office (NAVO) (http://www7320.nrlssc.navy.mil/global_ncom/index.html) (Barron et al., 2006). However, this procedure is not restricted to NCOM-NCOM nesting; any nest could be coupled with several other dynamical model formulations.

- During the nowcast, temperature (T) and salinity (S) fields are nudged to the nowcast fields of the parent simulations. The nudging during the hindcast phase has been suggested to provide a minimum connection with realtime data since NCOM-GL assimilates sea surface temperatures (SST) and Modular Ocean Data Assimilation System (MODAS) synthetics (with the surface height derived from the Naval Layer Ocean Model (NLOM) (http://www7320.nrlssc.navy.mil/global_nlom/). No data are nudged after the nowcast (0 hr).
- A short-term (2-day) forecast is provided. The 48-hour interval has been chosen because this is the typical period in which meteorological mesoscale forecasts are available and reliable.
- The nested domains run then in sequence using boundary conditions from the outer nests (i.e., one way nesting). Although NCOM provides a tile nesting approach, the default procedure allows an easy and rapid configuration and assessment of each domain, and more importantly, a possible different choice of the vertical coordinate between nests. Fig.1. illustrates the triple nested configuration for the MREA07 exercise.

In this model configuration, all domains are forced with the Coupled Ocean Atmosphere Mesoscale Prediction System (COAMPS®[†]) Europe-2 winds (27km) (Hodur, 1997) and heat fluxes from 0.5° Navy Operational Global Atmospheric Prediction System (NOGAPS, Rosmond et al., 2002). Monthly river discharges are extracted from the global river data set of NCOM-GL (Barron and Smedstad, 2002), with the Arno, Magra, and Serchio transports provided by the

[†] COAMPS is a registered trademark of the Naval Research Laboratory

Istituto Idrografico Italiano. The vertical resolution of each domain has 38 σ- and 7 z-levels (45 levels). The outer nest (nest0) is at 4km horizontal resolution with the primary purpose of serving as a buffer zone between NCOM-GL's NOGAPS forcing and the higher resolution wind data set. Nest I (2km resolution) include tides. Tides are specified at the boundaries from the Oregon State University tide model (Egbert and Erofeeva, 2002). Nest2 and nest3 are at about 0.6km resolution and configured for the BP07 (Elba) and LASIE07 (LaSpezia) domains, respectively. An ensemble of 10 independent runs of the inner nests was also made available in realtime, using similar set-ups but with perturbed atmospheric forcing using the space-time deformations method (Xiandong, et al., 2007).

[FIGURE I]

One of the most pressing issues of realtime operational forecasting is to provide the information in a timely manner. Ocean forecasts are usually one of the final components of a long string of products developed at several different centers: a delay in acquiring one of the input data (e.g., winds, boundary conditions), the classic computer breakdowns (just to mention a few issues) may create a domino effect and ultimately a late delivery of the forecast. In order to avoid delays in the queue submission which are often occurring at the supercomputer sites, the full forecast cycle is performed at the Naval Research Laboratory - Stennis Space Centre (NRLSSC) on dual processor Opteron-based LINUX platforms. The latest NOGAPS and COAMPS analysis and forecasts are usually available at NRLSSC before 1000GMT, but NCOM-GL daily hindcasts and forecasts arrive at about 1130GMT. Therefore, to speed up the delivery of the results, the OBC for nest0 are extracted from the NCOM-GL 72hr forecast of the previous day. This makes it possible to start the simulations at about 1000GMT and complete the forecast cycle usually before NCOM-GL latest files are available at NRLSSC. Unfortunately, only a partial COAMPS

data set is archived at NRLSSC, so the price for this procedure is the use of NOGAPS-0.5 heat fluxes.

The model results are written to NetCDF files at user specified z-levels and time increments. It is important that the z-levels be consistent with the NCOM vertical grid. A coarse vertical resolution in the NetCDF files may remove features reproduced by the model; a too fine vertical resolution increases the computational cost and memory requirement without increasing the physical accuracy of the solutions. For this real-time exercise, the NCOM fields were provided on 47-levels and at a 1hr increment. To reduce the amount of transferred data, only the 48 hr forecast (i.e., no hindcast) of the model and only a few upper vertical levels for the ensemble spread were posted on the MREA07 ftp server, generally at about 1230GMT and 1500GMT, respectively.

3. RELO-NCOM Control Analysis and data comparison

This note will focus the analysis and discussion for the period June 10 to 25, 2007 and for the nest 3 area only. In this region, dynamics were mostly dominated by a persistent cyclonic gyre centered roughly at 43 40N and 9 20W, modulated by smaller re-circulation cells north and east, closer to the coast. The shapes and temperature distributions of these smaller cells was strongly perturbed by the wind forcing. During the "sirocco" south-easterly winds (e.g. 06/19 06:00 snapshot displayed in Figure 2, left panel) the average surface temperatures were higher, with warmer waters trapped closer to the eastern coast. During the "libeccio" south-westerly winds ((e.g. 06/23 12:00 snapshot displayed in Figure 2, right panel), the cold eddy signature becomes more noticeable and different recirculation patterns can be found between the eddy and the coastline.

[FIGURE 2]

The Sea Surface Temperature (SST) images obtained from NOAA AVHRR displayed in Figure 3, although with different resolutions, concur with the analysis of the previous paragraph.

The water column was strongly stratified during the whole period. Model temperature hindcast and forecast estimates were compared with 160 CTD profiles collected during the trial in the period June 4-26, 2007 by three ships in the area (RV Planet, RV Leonardo and NI Galatea). The daily CTDs' covered both deep and shallow water throughout most of the surveying time. For this work only profiles inside the nest 3 domain were used. For each CTD, the nearest (in space and time) hourly model profile was extracted. No horizontal or temporal interpolation is performed on the model or data. Since observations are on a higher vertical resolution relative to model estimates, the model temperature at a specific z-level should be compared with the mean value of the observed values between the intermediate levels up and below (i.e. for the model estimate T_i at level Z_i, observations should be averaged between the levels $(Z_{i-1}+Z_i)/2$ and $(Z_i+Z_{i+1})/2$). The model data comparisons displayed in Figure 4 show that temperature errors were more noticeable on average at the bottom of the well mixed layer (at roughly 50m depth), with the surface waters typically cooler than observations and warmer waters below. Temperature errors were very small below the 200m depth. It is also noticeable these error characteristics did not change significantly during the analysis period, though significant changes occur in the forcing and dynamic responses as mentioned above.

[FIGURE 3]

From these comparisons one can assume the prediction skills of the model were limited, not significantly above model persistency, such that these free-run RELO-NCOM fields could be considered as an analysis tool capable of providing reasonable spatial distributions of the

temperature fields, up to at least 48 hours. This is mostly due to the persistent nature of the dominant local dynamics that did not change significantly during the analysis period. In other more dynamic areas one could expect these free-run errors to increase significantly after a few hours and differences between forecast lead times also to become more noticeable.

Since there were no significant differences between these errors, the discussion below regarding error prediction will use the 0–24 hours and 24–48 hours temperature forecasts as equivalent estimates.

4. Ensemble re-scaling using the Ensemble Transform

The ocean is driven by surface fluxes that are determined by the atmospheric state and are one major source of uncertainty. Predicted atmospheric fields often contain the forecast feature of interest, but they can be misplaced in space and time (e.g. Hoffman 1995). This characteristics motivated attempts to represent forecast errors in terms of a shift of a forecast in space and time similar to the pseudo-random fields method described by Evensen (2003) and applied in ocean ensemble generation problems (e.g. Demirov, et al., 2003). For the present work, the atmospheric forcing perturbations used to force the ocean ensemble members were produced using the method developed by Xiandong et al. (2007). It uses only time shifts of the forecast, with a choice of parameters to provide a good precision in the atmospheric perturbations, though accuracy may not be guarantee over the whole simulation period.

[FIGURE 4]

If we neglect bathymetry, error induced by numerical approximations and other sources of possible model bias, the ensemble transform (ET) method of generating initial perturbations applied in atmospheric ensemble forecasts (Bishop and Toth, 1999) can be used to re-balance and

re-shape the IC fields of the ensemble subset. Besides assuring all detected error growing modes will be equally represented, the advantage of this technique is such that: it respects hydrodynamic balances by ensuring that initial perturbations are a linear sum of forecast perturbations from the preceding forecast; and ensures that the initial perturbations are equally likely and orthogonal under a measure of the probability of initial condition error based on the best available estimate of initial condition error variance. This technique does not provide though an initial set of background perturbations that need to be introduced using complementary methods, such as forcing from an ensemble of atmospheric forecasts as mentioned in the previous paragraph.

As detailed in Toth and Bishop (1999), through the ET ensemble generation technique, K forecast perturbations of N state variables $\mathbf{X}^o$ (NxK), can be transformed into a set of perturbations $\mathbf{X}^r$ that are consistent with the background error analysis covariance $\mathbf{P}_g^a$, using

$$\mathbf{X}^r = \mathbf{X}^o\mathbf{T}$$

where $\boldsymbol{T}$ is a transformation matrix determined by the eigenvectors and eigenvalues of the projections of the magnitude of the predicted analysis perturbations on the inverse of the error analysis covariance matrix. If the number of ensemble members equals the number of state variables, this projection guarantees the perturbations covariance to be equal to the error covariance.

Through this transform we can then obtain a set of perturbed fields that are consistent with an independent estimate of the error covariance. In operational implementations these initial fields are used as new initial conditions for the K independent ensemble runs, providing a method to assimilate the observed errors into the ensemble forecasts. For the present application and to use this method in post-processing a persistency assumption during the 48hours forecast cycles is taken, regarding the projection of the ensemble covariances into the observed errors.

5. MREA07 Error Predictions

For the present application since no data is to be used the ET is computed using the temperature 48 hours forecast time variances, as estimated by the RELO-NCOM free runs, producing a diagonal error covariance matrix $\mathbf{P}_g^a$. Besides allowing for a faster transform, this approach allows to keep the shapes of the off-diagonal terms (spatial cross-correlations) as estimated by the ensemble, while consistently re-scaling the analysis errors, without introducing further analytical or numerical approximations.

The temperature estimates ensemble spatial correlations are then updated only by the RELO-NCOM independent runs. This method allows keeping error covariance updates, without the cost of computing and inverting very large matrices. Furthermore, since only a limited number of ensemble members are available, this method limits the growth of spurious cross-correlations. The same transform matrix **T** is applied to all time steps of the ensemble estimates.

The resulting ensemble spread (standard deviations) for each temperature estimate are then compared against the absolute value of the RELO-NCOM vs. data mismatches and displayed in scatter diagrams as those shown in Figure 5 for days Jun 13 and 14, before and after applying the ET. The statistical significance of each of these individual estimates (small blue dots) is negligible, such that they are grouped in equally populated bins with 1000 elements, defined along the ensemble spread axis. These bins displayed inside the scatter diagrams as large red dots will have similar likelihoods and will be statistically relevant. For the ensemble to be accurate, bins should be aligned along the main diagonal, highlighted as a black line on the plots. The green rectangles around the bins show the standard deviations of each bin along each axis (error

and ensemble spread). Other relevant statistic is the mean ratio between measured error vs. ensemble spread, (Err/Std in the figures) that should be close to 1 for the ensemble to be accurate.

[FIGURE 5]

The graphics in Figure 5 left of the black line show the scatter diagrams for days 13 (left upper plot) and day 14 (right upper plot) computed from the cnsemble before post-processing. From the bin distribution we can see the ensemble to have a positive spread-skill relationship, through all ranges of the observed errors, such that estimates of smaller ensemble spread are well correlated with smaller errors and estimates of larger error are well correlated with the larger errors, through all ranges of observed errors. However, we can see the ensemble was grossly under-predicting the magnitudes of the observed errors in roughly one order of magnitude. This is most likely due to the fact the initial fields and other major sources of error besides atmospheric forcing were not being properly perturbed.

The data of June 13 was used as the initial day to start the procedure and adjust the ensemble spread to the observed error. For this purpose, a multiplication factor of 4 was estimated from the data and applied to the temporal standard deviations used to compute the ET throughout the simulation period. This value was estimated iteratively in order to bring the ratio Err/Std from a value of 11 before the transform to 1. As a result, the red bins also became closer to the main diagonal as we can see on the scatter diagrams right of the vertical black line in Figure 5. For the following day represented by the 24-48 hour forecast this ratio increased slightly to 1.5, though the bins remained close to the main diagonal.

Other relevant result from Figure 5 is the spatial distribution of the error estimates. In the lower color maps one can see the ensemble spread at the surface for days 13 and 14. The black crosses

show the points were data was collected during those days respectively. One can see the spatial patterns were not strongly changed by the transform and the areas with larger estimated errors are shaped along the boundaries of the persistent cyclonic eddy in the SW portion of the domain as one could expect. The sampling locations during these two days included several runs across the boundaries of this cyclonic gyre.

Since the ET was using the temporal standard deviation to re-scale the ensemble spread one could argue that the information contained in the ensemble would be erased and time variability would be the dominant error-proxy. In order to evaluate this hypothesis the same scatter diagrams were computed using the temporal standard deviation instead of ensemble spread, as displayed in Figure 6. To keep an equivalent accuracy a multiplication factor of 7.8 was also applied to set the ratio Err/Std to 1 for the day 13 data. From the scatter diagrams one can see this error proxy keeps similar positive spread-skill relations, though the spatial distribution of errors is significantly different from those estimates by the ensemble and not so well correlated with the dominant dynamics.

Using the tuning parameters estimated for day 13, one can estimate the ensemble spread and the time variability error proxy for the following forecast days. Since observations were made until June 25, Figure 7 display the same diagrams for the last two days of June 24 (0/24 hours in the labels) and 25 (24/48 hours in the labels) when model-data comparisons were possible. The four plots panel in the left shows the results using the transformed ensemble and the panel in the right shows the same results using the time variability proxy. One can see the ensemble spread was kept consistent with the dynamics and the performance of both the transformed ensemble and time variability as error proxy seem close in performance. However, looking to the spatial distribution of the predicted surface temperature errors as displayed in the lower color maps for days June 24 and 25 one can see the ensemble responded consistently with the "Sirocco" and

"Libeccio" wind events, spreading the areas of larger uncertainty around the cyclonic eddy, not so well represented by the time variability proxy.

[FIGURE 6]

In order to obtain more objective performance estimates, daily performance statistics were computed as displayed in table 1. These include the ration Err/Std as an estimate of the error estimate accuracy, the bins correlation coefficient (C) as an estimate of the spread-skill and the bin deviation from the main diagonal (Bin Bias - BB) as an estimate of the error estimates bias.

[FIGURE 7]

Overall, during the period June, 13 to 25 the positive spread-skill was kept for all estimates (ensemble with and without transform and time variability), with the ensemble performing slightly better showing a 0.8 correlation coefficient among the bins while the time proxy had a 0.7 coefficient. The ratio Err/Std was also kept consistently through this period such that on average through this period the ensemble value was 13.4, the ET was kept as 1 and the time proxy as 1.1.

The mean differences between bin coordinates (i.e. deviations from the main diagonal) can also be used as an error bias estimate. Through this 12 days period (June 13 to 25) the ensemble estimates after the transform remained unbiased while the original ensemble had a value of 0.4 and the time variability proxy showed also a negligible negative bias of 0.03.

6. Concluding Remarks

The work presented above showed that some level of predictability of stochastic environmental variables through numerical modeling could be achieved using Monte-Carlo methods, producing

ensemble based error estimates along with the predicted state variables, even using a limited number of ensemble runs. However, the system performance will be space and time dependent requiring an accurate metrics system to produce both diagnostics and prognostics of the precision and accuracy of the outputs.

The Ensemble Transform (ET) approach was successfully applied for free-run ocean Mesoscale error prediction calibration, by re-scaling RELO-NCOM ensembles produced through atmospheric perturbations. Independent data was used for this analysis where the model runs were not assimilating any local data. Results show the ensemble spread did not diverge and was consistent with the observed dynamics throughout the simulation period. The ensemble showed a positive spread-skill through all ranges of the observed errors.

Comparisons of ensemble spread of the temperature profiles with local observed errors and time variability (assumed as an error proxy) showed they were consistent through a 12 days analysis period. The ET calibrated ensemble had slightly better performance statistics then the time-variability error proxy, most likely due to the fact the ensemble predicted errors were better correlated with the local observed dynamics.

Results show the ensemble spread did not diverge and was consistent with the observed dynamics throughout the simulation period. Furthermore, comparisons of ensemble spread of the temperature profiles with local observed errors and time variability (assumed as an error proxy) showed they were consistent through the 12 days analysis period, with performances above the non-calibrated ensemble estimates and time-variability used as error proxy. Overall error estimates became unbiased and the system was able to accurately separate large errors from smaller errors with a positive spread-skill relationship, through all ranges of the observed errors.

[TABLE 1]

Acknowledgment

This work was supported by the Office of Naval Research under the grant N00014-08-2-1146. Thc authors thank the MREA07 technical and science teams and the ships crews that carried the in-situ data collection.

References:

Barron, C.N. et al., 2006: Formulation, implementation and examination of vertical coordinate choices in the global Navy Coastal Ocean Model (NCOM). Ocean Modeling, 11, 347-75.

Barron, C.N. and L. F. Smedstad: 2002; Global river inflow within the navy coastal ocean model. Proceeding of MTS/IEEE Oceans 2002 Conference. Biloxi, MS, 29 October 2002, 1472-1479.

Bishop, C. H., and Z. Toth, 1999: Ensemble transformation and adaptive observations. *J. Atmos. Sci.*, 56, 1748–1765

Carriere, O., Hermand, J-P, LeGac, J.C, and Rixen, M. this issue. Full-field tomography and Kalman tracking of the range-dependent sound speed field in a coastal water environmcnt. Journal of Marine Systems, Special issue on Rapid Environmental Assessment.

Coelho, E.F., Rixen, M. and Signell, R., 2005. NATO Tactical Ocean Modeling System: Concept Applicability, NATO Undersea Research Centre Serial Report, SR411.

Coelho , E.F., Peggion G., Rowley C., Bishop C., Xiaodong X., Jacobs G., "Error Modeling And Sampling Guidance Using the Ensemble Transform and Ensemble Transform Kalman Filter During The BP07 Trial" ", in Rapid Environmental Assessment Conference. Coastal Processes: Challenges for monitoring and prediction, NATO Undersea Research Centre,

September, 2007

Coelho, E.F., Rixen, M., 2008 "Maritime Rapid Environmental Assessment. New Trends in Operational Oceanography", Journal of Marine Systems, Vol 69, issues 1-2.

Coelho, E.F., 2008 "Operational oceanography. Zoom-in modeling for local applications", in Proceedings of the International Conference on Mathematics and Continuum Mechanics. ISBN: 978-989-95011-2-6, Centro Internacional de Matematica (CIM), 207-217, Porto-Portugal .

Cummings, J., 2005. Operational multivariate ocean data assimilation. Q. J. R. Meteorol. Soc., 131, pp. 3583–3604

Demirov, E. N. Pinardi, C. Fratianni, M. Tonani, L. Giacomelli, P. De Mey, 2003. Assimilation scheme of the Mediterranean Forecasting System: operational implementation" *Annales Geophysicae,* 21: 189-204.

Doblas-Reyes, F.J, Hagerdorn, R. and Palmer, T.N, "The rationale behind the success of multi-model ensembles in seasonal forecasting – II. Calibration and Combination", Tellus, 57A, 234-252, 2005

Egbert, G.D and S.Y. Erofeeva, 2002: Efficient inverse modeling of barotropic ocean tides. J. Atmosph. and Oceanic Techn., 19, 183-204.

Evensen, G., 2003. The Ensemble Kalman Filter: theoretical formulation and practical implementation. *Ocean Dynamics*, 53: 343–367

Fabre, J.P, C.Rowley, G. Jacobs, E.F. Coelho, C. Bishop, X. Hong and J. Cummings, "Environmental Acoustic Variability Characterization for Adaptive Sampling", in Naval Research Laboratory Reviews, 2008

Gneiting, T., Westveld III, A., Raftery, A. and Goldman, T., 2004. Calibrated Probabilistic

Forecasting Using Ensemble Model Output Statistics and Minimum CRPS Estimation. Technical Report no. 449, Department of Statistics, University of Washington-USA

Hamill, T.M and Whitaker, J., "Ensemble Calibration of 500-hPa Geopotential Height and 850-hPa and 2-m Temperatures Using Reforecasts", Monthly Weather Review, vol 135, 2007

Haven, K., Majda, A., Abramov, R., 2005. Quantifying predictability through information theory: small sample estimation in a non-Gaussian framework. *Journal of Computational Physics* 206 (2005) 334–362

Hodges, B., Laval, B., Wadzuk, B., 2006. Numerical error assessment and a temporal horizon for internal waves in a hydrostatic model. *Ocean Modelling* 13 (2006) 44–64

Hoffman, R. N., Z. Liu, J.-F. Louis, and C. Grassotti, 1995: Distortion representation of forecast errors. *Mon. Wea. Rev.*, 123, 2758-2770

Hodur, R.M., 1997: The Naval research laboratory's Coupled Ocean/Atmosphere Mesoscale prediction System (COAMPS). Mon. Wea. Rev., 135, 1414-30.

Judd, K., Smith, L.A. and Weisheimer, A., 2007: How good is an ensemble at capturing truth? Using bounding boxes for forecast evaluation. *Quarterly Journal of the Royal Meteorological Society,* 133, 1309–1325

LeGac, J.C, and Hermand, J.P., 2007: MREA/BP07 cruise report. Tech.Rep. Technical Document. NURC-CR-2007-04-1D1.NATO Undersea Research Centre, La Spezia, Italy.

Lermusiaux , P., Chiu, C-S., Gawarkiewicz, G., Abbot, P., Robinson, A.R., Miller, R., Haley, P., Leslie, W., Majumdar, S., Pang, A., a n d Lekien, F., 2006: Quantifying Uncertainties in Ocean Predictions. *Oceanography* Vol. 19, No. 1, Mar. 80-93

Martin P.J., 2000: Description of the Navy Coastal Ocean Model Version 1.0, NRL/FR/7322-00-9962. Naval Research Laboratory. 42 pp.

Ngodock, H, Smith, S., and Jacobs, G., "Cycling the representer algorithm for variational data assimilation with a nonlinear reduced gravity ocean model", Ocean Modelling, Volume 19, Issues 3-4, 2007

Rixen, M, Coelho, E., Signell, R., 2007. Surface drift prediction in the Adriatic Sea using hyper-ensemble statistics on atmospheric, ocean and wave models: uncertainties and probability distribution areas. Journal of Marine Systems, doi:10.1016/j.jmarsys.2007.02.015

Rixen, M. and Coelho, E.F., 2006(2). Operational prediction of acoustic properties in the ocean using multi-model statistics. Ocean Modelling 11 (2006) 428-440

Rosmond, T.E, Teixeira, J., Peng, M., Hogan, T.F, and R. Pauley; 2002: Navy Operational Global Atmospheric Prediction System (NOGAPS): Forcing for ocean models. Oceanography, 15, 99-108.

Rowley C.; 2007: Relo_Ncom Validation Test Report. NRL document in preparation

Xiandong, H. and Bishop, C, 2007: Ensemble and Probabilistic Forecasting. *IUGG XXIV General Assembly 2007*, Perugia, Italy, 2-13 July.

Table 1 – This table shows the daily mean values of the ration between individual observed error magnitudes vs the correspondent ensemble standard deviation(Err/Std), the correlation coefficient or linear regression slope of the 1000 point bin averages (Corr.Coef) and the difference between the bins ensemble standard deviation and bin errors in degrees C (Bin Bias BB). Each one of these estimates was computed for the ensemble withouth post-processing (Ens), with the ET post-processing (ET) and for the post-processed time variability used as an error proxy (Time). The raw at the bottom shows the overall averages during the experiment.

Day	Err/Std			Corr.Coef.			Bin BIAS (BB)		
	Ens	ET	Time	Ens	ET	Time	Ens	ET	Time
06/13	11.0	1.0	1.0	0.84	0.84	0.75	0.3	0.0	0.0
06/14	16.3	1.5	1.5	0.74	0.73	0.67	0.4	0.1	0.1
06/17	20.3	1.6	1.8	0.79	0.80	0.55	0.3	0.1	0.2
06/18	10.0	0.8	1.0	0.67	0.67	0.89	0.5	-0.2	0.0
06/20	17.4	1.4	1.8	0.48	0.53	0.38	0.4	0.1	0.2
06/21	12.1	0.9	1.0	0.89	0.90	0.85	0.3	0.0	0.0
06/22	10.3	0.8	0.9	0.85	0.86	0.76	0.3	-0.1	-0.1
06/23	13.0	1.0	0.9	0.90	0.91	0.90	0.3	0.0	0.0
06/24	11.9	0.8	0.6	0.85	0.85	0.94	0.2	-0.1	-0.2
06/25	11.9	0.8	0.7	0.70	0.69	0.46	1.3	-0.3	-0.5
MEAN	13.4	1.0	1.1	0.8	0.8	0.7	0.43	0.00	-0.03

Fig.1. The triple nest configuration for MREA_07.

Fig. 2 – RELO-NCOM upper layer temperature snapshots for the days 06/19 (left panel) and 06/23 (right panel). The shapshots hours, displayed in the images, correspond to the wind maximum stress for each day. During the 19th winds were predominantly south-easterly ("Sirocco") and during the 23rd they were predominantly south-westerly ("Libeccio"). Both panels display how flow patterns changes around the persistent gyre in the South-West corner, with warmer waters intruding northward during the "Libeccio" event.

Fig. 3 – NOAA AVHRR Sea Surface Temperature estimates for 06/19 (left panel) and 06/23 (right panel). During the 19th winds were predominantly from the south-east ("Sirocco") and during the 23rd from the south-west ("Libeccio"). Images were produced by automatic processing using NURC TERASCAN software.

Fig. 4 – RELO-NCOM water temperature bias and RMS error estimates. The four panels in the left show the RMS errors along each simulation day (24 hours period), using different model estimates compared with the observations. The color plot named "A04" in the upper left uses hindcast atmospheric forcing fields, the plot named "Pers" uses model persistency (hour 0 snapshot) and the plots below named "F24" and "F48" use 24 and 48 hours lead forecasts respectively. The four panels in the right show the error bias (24 hours mean errors) using the same model estimates.

Fig. 5 – Error scatter plots computed using the run of June 13. The upper scatter diagrams show the ensemble spread vs. observed forecast error before re-scaling (Figure 5-a) and after re-scaling

(Figure 5-b). The forecast errors were computed using the 0-24 hour forecasts (panels in the left) and using the 24-48 hour model forecasts (panels in the right). The color plot below each scatter diagrams show the surface temperature error estimate (ensemble standard deviation) at hour 00:00 (left) and 24:00 (right) relative to the simulation day and the white crosses depicts the locations used for model-data comparison.

Fig. 6 – Same as Figures 5-b, but using the time variability as an error proxy instead of the ensemble spread as an error estimate

Fig. 7 – Same results as described for Figure 5-b (on the left) and Figure 6 (on the right) but for the model run of June 24. The panels left of the vertical line show the results using the calibrated ensemble. Panels in the right show the same results but using the time variability as an error proxy.

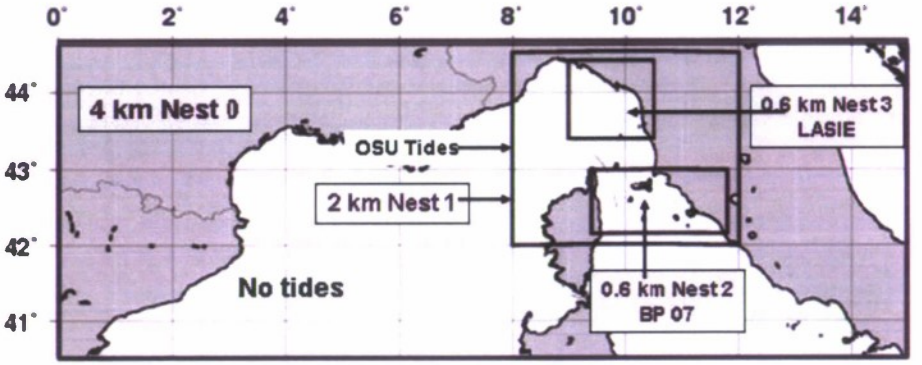
0°
2°
4°
6°
8°
10°
12°
14°
44°
43°
42°
41°
4 km Nest 0
OSU Tides
2 km Nest 1
No tides
0.6 km Nest 3
LASIE
0.6 km Nest 2
BP 07

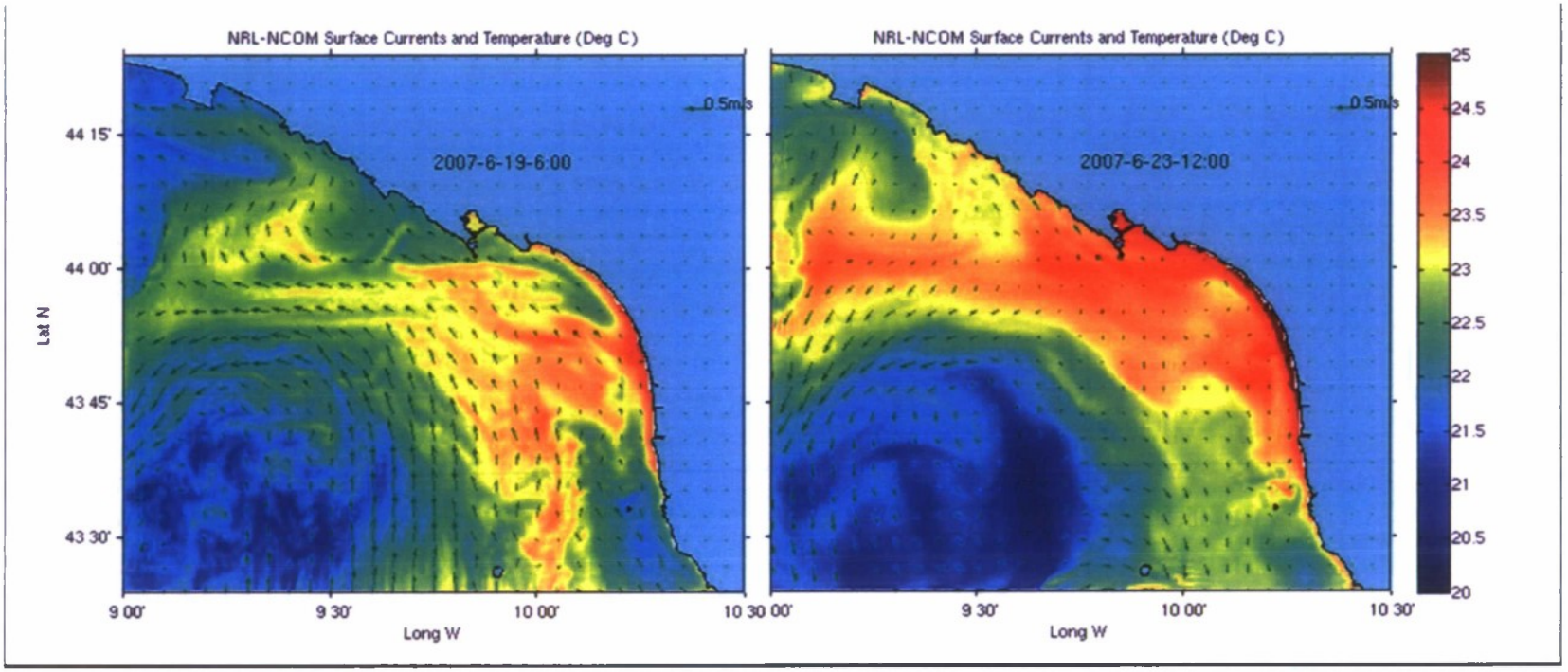
NRL-NCOM Surface Currents and Temperature (Deg C)
0.5m/s
2007-6-19-6:00
44 15'
44 00'
43 45'
43 30'
Lat N
9 00'
9 30'
10 00'
10 30'
Long W
NRL-NCOM Surface Currents and Temperature (Deg C)
0.5m/s
2007-6-23-12:00
9 30'
10 00'
10 30'
Long W
25
24.5
24
23.5
23
22.5
22
21.5
21
20.5
20

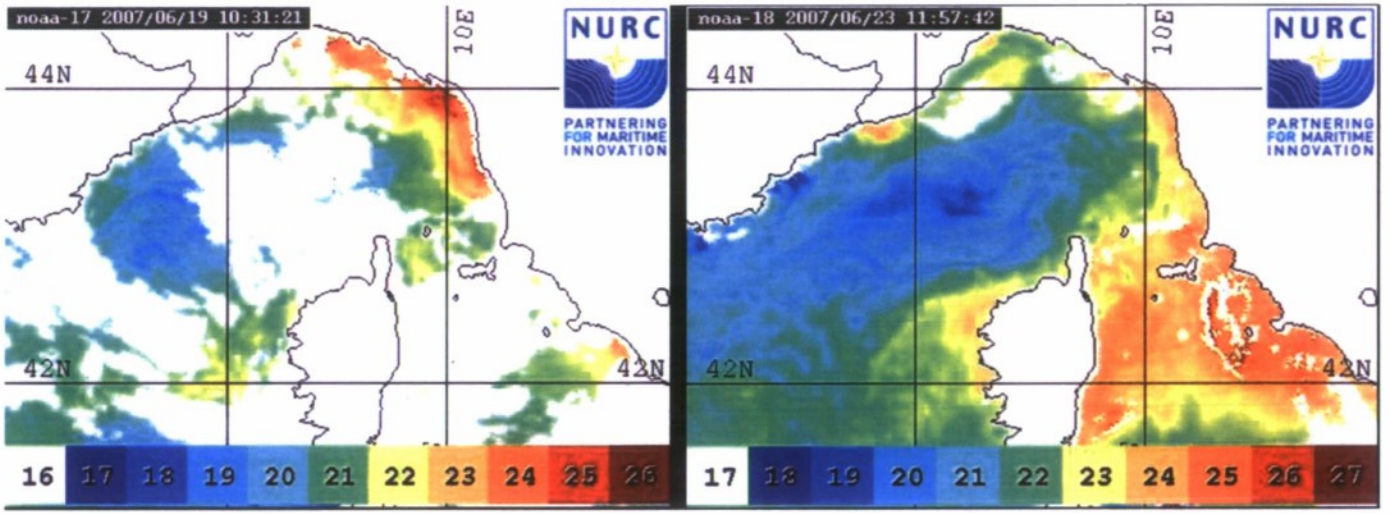
noaa-17 2007/06/19 10:31:21
NURC
PARTNERING FOR MARITIME INNOVATION
44N
42N
10E
16 17 18 19 20 21 22 23 24 25 26
noaa-18 2007/06/23 11:57:42
NURC
PARTNERING FOR MARITIME INNOVATION
44N
42N
10E
17 18 19 20 21 22 23 24 25 26 27

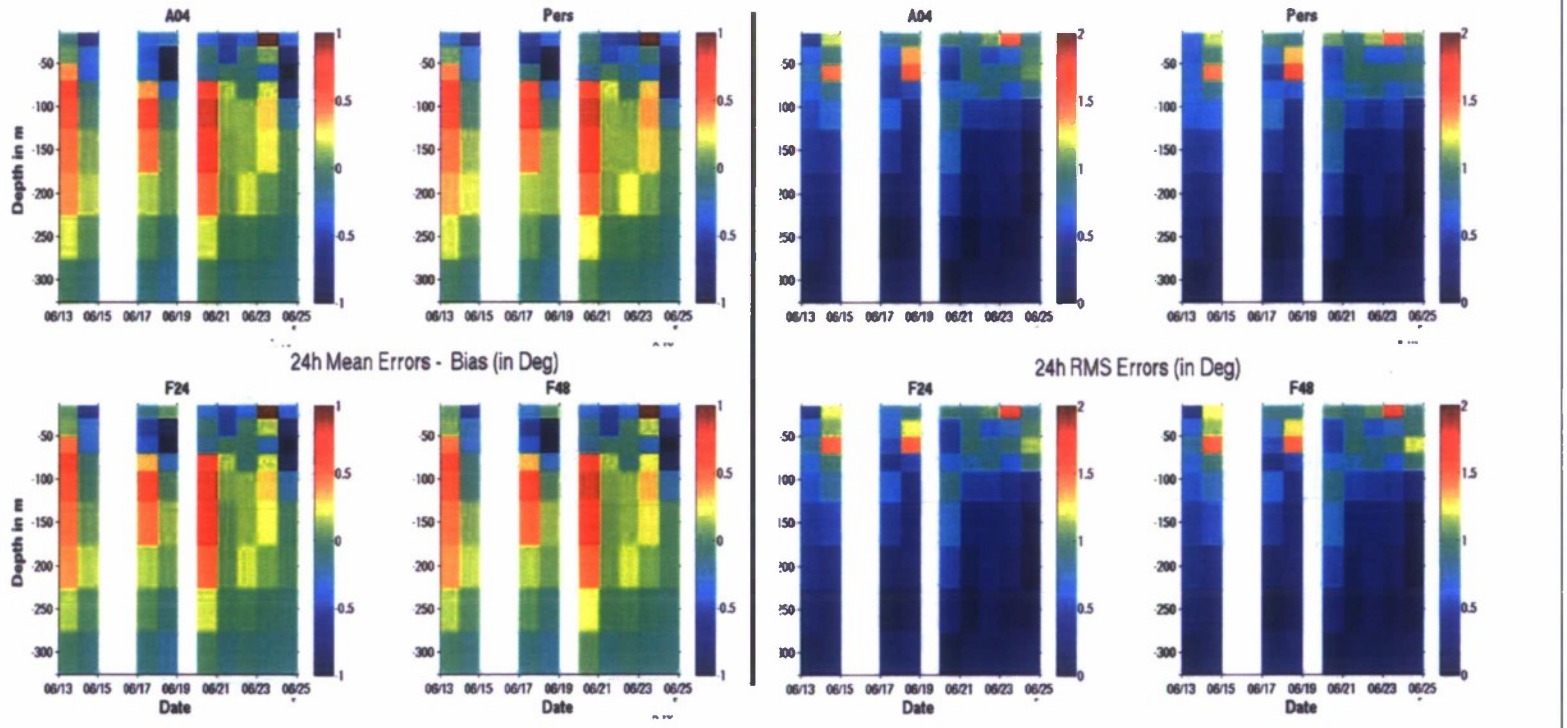
A04
Pers
A04
Pers
Depth in m
24h Mean Errors - Bias (in Deg)
24h RMS Errors (in Deg)
F24
F48
F24
F48
Depth in m
Date
Date
Date
Date

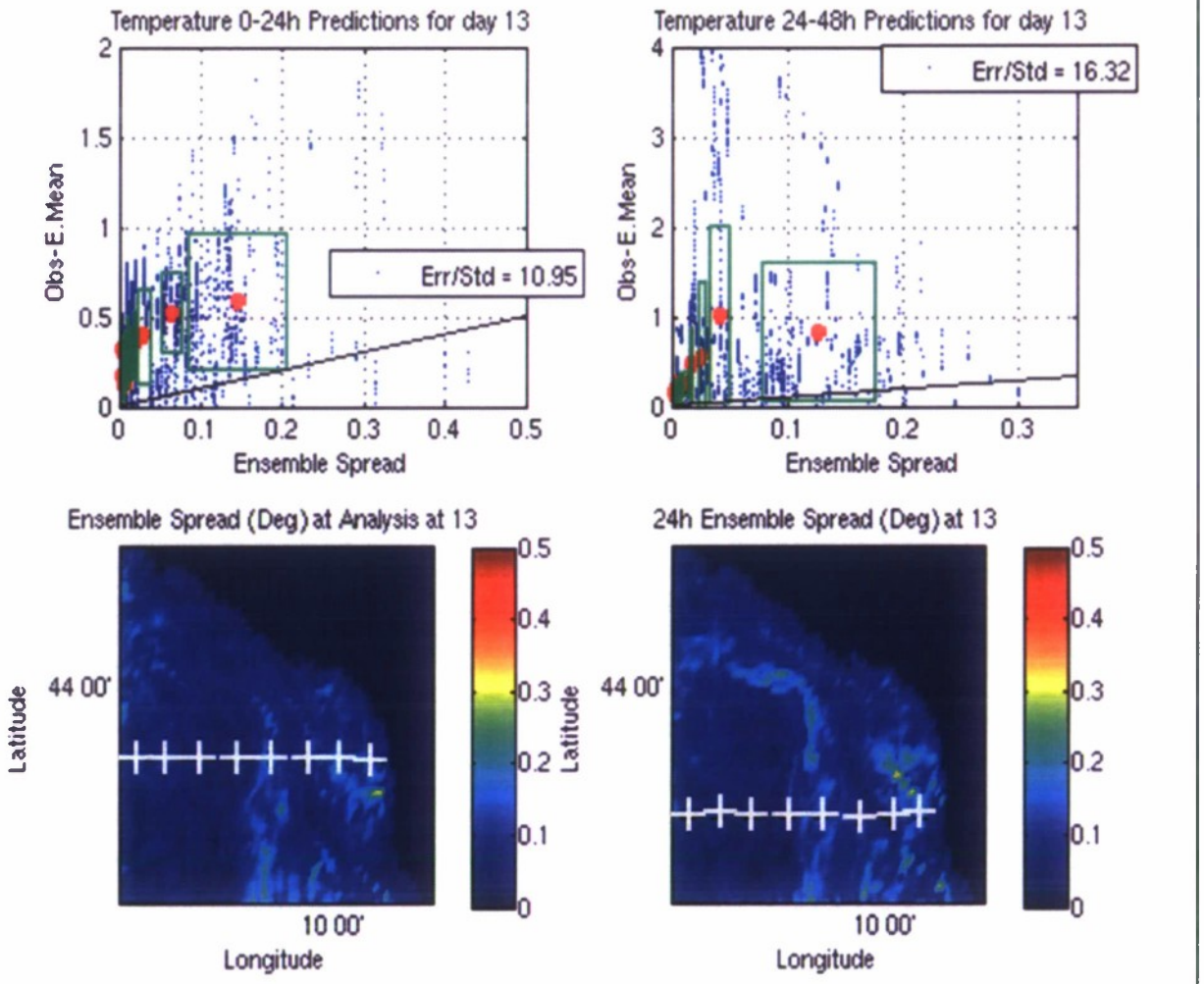
Temperature 0-24h Predictions for day 13
Obs-E.Mean
Ensemble Spread
Err/Std = 10.95
Temperature 24-48h Predictions for day 13
Obs-E.Mean
Ensemble Spread
Err/Std = 16.32
Ensemble Spread (Deg) at Analysis at 13
Latitude
44 00'
10 00'
Longitude
24h Ensemble Spread (Deg) at 13
Latitude
44 00'
10 00'
Longitude

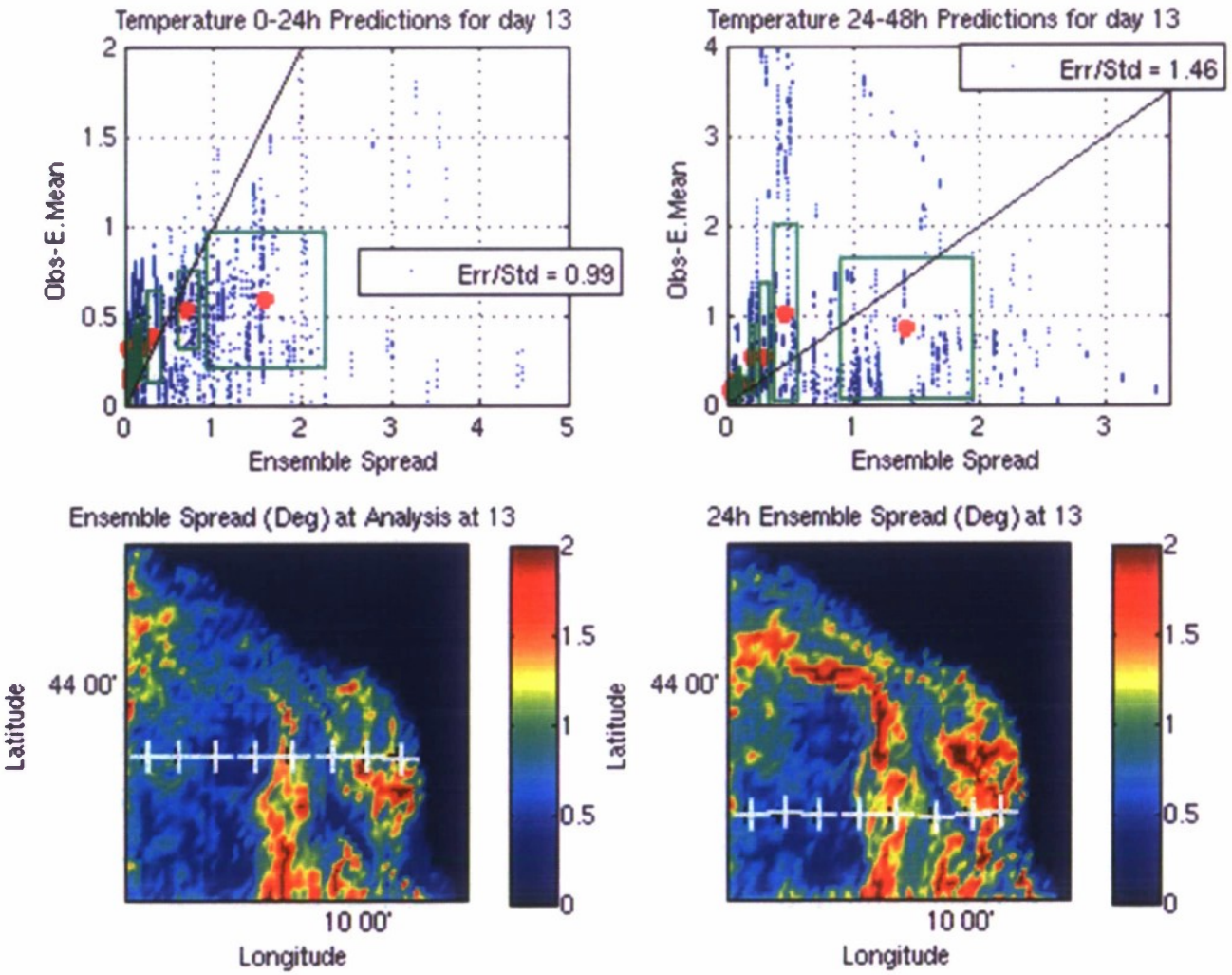
Temperature 0-24h Predictions for day 13
Obs-E.Mean
Ensemble Spread
Err/Std = 0.99
Temperature 24-48h Predictions for day 13
Obs-E.Mean
Ensemble Spread
Err/Std = 1.46
Ensemble Spread (Deg) at Analysis at 13
Latitude
44 00'
10 00'
Longitude
24h Ensemble Spread (Deg) at 13
Latitude
44 00'
10 00'
Longitude

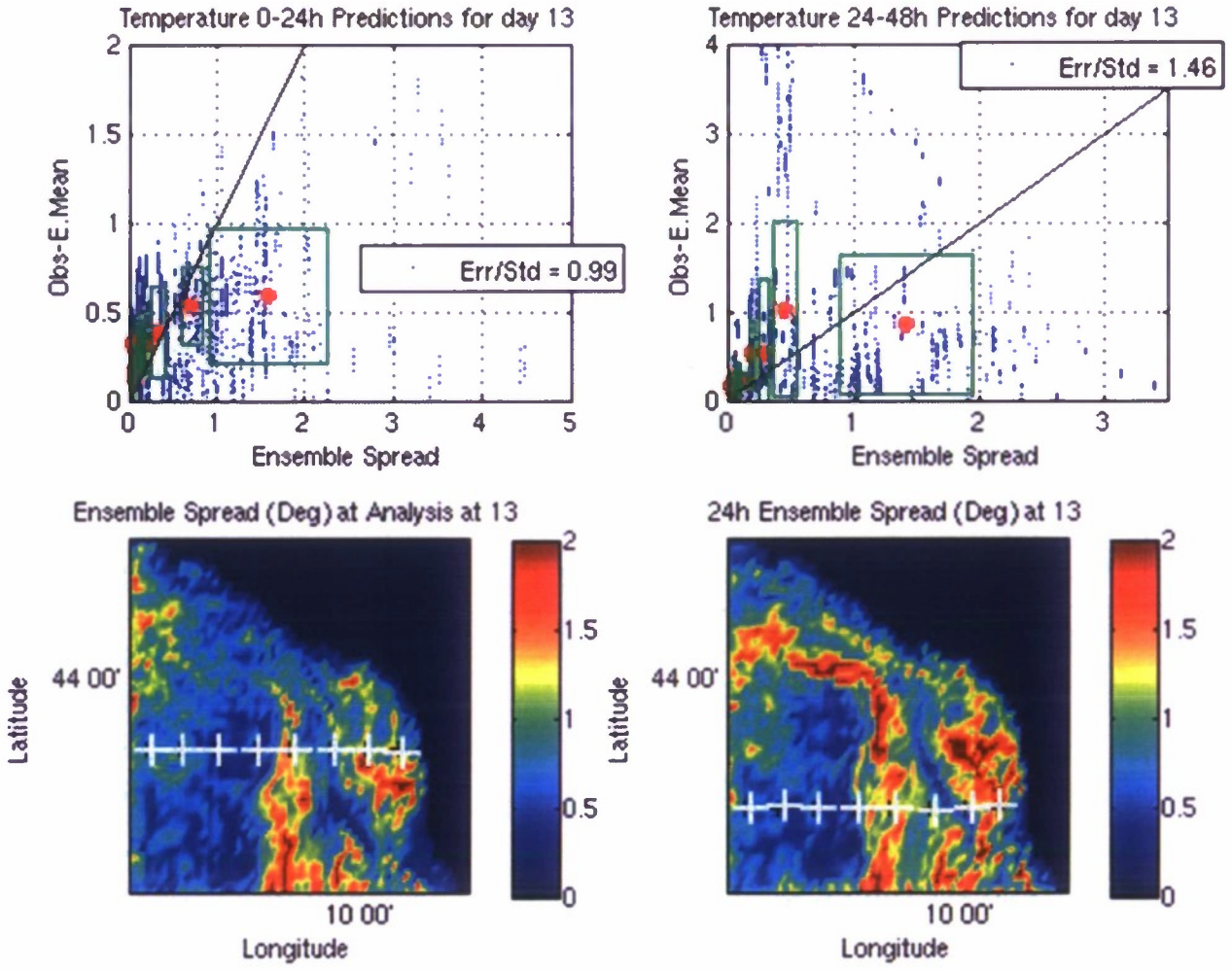
Temperature 0-24h Predictions for day 13
Obs-E.Mean
Ensemble Spread
Err/Std = 0.99
Temperature 24-48h Predictions for day 13
Obs-E.Mean
Ensemble Spread
Err/Std = 1.46
Ensemble Spread (Deg) at Analysis at 13
24h Ensemble Spread (Deg) at 13
Latitude
44 00'
10 00'
Longitude

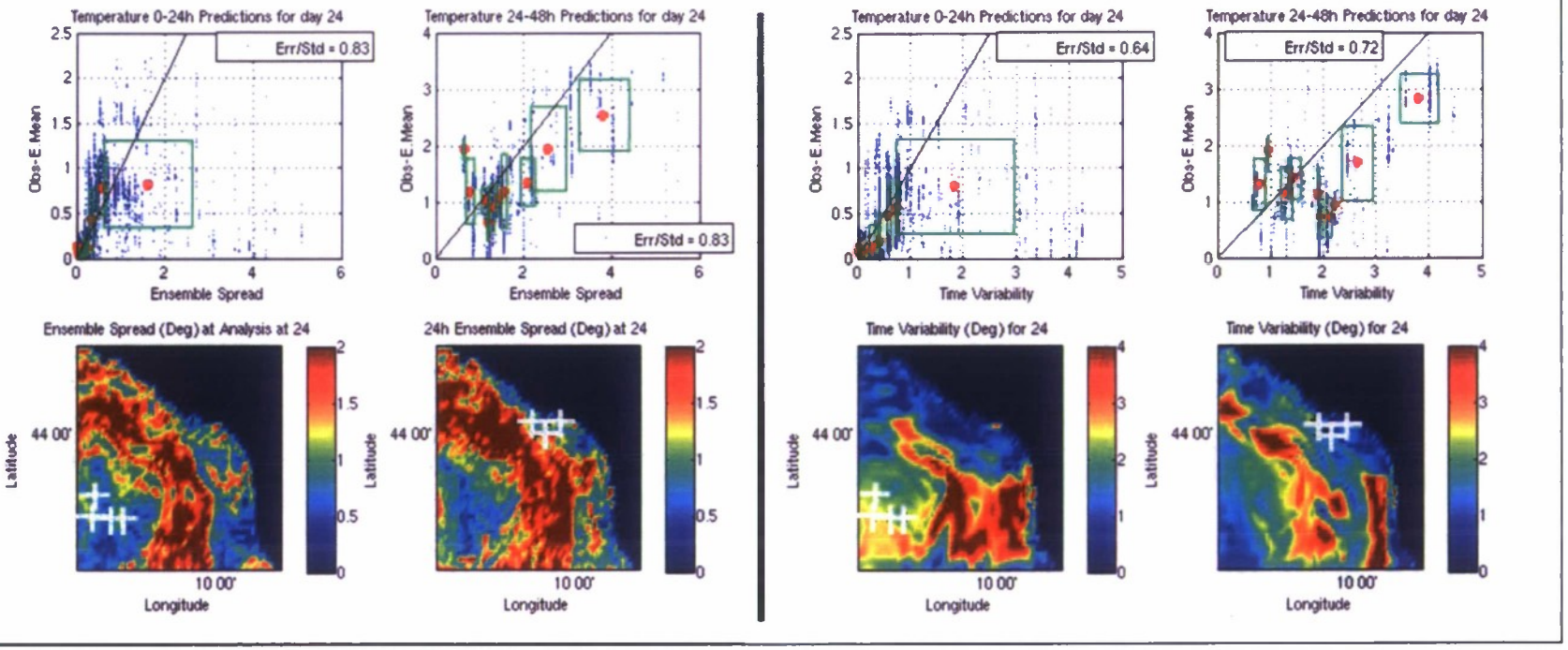
Temperature 0-24h Predictions for day 24
Err/Std = 0.83
Obs-E Mean
Ensemble Spread
Temperature 24-48h Predictions for day 24
Err/Std = 0.83
Obs-E Mean
Ensemble Spread
Temperature 0-24h Predictions for day 24
Err/Std = 0.64
Obs-E Mean
Time Variability
Temperature 24-48h Predictions for day 24
Err/Std = 0.72
Obs-E Mean
Time Variability
Ensemble Spread (Deg) at Analysis at 24
24h Ensemble Spread (Deg) at 24
Time Variability (Deg) for 24
Time Variability (Deg) for 24
Latitude
Longitude
44 00'
10 00'

Super-ensemble forecasts and resulting acoustic sensitivities in shallow waters

Michel Rixen, Jean-Claude Le Gac, Jean-Pierre Hermand, Germana Peggion, Emanuel Ferreira-Coelho

PII: S0924-7963(09)00157-2
DOI: doi: 10.1016/j.jmarsys.2009.01.013
Reference: MARSYS 1827

To appear in: *Journal of Marine Systems*

Received date: 18 August 2008
Revised date: 22 September 2008
Accepted date: 22 January 2009

Please cite this article as: Rixen, Michel, Le Gac, Jean-Claude, Hermand, Jean-Pierre, Peggion, Germana, Ferreira-Coelho, Emanuel, Super-ensemble forecasts and resulting acoustic sensitivities in shallow waters, *Journal of Marine Systems* (2009), doi: 10.1016/j.jmarsys.2009.01.013

Super-ensemble forecasts and resulting acoustic sensitivities in shallow waters

Michel Rixen[1], Jean-Claude Le Gac[1], Jean-Pierre Hermand[2], Germana Peggion[3*], Emanuel Ferreira-Coelho[4*]

[1]NATO Undersea Research Center (NURC), La Spezia, Italy

[2]University of Brussels (ULB), Belgium, and Royal Netherlands Naval College

[3]University of New Orleans, USA

[4]University of Southern Mississippi, USA

Abstract

Multi-model Super-Ensembles (SE) which optimally combine different models, have been shown to significantly improve atmospheric weather and climate predictions. In the highly dynamic coastal ocean, the presence of small-scales processes, the lack of real-time data, and the limited skill of operational models at the meso-scale have so far limited the application of SE methods for acoustic Rapid Environmental Assessment purposes. In the framework of the BP07 experiment conducted South East of Elba, sound speed prediction skills of various SE techniques combining operational model outputs and in-situ measurements are assessed. Results suggest that SE-based predictions provide more robust 24hr forecasts. A detailed acoustic propagation sensitivity study at different frequencies and ranges also reviews the potential of these predictions for acoustic inversion and tomography efforts.

Keywords: Ocean-acoustic predictions, multi-model super-ensemble, sound speed, Kalman filter, data assimilation, tomography

1. Introduction

An increasing number of models are routinely providing operational (atmospheric) weather forecasts and climate predictions (Palmer, 2004) but prediction skill is inherently limited for a number of reasons, including simplifications in physical processes, errors in initial conditions and boundary conditions, numerical schemes, *etc.* The use of data assimilation techniques (*e.g.* Bennett, 1992; Wunsch, 1996; Robinson et al, 2004; Bennett, 2002; Evensen, 2006) to regularly correct for model drifts may compensate to some extent for loss of predictability with time (Lorenz, 1963). Model ensembles have become an important means of investigating dispersion problems (Galmarini et al 2001, 2004), tracking individual model errors, increasing forecast skill, and reducing uncertainties (Lermusiaux et al, 2006) in highly dynamic and complex environments where predictability is limited. The multi-model Super-Ensemble (SE) technique

---

[*] Naval Research Laboratory visiting scientist

(Krishnamurti et al 1999, 2000a, 2000b), which uses an optimized combination of an ensemble of models has previously been demonstrated to improve weather, seasonal and interannual forecast skill in atmospheric (Kumar et al 2003; Shin and Krishnamurti 2003a; Yun et al 2005; Mutemi et al 2007) and ocean (Logutov and Robinson 2005; Rixen and Ferreira-Coelho 2005, 2007; Rixen et al, 2007, 2008) models over simple-ensemble and bias-removed ensemble means. SE methods (Williford et al 2003) have been further improved by the use of dynamic (Shin and Krishnamurti 2003b, Rixen et al 2008), regularization (Yun et al 2003), non-linear (Rixen and Ferreira-Coelho 2007) and probabilistic (Rajagopalan et al 2002) techniques. These methods all aim at finding a combination of models that optimally agrees with reference data over a training period (the hindcast, regression or fit); this combination is subsequently used to produce a SE forecast obtained by weighting individual model forecasts. A critical aspect for all super-ensemble methods is therefore whether the regression solution is capable of extrapolation in time and is applicable to future events. In other words, is the learning adequate to provide generalization skills?

Operational implementation of SE methods in Numerical Weather Prediction (NWP) centers is quite straightforward due to the reliability of observational data streams and the robustness of the models. On the other hand, in the ocean, the lack of long real-time data time series – especially in shallow waters – and a limited suite of operational models have so far limited the application of such promising techniques in an operational framework. The limitations for in-situ observations in the coastal and shallow water environment are mostly due to heavy maritime traffic, intense fishing activity and mechanical and biological stress on sensors and platforms.

A pioneering study was conducted during the MREA04 (Maritime Rapid Environmental Assessment) field experiment along the Portuguese coasts to investigate the potential benefit of SE techniques for acoustic purposes and concluded that simple linear-regression based multi-model prediction were able to improve significantly sound speed prediction skills at 24hr lead time (Rixen and Ferreira-Coelho, 2004).

Real-time ocean-acoustic predictions and data assimilation can be very useful but require a precise understanding of the full transfer of uncertainties from the ocean to the acoustic, e.g. using ensemble schemes (Lermusiaux et al 2002; Lermusiaux and Chiu, 2002; Robinson and Lermusiaux, 2004; Lermusiaux et al, 2006. Adaptive sampling schemes and their impact on acoustic propagation may help reducing uncertainties in specific regions of interest (e.g. Heaney et al, 2007; Wang et al, 2008 this issue; Yilmaz et al, 2008).

In the framework of the BP07 field experiment conducted South-East of Elba in Spring 2007 (Le Gac and Hermand, 2007), we investigated the use of *dynamic* SE techniques based on the Kalman filter (Kalman, 1960) to allow for a temporal evolution of model combinations, which form the basis of the present work, described in section 2. A thorough acoustic propagation sensitivity study is carried out in section 3 to assess the potential of SE predictions for acoustic inversion and tomography purposes. Specifically, multi-frequency correlations and uncertainties are investigated in detail. In a companion

paper (Carrière et al, 2007, this issue), full-field tomography and Kalman tracking of the range-dependent sound speed is investigated for the same field experiment.

2. The BP07 experiment: ocean observations and predictions

An intense joint ocean-acoustic observational program and prediction effort took place during the BP07 experiment and is described in details in the field trial report (LeGac and Hermand, 2007) and in a number of companion publications (Carrière et al, Meyer et al, Lam et al, Coelho et al, this issue).

The main focus of the experiment was on a small area Southeast of Elba Island, Italy and in particular on a section in the middle of area 'REA I' (AB transect in Fig. 1) for which a detailed geoacoustic characterization of the seafloor and subseafloor is available following the Yellow Shark 94 inversion results (Hermand and Gerstoft 1996, Hermand 1999). However the ocean monitoring effort was not entirely focused on the A-B transect but also covered the wider BP3 area in general.

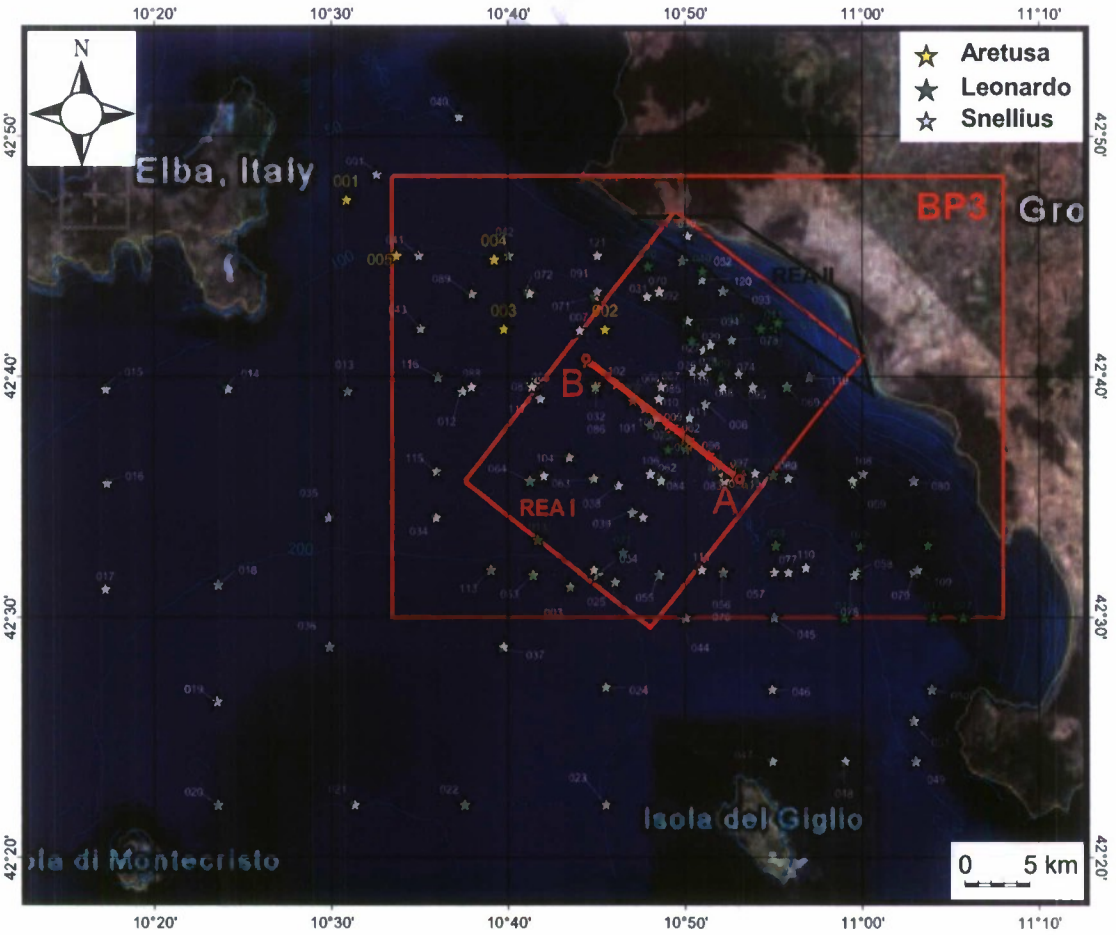

Fig. 1. MREA/BP07 test areas. The boxes for ocean monitoring and prediction (BP3) and for acoustic characterization (REA1) are shown. Stars in yellow, green and gray show CTD casts collected by R/V Aretusa (Italian Navy), R/V Leonardo

(NURC) and R/V Snellius (Royal Netherlands Navy), respectively, during the BP07 time frame, April 16 – May 4, 2007. Section AB has been one of the focuses of the ocean-acoustic experiments.

Regular CTD were collected by three vessels and provided a reasonable spatio-temporal coverage. In addition, two thermistor strings 15km apart and equipped with 11 sensors, were deployed by NRV *Leonardo* at position A and B from 19 April to 1 May. They covered water depths respectively from 13.3m to 63.5m and from 13.5m to 53.5m with spacing of 5m. Sampling rate was set to 2 minutes. Sensors 7 and 11 at mooring A failed and were withdrawn. Note (Fig. 2) the high temporal variability (some patterns have cycles shorter than an hour) and the strong differences between the two moorings. Surface heating is obvious at station B, whilst station B shows the presence of a more complex mixed layer on two occasions and a more cyclic pattern in temperature evolution.

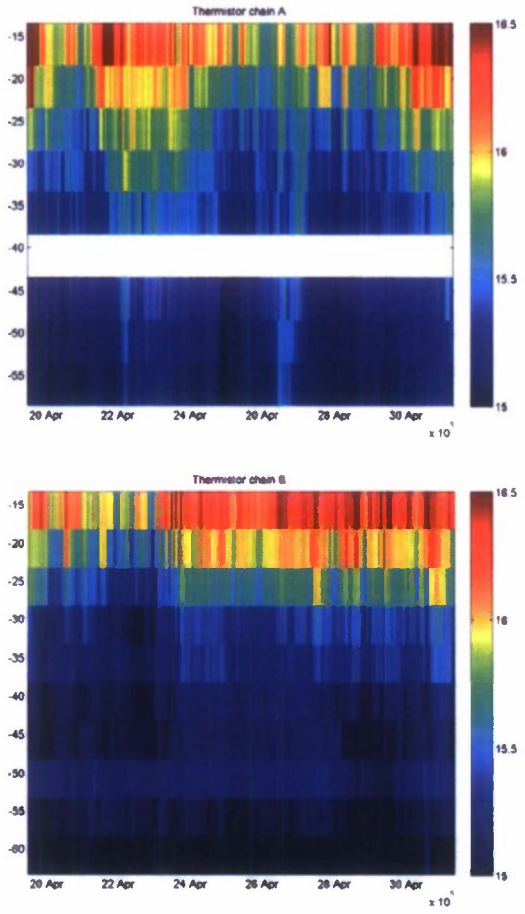

Fig. 2 Raw temperature thermistor string data time series over depth (m) collected respectively at the A and B endpoints of the transect.

These measurements were complemented by selected MVP surveys (see Lam *et al*, this issue), oceanographic data from acoustic drifting buoys and profiles collected from R/V *Snellius* launch or rubber boat (not shown here).

All data collected in the vicinity of the AB transect represent a pool of 18866 temperature data and 6882 salinity data, which were objectively analyzed and gridded using an Optimal Interpolation (OI) technique (*e.g.* Bretherton *et al*, 1976; Rixen *et al*, 2001) with an horizontal grid resolution of 715m, a vertical resolution of 1m and a temporal resolution of 3hrs. The 3D box over section AB for period 16 April-3 May 2007 was spanning 15km, 110m and 13 days. To compensate for sensor noise and sensor inter-calibration issues, the noise-to-signal ratio was set to 1 after cross-validation of this parameter. Because of the amount of data, intractable for direct optimal interpolation techniques, the domain of analysis was split into sub-domains larger than typical correlation lengths to overcome the computational burden, a technique known as sub-optimal interpolation. The spatial correlation lengths were set to 4m on the vertical and 2km on the horizontal. The temporal correlation length was set to 1 day. Lower values were creating unphysical results because of the non-uniform distribution of observations in space and time. A background field was obtained by spatio-temporal linear regression over the whole experimental period (also known as First Guess At Appropriate Time - FGAT) and the OI analysis was computed on resulting anomalies. Multivariate analysis techniques were not explored here. Sound speed fields were derived from the T/S analyses (Fofonoff and Millard, 1983).

The sound-speed field over section AB exhibits both spatial and temporal variability as illustrated in Fig 3 and 4. Strong heating can be observed on the upper 10m at the surface over the period resulted in a strong pycnocline and high sound-speed vertical gradients at around 15m depth.. The area was subject to strong mesoscale activity as well (see also Carrière *et al*, this issue), as illustrated in the two high sound speed surface cells (Fig. 4). The diurnal cycle has been smoothed out by the analysis which was not able to preserve all the spectral information because of the limited amount of data.

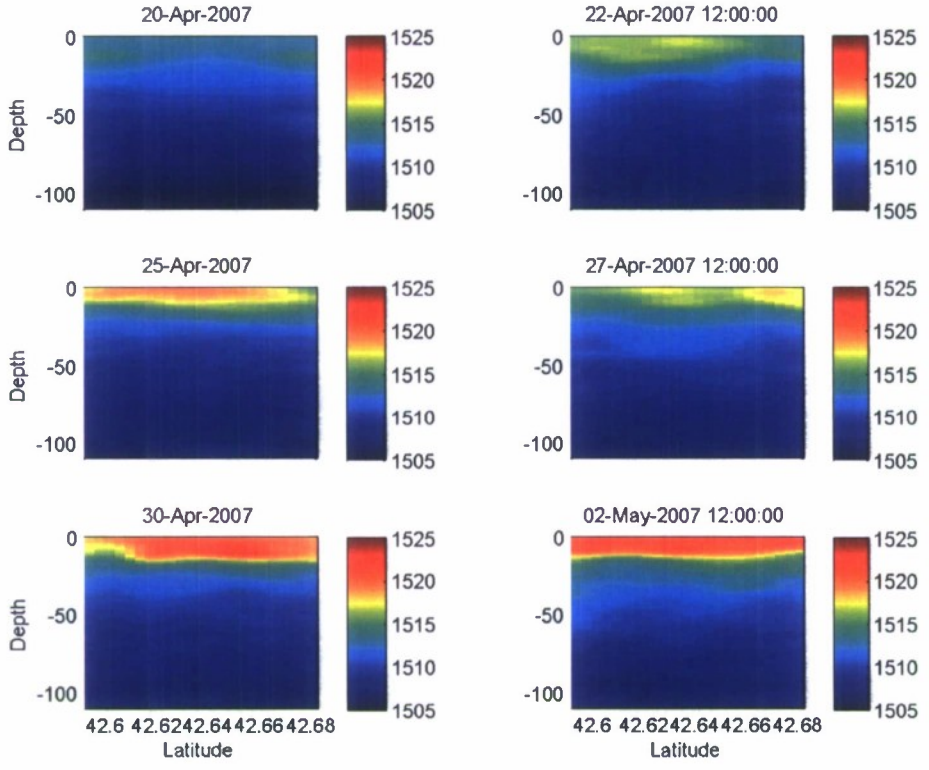

Fig 3. Sound speed (m/s) on section AB versus depth for the start (top left) to the end (bottom right) of the experiment.

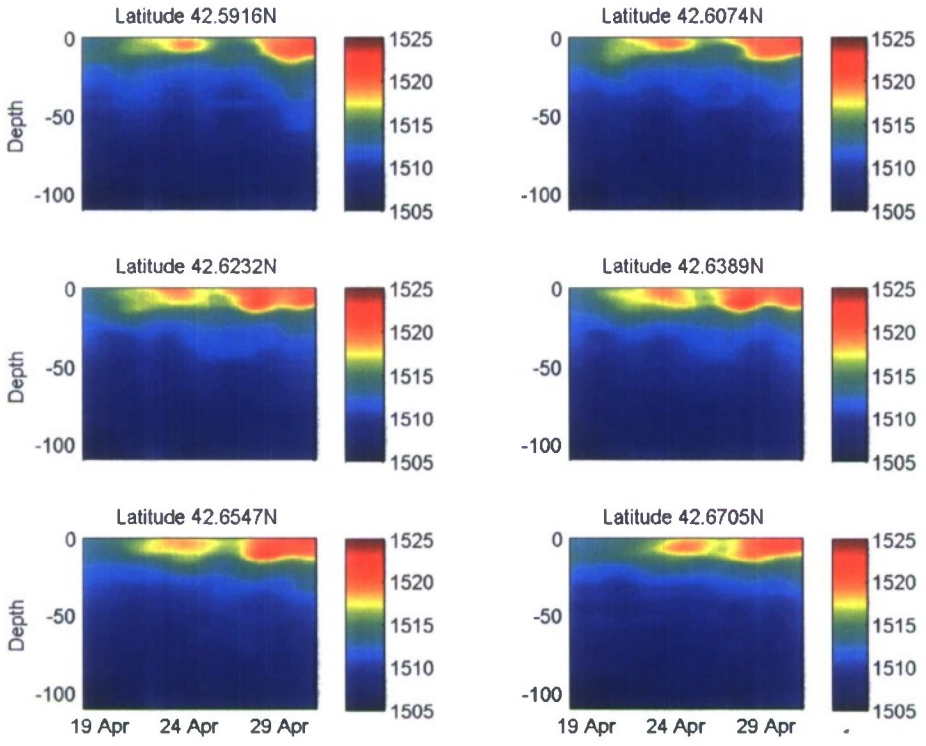

Fig 4. Sound speed (m/s) temporal evolution over depth at different latitudes from location A (top left) to B (bottom right).

2.2 Models and adaptive sampling

A specific prediction system was set up at NRLSSC for the MREA/BP07 sea trial. As described in details in Coelho *et al* (this issue), it was built around the NCOM model. Starting from the global NCOM model at 4-km resolution, two nested models were set up in order to cover the full MREA07 area respectively with a 2-km coarse resolution (NCOM_COARSE) and a 0.6 km fine resolution (NCOM_FINE). SST data and MODAS synthetics were indirectly assimilated in the models through the Global-NCOM models, while the nested ones directly assimilated COAMPS-Europe 2 wind forcing and NOGAPS heat fluxes. 48-h forecasts were made available on a daily basis.

NCOM ensemble runs were used to minimize forecast error covariance by exploring various observational patterns (see Coelho *et al*, this issue). Error covariance analyses were transmitted by NRLSSC to NURC and two CTD surveys were specifically designed for this purpose and used in a parallel for the MSEAS-HOPS ocean modeling effort with a sensitivity study of acoustic propagation and probability of detection at low frequencies (see Lam *et al for details*, this issue). The proposed CTD sampling strategy was then adapted according to real-time on-site constraints (ship time available in between acoustic and geoacoustic runs, weather and sea-state, *etc*).

2.3 Super-ensemble predictions

The analysis field and NCOM model outputs were used to explore various ensemble predietion teehniques.

The simple ensemble mean (hereafter ENSMEAN) does not use observations over the training period and thus, eannot really be eonsidered as a SE teehnique. However it is also a used method, sinee it is usually expeeted to provide better foreeasts than individual models (Kalnay and Ham, 1989).

The unbiased ensemble mean (hereafter UNBIASED_ENSMEAN) eorreets for biases on eaeh individual model, based on observations during a training period. These unbiased models are then averaged.

The linear regression SE teehnique (LINREG) eonsists in finding a linear combination of the models, minimizing (in the least mean squares sense) its departure from observations during a training period. The resulting weights are then used to eombine numerical foreeasts. This method ean be improved by normalizing models and adding a eonstant model (*i.e.* bias or independent term), hereafter appended with suffix NORM). Collinearities between the models ean also be removed by retaining only a eertain pereentage of variability of the models by applying an Empirieal Orthogonal Funetion (EOF) (also known as Prineipal Component Analysis - PCA) on the models - in the present study 95% of the varianee, with suffix EOF - whieh results in fewer models and improves the generalization eapabilities of the SE. This method is hereafter referred to as LINREG_NORMEOF.

These teehniques are well known and have been tested in various oeeanographie eontexts (Rixen and Ferreira-Coelho 2005, 2007, Rixen *et al* 2007, 2008; Lenartz *et al*, this issue; Vandenbuleke *et al*, submitted). Training period is chosen *a priori* and all observations are equally important. Naturally however, more reeent data should be more relevant and weights should be adapted aeeording to reeent model skills.

Sequential data assimilation teehniques ean eontinuously adapt the weights during a training period when observations are available up to the present time when weights are frozen and used to eombine available foreeasts for the future. The reeursive Kalman filter (Kalman, 1960) solution is well suited for this purpose and is briefly described in the eontext of SE. It eonsists of two eonseeutive steps.

1) predietion step:

$$x^f(t_i) = M_{t_i} x^a(t_{i-1}) \quad (1)$$

$$P^f(t_i) = M_{t_i} P^a(t_{i-1}) M_{t_i}^T + Q \quad (2)$$

2) eorreetion step:

$$K = P^f(t_i)H^T[R + HP^f(t_i)H^T]^{-1} \quad (3)$$

$$x^a(t_i) = x^f(t_i) + K[y^0 - Hx^f(t_i)] \quad (4)$$

$$P^a(t_i) = P^f(t_i) - KHP^f(t_i) \quad (5)$$

The state vector x with covariance P, contains the weights on the models in the SE combination. Superscript f denotes forecast state after prediction steps; and superscript a stands for analyzed state after the correction steps using observations. The state vector x is initialized with a best guess obtained from the LINREG solution. The P is set to 0.5 initially as we expect P to be far off the optimal value at the beginning of the training.

In the context of SE, the model matrix M, with error covariance Q, is the identity matrix. Standard deviations of the model error for individual weights are set to the variability of weights for LINREG solutions of various short sub-training periods, providing the diagonal terms for the error covariance Q.

Observations are represented in the vector y, with error covariance R. In the present study, y is the analyzed sound speed, obtained by optimal interpolation of temperature and salinity data and R is the expected error from the OI.

The observation operator H links the state vector space with the observation space and contains the individual sound speed forecasts of the NCOM models.

Similarly to the LINREG method, the SE Kalman filter based method (KALMAN) can be applied to models resulting from an EOF regularization and is denoted KALMAN_NORMEOF hereafter. This approach again is expected to increase generalization skills of the SE.

In oceanography, usually, the state vector contains hundred of thousands of grid points, so that low-rank approximations of the Kalman iteration must be adopted (e.g. Pham *et al.*, 1998). Here, the state vector is very small (*i.e.* the three weights, two on the numerical models and one on the independent term, which may be reduced down to 2 or 1 after the PCA regularization), and hence the full Kalman is applied at every grid point. The only assumption required for this method is that of a linear model transforming the weights in time and Normal weight distributions.

The methods described above have been tested on 0-24hrs forecast for 3 consecutive days with a running window from 29 April- 1May with 3 hrs steps. The training period starts on April 16 and ends on 29 April 00h00. Figure 5 shows resulting sound speed deviations from the OI analyzed fields for days 29 April 2007 12h00. One notes that both NCOM_COARSE and NCOM_FINE are rather well tuned in the middle of the water column, except that the fine resolution NCOM shows some larger 'spotty' errors. However strong biases can be identified in the upper 15m at the surface and the bottom 10m, mainly because only few CTD reached the bottom layers. The ENSMEAN is strongly biased as well. The UNBIASED_ENSMEAN seems to correct most of the surface and bottom bias but has larger errors in the 15-60m range. The LINREG and

KALMAN forecasts correct for most of the errors, the larger discrepancies at the surface having been decreased significantly. Qualitatively, the EOF regularization benefit for KALMAN is not directly apparent from the figure. Results for 1 May 12h00 are qualitatively similar except that here, the benefit of the regularization on the KALMAN method is clearly apparent.

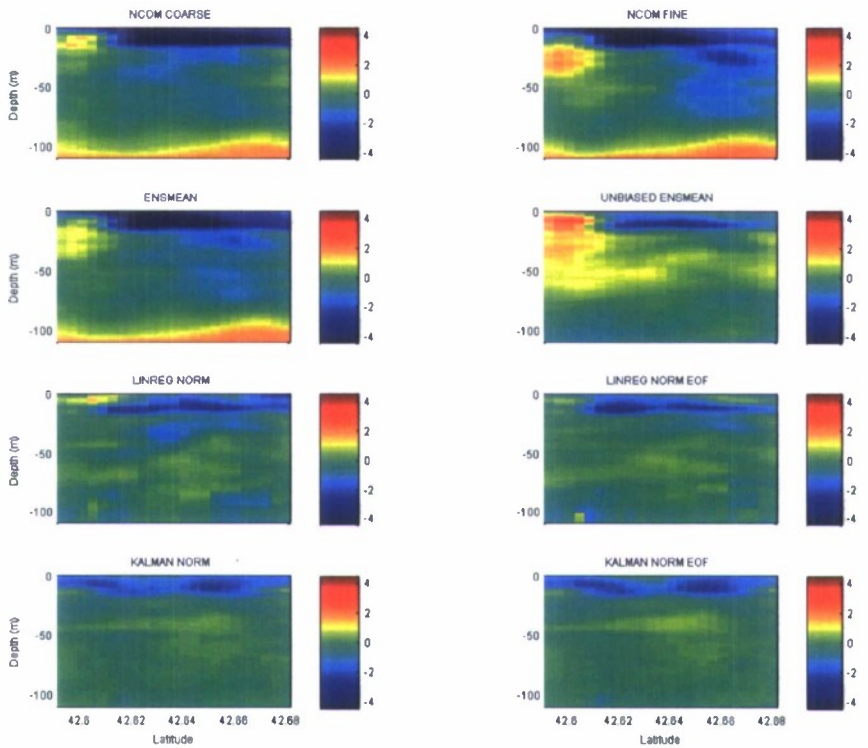

Fig 5. 24hrs sound speed (m/s) forecast errors on section A-B on 29 April 12h00 for the various models. From left to right and top to bottom: NCOM_COARSE, NCOM_FINE, ENSMEAN, UNBIASED_ENSMEAN, LINREG_NORM, LINREG_NORMEOF, KALMAN_NORM and KALMAN_NORMEOF

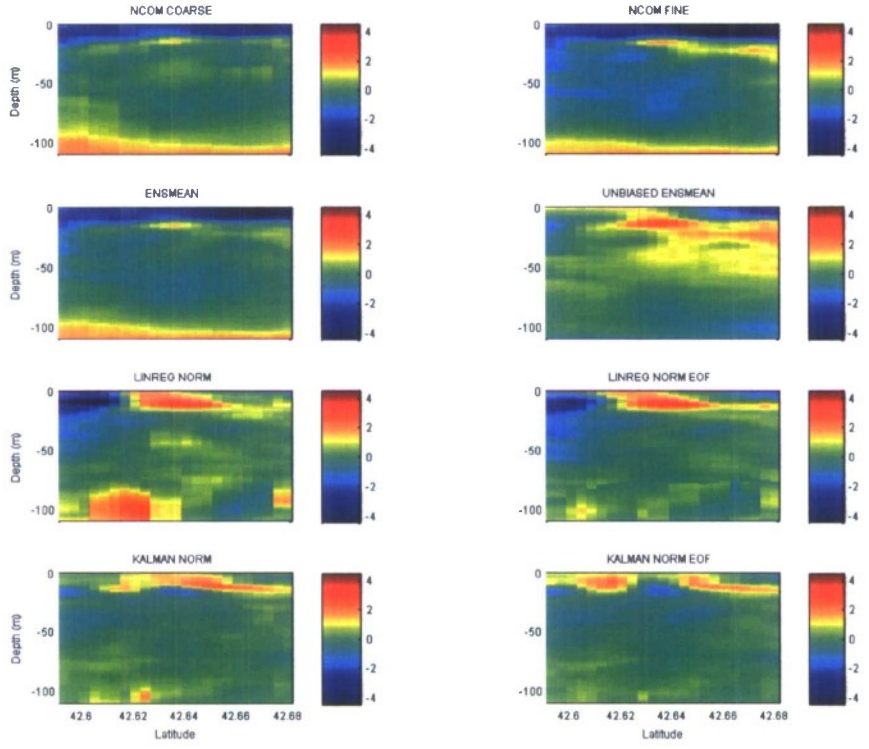

Fig. 6 Same as figure 5 but for 1 May 12h00.

The relative weighting on the 2 numerical models and the independent terms, and on the EOF compressed models, were examined carefully and show a strong variability, both in space (vertical and horizontal) and time, with values usually in the range [-2 2].

The weights on NCOM_COARSE and NCOM_FINE for the LINREG method (Fig. 7) suggest that the coarse NCOM model is usually more reliable and contribute significantly to the SE skill: weights are usually closer to one over the whole section AB. Contribution from NCOM_FINE are smaller and sometimes negative, indicating than this model may be out-of-phase at specific locations. Note also some higher magnitudes of the weights, up to 2, below 100m around latitude 42.61°N, illustrating the poor correlations between numerical models and data at this particular location.

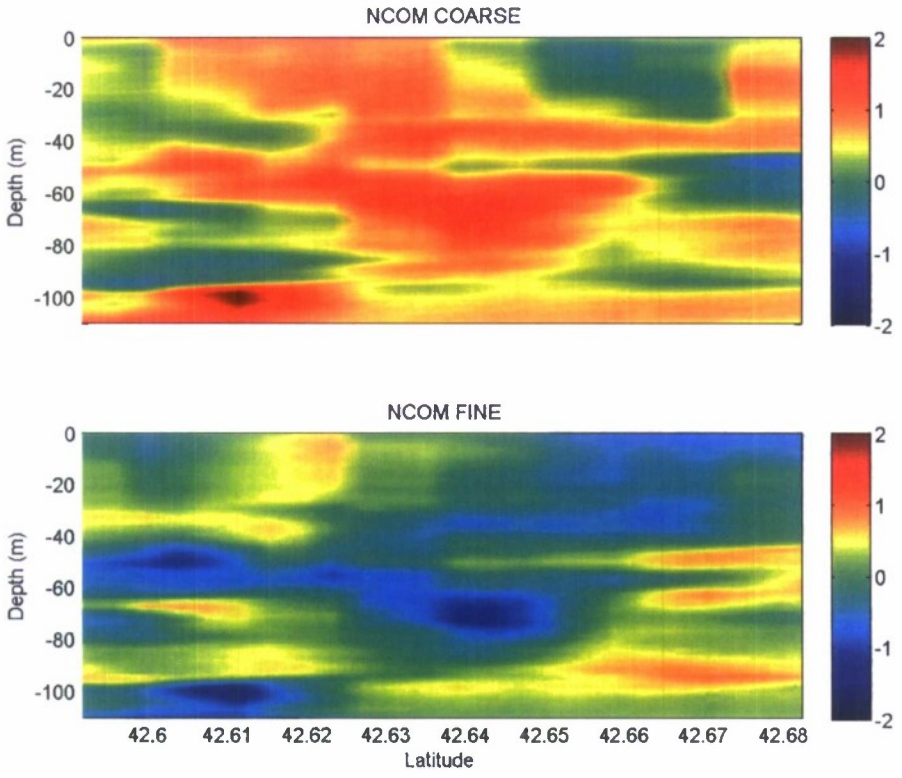

Fig 7 Weights on NCOM_COARSE (top) and NCOM_FINE (bottom) for the LINREG method on section AB versus depth (m).

Interpretation of these weights in physical terms, especially for the KALMAN-based methods, remains difficult as illustrated in Fig 8. The weights on NCOM_COARSE remain usually stronger and contribute more to the SE skills, especially on the upper and lower 10m of the water column in the first half of the learning period. One also notes the important role of the independent term which evolves significantly in time. This may be an indication of the strong variability of skills of the underlying numerical models.

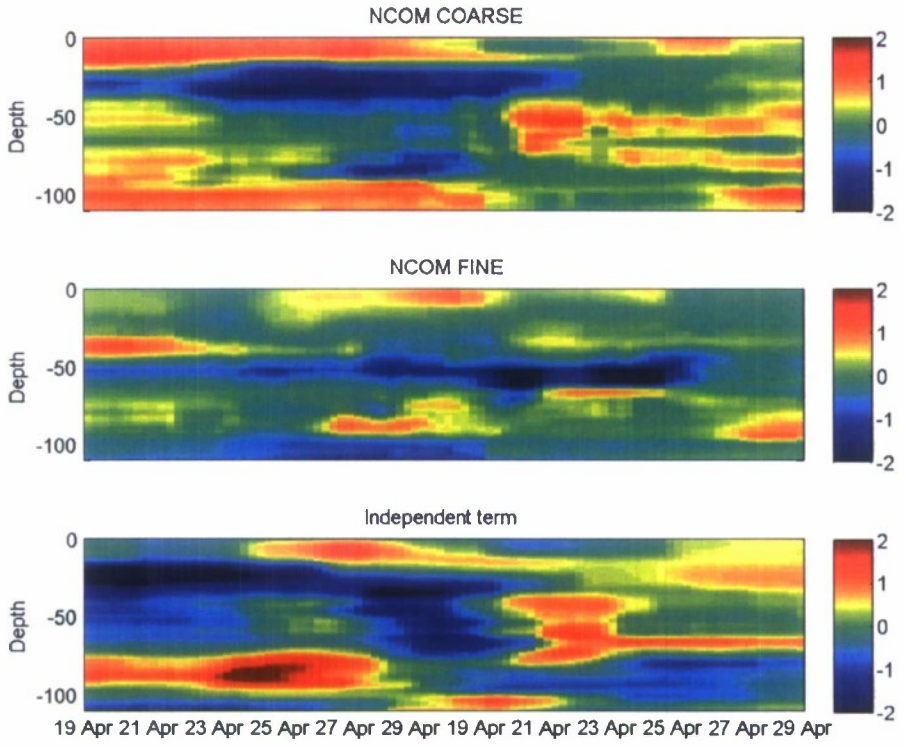

Fig. 8 Evolution of weights on NCOM_COARSE (top), NCOM_FINE (middle) and the independent term (bottom) over the learning period versus depth (m) for the KALMAN_NORM method for a profile at 42.64°N (middle of section AB).

Error statistics between the various models and the OI analysis have been computed for the whole 29 April-1May forecast period, and are shown in Fig. 9. As expected, root mean square (RMS) errors for NCOM_COARSE, NCOM_FINE and ENSMEAN are quite large, mainly due the model biases at the top 15m and the bottom 10m of the water columns. NCOM_FINE errors are also larger than NCOM_COARSE. The UNBIASED_ENSMEAN method corrects for a large portion of the bias and illustrates the benefit of the method. Further methods decrease the RMS error even further, the optimal approach being the KALMAN_NORMEOF. Hence, by adapting the weights dynamically on EOF compressed models, the generalization skills of the SE have been maximized. NCOM_COARSE shows very good correlation to *in-situ* analyzed data contrary to NCOM_FINE. This illustrates the fact that most of the error in NCOM_COARSE is due to the bias, whilst NCOM_FINE, although better suited for eddies and fine-scale processes, is not able to correct for the phase of such features. It should be stressed at this point that the NCOM runs were not assimilating any local profile data which are used here as independent validation set by comparison with numerical and SE numerical forecasts. Note however that the analysis is smoothing the observations to scales that are more comparable to NCOM_COARSE (2km-3hrs), hence not resolving the fine structures eventually simulated by the NCOM_FINE runs.

Validation against in-situ sparse data was tested but conclusions were less conclusive due to the scarce and inhomogeneous data distribution.

The bias of all SE methods using observations is lower than the numerical models and their ensemble average. The standard deviation of the forecasts also suggests that SE methods, and KALMAN_NORMEOF in particular, result in better representation of energy spectrum of the predictions. The synthetic Taylor skill score (Taylor, 2001) is a function of both signal energy and correlation and shows the improvements in skill obtained by using progressively more complex methods, starting from the numerical models to the dynamic weight adjustment with regularization.

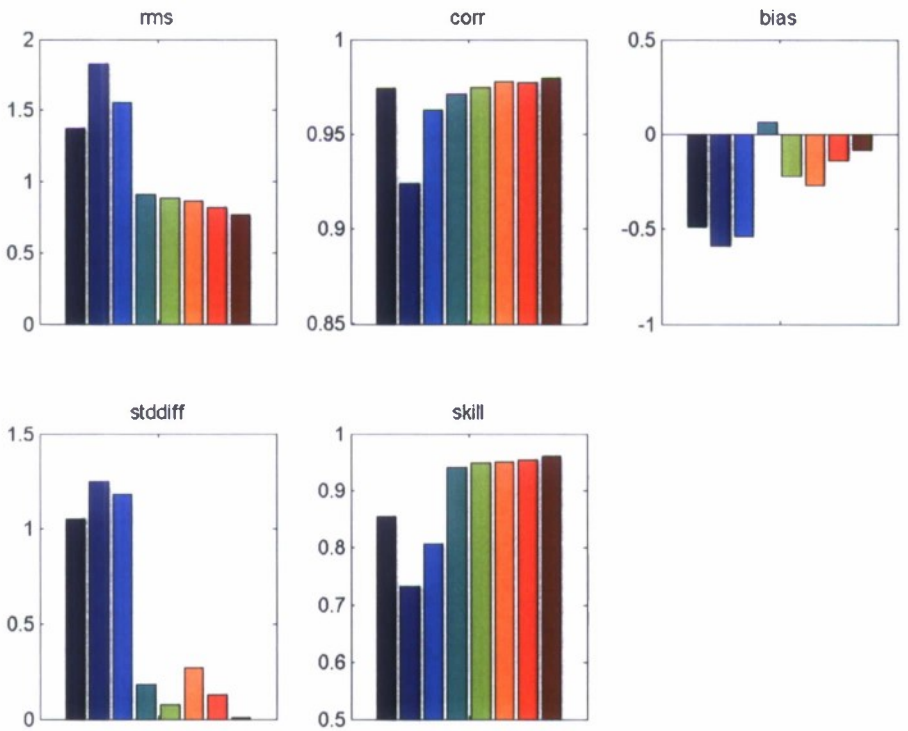

Fig. 9. Error statistics for 24 hrs sound speed (m/s) forecast from 29 April to 1 May 2007 for the 8 prediction methods. From left to right and top to bottom: RMS error, correlation, bias, energy difference and Taylor skill. Bars from left to right correspond respectively to NCOM_COARSE, NCOM_FINE, ENSMEAN, UNBIASED_ENSMEAN, LINREG_NORM, LINREG_NORMEOF, KALMAN_NORM and KALMAN_NORMEOF.

3. Ocean-Acoustics sensitivity analysis

Ocean modeling outputs can be used for a number of applications, among which the assessment of acoustic propagation constitutes an important matter of interest. For shallow water environments in particular, it is well known that the environment strongly influences the propagation of sound. A proper description of the environment is thus

required eomprising the water-eolumn aeoustie propertics (sound speed profile *versus* time and range, sea-surfaec roughncss) and thc seabottom geoacoustic properties. It is well established that for shallow waters, a prccise asscssment of the range-dependent seafloor and subseafloor properties is essential, whilst the acoustical field is less sensitive to thc watcr column properties. As a result, thc oeean-aeousties eommunity has spent mueh efforts in the last decade to properly assess thc seabottom properties. Reeently, emphasis was put on comparing the relative effects of uncertain seabottom deseription *versus* uncertain water column description. Though, no general statement about thc importanee of one environmental parameter over the other ean be made (the basic eonelusion being that it is generally ease-dependent), it was nevertheless eoncluded that effeetive modeling of the water eolumn is an important eomponent of acoustic REA even though thc seabottom geoacoustic properties prevails in most shallow water environments. Interestingly, such statements had alrcady been made previously for studies devoted to the assessment of thc seabottom properties in which geoacoustic inversion methods were reported to havc performance limitations due to inadequate description of the water column and in particular, thc range depcndence of thc sound speed profile and its time variability during thc measurements. In the light of these observations, the ocean modeling approaehes presented in thc previous sections eonstitute an interesting test ease in order to investigate thc impaet of ocean modeling upon acoustic propagation assessment. More precisely, the AB transect of the MREA/BP07 sea trial is characterized by a range- and time-dcpendent sound speed profile, diversely modeled as illustrated in the previous seetions. Transposing the ocean predictions in acoustic predictions, *i.e.* mapping ocean modeling into acoustic modeling, provides a way to estimate how mueh aeousties foreeasts ean be affected by oeean predietions. Subscquently, thc idea is to adopt thc end-user viewpoint of an acoustician to estimate the neeessary and suffieient degree of sophistieation of oeean modeling required for aeoustie modeling. In other words, is there an interest to model precisely the ocean conditions when an approximate deseription of the water column is already available? Moreover, another viewpoint that is worth being investigated with the framework of thc BP07 sea trial is closely linked to one major objective of the experiment, *i.e.* thc assessment of the seabottom properties by means of fused seismie imaging and geoacoustic inversion teehniques. Considering that the sampling of the seawater properties is relatively searee both in time and in geographical extension, one may wonder whether available 4D ocean modeling fields could be directly used as inputs to the geoaeoustic inversion algorithm.

To analyze the two viewpoints, a sensitivity study based on intensive aeoustie propagation simulation was conducted. For thc following simulations, the sea surface was considered to be perfectly flat and thc seabottom properties were kept eonstant for every acoustic run. A range-dependent bathymetry, stratigraphic and aeoustie model of the sediment along the AB transeet was taken from previous seabottom characterization studies along thc same transect (Hermand and Gerstoft, 1996; Hermand, 1999) and an additional geophysical survey of the transect with a multibeam-echo sounder and a seismic subbottom profiling system (Fig. 10). As in Hermand and Gerstoft (1996) and Hermand (1999), the stratigraphy of the seabottom was simplified in order to keep thc most important features that have an impaet at aeoustie frequencies from few hundreds

Hertz (300) to few kHz (1.8). The seabottom was modeled by an overlying very soft sediment layer of clayed unconsolidated sediments with a variable thickness (from 5 m to 9 m), over a silty harder sediment. The geoacoustic parameters of those layers are illustrated in Fig. 11. To compute the complex acoustic pressure fields, the range-dependent propagation model based on the parabolic approximation RAM (Collins,1989) was employed. The complex acoustic pressure fields were computed for a series of 9 frequencies from 300 Hz to 1800 Hz along the AB transect, and for each available time step of the ocean modeling (24 steps with 3-h interval from April 29 to May 1). A typical environmental model that was used is presented in Fig. 11.

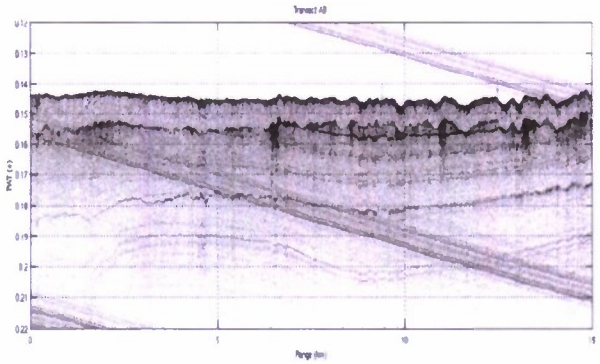

Fig. 10. Seismic survey of the AB transect using a seismic towed sub-bottom profiler

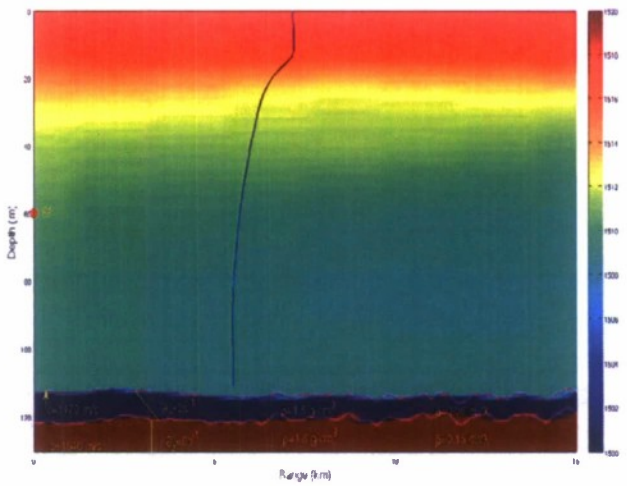

Fig. 11 Typical scenario for the acoustic prediction runs along the AB transect. A range-dependent sound speed profile from the ocean-modeling work is assumed. The seabottom is composed of a range-dependent overlaying clayed layer over a silty basement.

Though sensitivity studies are quite often applied in ocean-acousties to examine the effect of various environmental parameters on the acoustic propagation in a particular environment, very little has been done to provide a quantitative approach to that issue. Typically, the sensitivity analysis is often carried out qualitatively by observing the change in acoustic fields that results from an environmental change (e.g. Fig.12). In

Dosso *et al* (2007 and references herein), quantitative approaches have been proposed based on normalized bias estimates between the reference transmission losses field and the perturbed ones. In the present paper, a different approach based on the cross-correlation of the fields is applied. In Dosso *et al* (2007), it is shown that the sensitivities are range, depth and frequency dependent. Here, the depth dependency is not investigated. Instead, the measure of sensitivity consists in a normalized cross-correlation of the acoustic pressure fields at every range along a synthetic vertical line array (VLA) with an inter-element spacing of 1 m for a set of frequencies. The VLA coverage is limited to the water column. This metric is related to the classical "Bartlett processor" applied within the geoacoustic inversion framework based on matched field processing (MFP) (Tolstoy, 2003). Two normalized cross-correlations have been used in the analysis:

$$\phi_1(r,f) = \frac{\left|\sum_{j=1}^{N_z} p_j^*(r,f) q_j(r,f)\right|^2}{\sum_{j=1}^{N_z}\left|p_j(r,f)\right|^2 \sum_{j=1}^{N_z}\left|q_j(r,f)\right|^2}, \tag{6}$$

$$\phi_2(r,f) = \frac{\left[\sum_{j=1}^{N_z}\left|p_j(r,f)\right|\left|q_j(r,f)\right|\right]^2}{\sum_{j=1}^{N_z}\left|p_j(r,f)\right|^2 \sum_{j=1}^{N_z}\left|q_j(r,f)\right|^2}, \tag{7}$$

where p is the reference acoustic pressure field using the ocean optimally interpolated data presented in the previous section, q is the pressure field with the ocean forecast under investigation, N_z the number of hydrophones of the synthetic VLA, p^* is the conjugate of the complex acoustical pressure field p. *As this point, it should be mentioned that the optimal interpolation field is considered as the best reference water column model. It is remembered though that it is limited in range and time resolution.*

Both measures are bounded within the interval [0 1], 1 corresponding to a perfect match of the compared pressure fields. ϕ_1 investigates the correlation of the vertical spatial structure of the acoustic pressure fields in phase and amplitude, while, ϕ_2 investigates only the vertical spatial structure of the amplitude of the acoustic pressure fields (or the transmission loss).

The sensitivity measures defined so far consider changes in the acoustic field at a fixed range in space. However, the acoustic field perturbation due to an environmental perturbation generally includes a component representing a spatial shift of the field in addition to a change to the shifted field (*e.g.* Dosso *et al*, 2007). By not taking into account that field shifting effect, our approach can lead to over-estimated impacts of the environment upon the acoustics, whilst an analysis of the acoustic fields shows qualitatively that the impact may be lower. To avoid that effect, a numerical spatial field shifting was applied. A range-depth window of preselected size is defined for the reference field, centered on the current range. The tested field is correlated with each of the combination of the reference field inside the window. Finally, only the maximum of the obtained results is retained. For the study, the acoustic field was computed with an elementary cell-size of 20m x 1m. The reference window was defined +/- 100m about the current range and the vertical shift was +/- 5m about the current depth (*i.e.* for each cell

in the frequeney x range domain, 121 eombinations of the pressure fields were eonsidered).

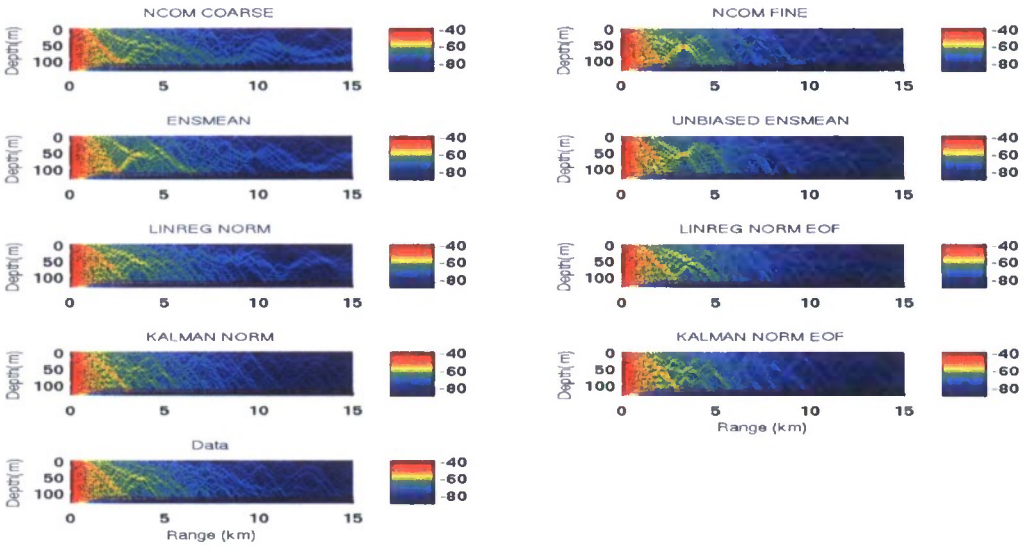

Fig. 12 Example of the acoustical pressure fields obtained with the various ocean modeling outputs and the optimally interpolated data field.

The results of the sensitivity analysis ean be eonsidered from several perspeetives presented in the following subseetions.

3.1 Sensitivity analysis from an acoustic propagation perspective

In Fig.13a,b, the resulting ϕ_1 and ϕ_2 fields in the frequeney times range domain are plotted for the oeean-modeling outputs produeed for 1 May, 12:00. Some trends ean be elearly identified. They obviously overeome the sole framework of super-ensemble ocean modeling and ean be generalized to the need of a proper deseription of range-dependent properties of the water column as illustrated below:

- The eorrelation levels are frequeney- and range-dependent.
- The lower the frequency, the lower the sensitivity. At very low frequeney (typieally from 300 to 500 Hz), little effeet on the aeoustie field ean be observed, meaning that a relatively eoarse deseription of the water eolumn is aeeeptable. At higher frequeneies this is no longer the ease. In partieular, it ean be seen that aeeurate aeoustieal predietions are limited to the very elose neighborhood of the sound souree at those frequeneies. This is a well-known effeet related to the faet that the higher the frequeney, the lower the aeoustie wavelength, the higher the impaet of the small scale environmental features.
- The greater the distanee, the higher the sensitivity. This result is quite trivial sinee, the aeoustie propagation at long ranges is directly linked to the past propagation. Differenees tend to aeeumulate with inereasing range.

Interestingly, it should be noticed the stronger impact of the environment when the full complex pressure field (amplitude and phase) is kept, rather than when only the amplitude is considered. Though the same range-frequency dependency can be observed on both types of fields, the correlation levels are much lower when the phase information is kept, which demonstrates how much this information is sensitive to the description of the environment. As soon as the correlation level is frequency dependent, it is emphasized that an accurate range dependent description of the water column properties needs to be fed to the acoustic models involved in applications based on full field estimates, *e.g.* matched-field processing (MFP), and model-based matched filter (MBMF) processing, the latter involving the prediction of the band-limited impulse response of the medium. The importance of such a need increases with frequency and range.

In Figs. 14a,b, a multi-frequency correlation measure was deduced from the 2D frequency times range intercorrelation matrices. This is straightforwardly obtained by computing, for each range and each model, the mean of the ϕ_1 and ϕ_2 outputs over frequency, which leads to the generalized multi-frequency Bartlett processor outputs that are routinely in acoustic inversion works based on matched field processing (MFP). Whatever the frequency and the range, multi-frequency correlations of the amplitude fields remain relatively high (over 0.85) reinforcing the conclusion that for these frequencies, ocean modeling efforts might have a limited scope (no measure of the degree of adequacy of the water column model is discussed here though). For full complex pressure fields, the decay of the inter-correlation fields is much higher with range. Only the two KALMAN filter-based models are shown to maintain good performances (correlation values higher than 0.7 for ranges up to 5 km), whilst the remaining models are much more limited in range. Here also, the conclusions are identical: the computation of the full complex pressure field requires a more accurate description of the water column conditions..

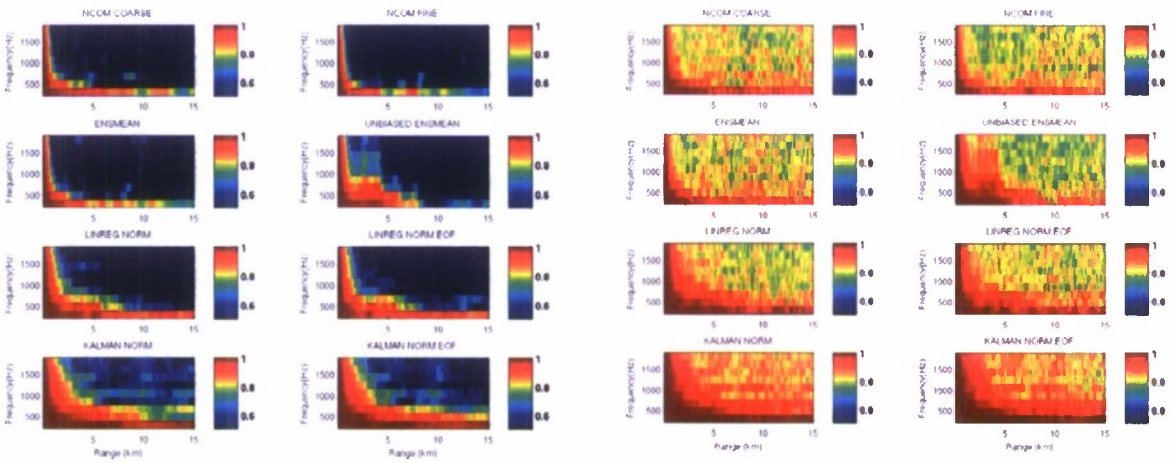

Fig. 13. 2D sensitivities of (a) the complex-valued acoustic pressure field for the eight ocean modeling outputs and (b) the amplitude of the acoustic field on 1 May 2007, 12h00.

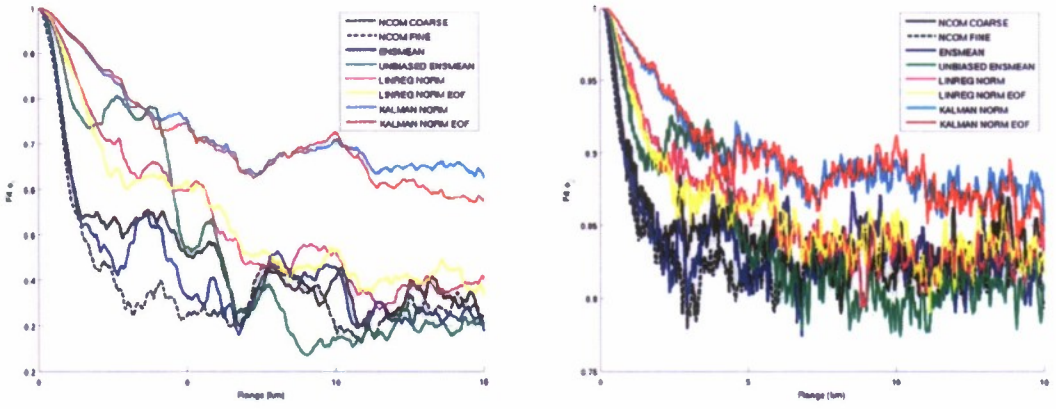

Fig. 14 Multi-frequency sensitivities for 1 May 2007 at 12h00: (a) complex-valued acoustic pressure field and (b) corresponding amplitude.

3.2 Sensitivity analysis from an ocean-modeling perspective

From an ocean modeling perspective, the sensitivity analysis allows to extract interesting features about the performances of the different environmental forecasts.

As expected from the evaluation of the super-ensemble ocean-modeling skills presented in the previous sections, better matches of the acoustic fields can generally be obtained when the super-ensemble outputs are employed in place of the initial NCOM simulations. In some instances though, the improvements are quite low especially for the less sophisticated super-ensemble techniques (ENSMEAN, UNBIASED_ENSMEAN). The UNBIASED_ENSMEAN technique was even seen to lead to less accurate acoustic forecasts for the very first predictions on 29 April (see Fig 15a).

A hierarchy of the skills of super-ensemble techniques from an acoustic modeling viewpoint can be established from the intercorrelation fields. The improvement given by the ENSMEAN based techniques are generally lower than those of the LINREG ones, which are also less skilled than the KALMAN-based techniques. More interestingly, it can be emphasized that the KALMAN filter techniques shows rather constant consistency (both in range and frequency) over the 3 days of the test (see Fig. 14a and 15a,b). Meanwhile, the two other types of methodologies are far less robust over time. For example, the UNBIASED_ENSMEAN approach starts with poorer skills than any other forecast (see Fig. 15a), and about the middle of the runs, it suddenly improves over the other methods, except the KALMAN-based forecasts (see Fig. 14a). The reasons for such an improvement seem to be linked to a more accurate assessment of the thermocline for this method after several runs.

Though the most sophisticated methods showed better matches of the acoustic fields with respect to the reference water-column field, none of them was nevertheless able to cope with all the characteristics of this reference field, with a higher impact at long ranges and high frequencies. Moreover, it should also be emphasized, that though the oceanographic survey was rather important, the optimally interpolated data still present some limitations in range and time resolutions, i.e. 2 km and 1 day respectively. Therefore, for the purpose

of acoustic predictions, there is a need for improvement of the ocean forecasts. Several ways are possible to enhance ocean modeling skills for the specific requirements of acoustics. A denser hydrographic survey and a better assimilation of *in situ* ocean data at earlier stages of the ocean-modeling phase are likely to provide better initial forecasts. Anyway, this approach can be constrained by the number of measuring platforms and there may also be conflicts between the measurement strategies for ocean-modeling solely and those dedicated to acoustics. An alternate approach which could be particularly worthwhile within the current ocean-acoustics framework is to use acoustic observations to resolve range-dependent oceanographic fields that can be used in a second step to improve, within a feedback loop the ocean modeling outputs. The interesting aspect of this approach is that acoustic observations lead to synoptic observations of the ocean that presumably should allow catching the oceanic variability at fine scales and long ranges. Moreover, these measurements are more closely linked to the final application. The most relevant features of the environment are likely to be caught through the acoustic observation and thus the resulting ocean modeling is expected to more closely serve the acoustic needs. A companion paper investigates the feasibility of such a range-dependent tomography scheme (Carrière *et al*, this issue) and discusses some of the basis for such a general ocean-acoustics feedback loop.

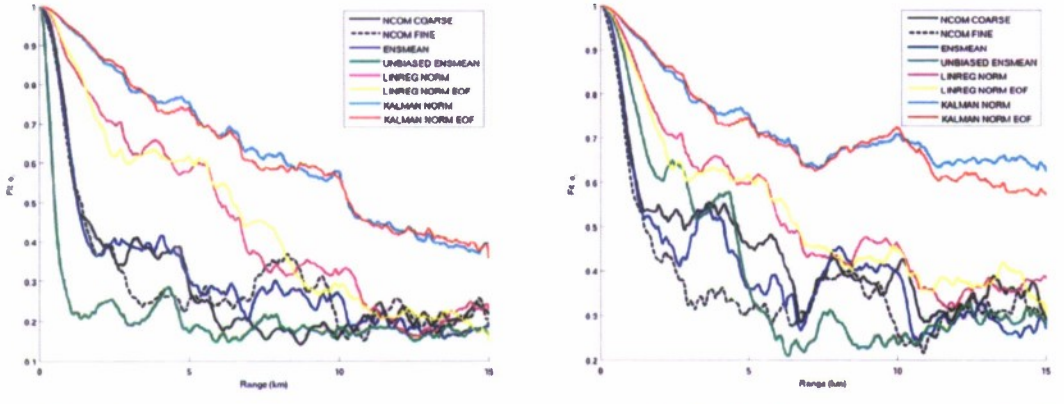

Fig. 15 Multi-frequency sensitivities on (a) 29 April 2007, 12h00 and (b) 1 May 2007, 00h00.

3.3 Sensitivity analysis from a seabottom geoacoustic inversion perspective

The use of 4D ocean modeling outputs constitutes an interesting alternative for the geoacoustic inversion community. Since range dependency of the water column affects acoustic propagation, any inversion scheme for seabottom acoustic properties has to constrain the environmental model with measured or predicted sound speed profiles or to search for the best (ad-hoc) sound speed field in searching for the seabottom properties (range-dependent geoacoustic inversion). Another viewpoint from the inversion perspective is to investigate the problem with a "system-oriented" approach, *i.e.* what are the impact of range dependency on the inversion results and whether we can cope with water column range dependency when performing geoacoustic inversion with a range

independent model. Since range dependency of the water column can limit the performances of the range-independent approach efforts have been spent on developing the range-dependent approach. However the resulting methods are often quite time consuming because they require computationally-expensive forward acoustic propagation models. Moreover, they often require good *a priori* knowledge of the range dependency to better pose the inverse problem. To simplify the inverse problem, it can thus be useful to limit the inverse problem to a geometrical set up that limits the impact of the range dependency. Here it appears that at close ranges i.e., from a few hundreds meters to a few kilometers, the correlations between predicted and measured fields remain high over the whole water column (over 0.8–0.9), whatever the water column conditions are. This gives confidence that experimental configurations involving short ranges are most likely to be weakly impacted by range dependency. Such an approach has been followed during the BP07 sea trial during which dedicated seabottom geoacoustic inversion runs were designed to assess the seabottom properties in parallel to the ocean modeling efforts. For these runs, a sound source emitting broadband-coded signals within the frequency range 300–1800 Hz was employed and the signals were received along sparse VLAs at distances not exceeding 1–2 km. Though the full vertical intercorrelation measure is not completely representative of the VLA design employed (sparse arrays limited to a part of the water column), it provides good confidence that such a setup is suited for geoacoustic inversion purposes with little impact of the range dependency of the water column as was recently confirmed by the first BP07 geoacoustic inversion results along the AB transect (Hermand and Le Gac, 2008). Hopefully, this is expected to be extended to the small-scale time variability. Further work shall be dedicated to investigate that assumption.

4. Conclusions and perspectives

This work presents an innovative approach to the coupled ocean-acoustic problem. Despite scarce hydrographic monitoring which is obviously a strong limitation for accurate and reliable ocean forecasting, sophisticated – but cheap – methods can be used to exploit both observational and prediction information streams. We have demonstrated the potential benefit of combining dynamically various observational data sources (*i.e.* CTD, thermistor strings and others) and traditional ocean prediction into a super-ensemble forecast to better characterize and predict ocean and acoustic properties.

In a companion paper (Carrière *et al*, this issue), tomography-derived synoptic data provides a promising complement (or even an alternative approach) to standard hydrographic measurements. In particular, range dependent temperature or sound speed profile obtained by acoustic inversion may be in turn assimilated in ocean models or multi-model super-ensembles (SE). Subsequent nowcast and forecast can then further help refining the inversion process.

Ongoing efforts on SE include the exploitation of remote sensing information to better understand SE error covariance and to overcome the lack of in-situ observations.

The prediction of the SE error statistics also deserves some increased efforts. The uncertainties may be exploited in the inversion process because they help better constraining the search space. These uncertainties may also be used in adaptive sampling efforts to optimize the observational network and asset allocation by focusing on areas where errors are expected to be higher.

This multidisciplinary ocean-acoustic feedback approach offers some promising perspectives in the context of Rapid Environmental Assessment.

Acknowledgments

The support of all individual and institutions involved in the BP07 Joint Research Program is highly appreciated. Especially, the contribution of the Italian Navy (Maurizio Demarte), the Royal Netherlands Navy and University of Algarve (Sergio Jesus) in the observational program are hereby deeply acknowledged. This work was supported by the NURC (North Atlantic Treaty Organization). The Naval Research Laboratory was partially funded by the Office of Naval Research under grant N00014-08-2-1146.

References

1. Bennett AF (1992) Inverse Methods in Physical Oceanography. Cambridge Monographs on Mechanics and Applied Mathematics. Cambridge: Cambridge University Press.
2. Bennett, 2002: Inverse Modeling of the Ocean and Atmosphere. Cambridge University Press, Cambridge.
3. Bretherton, F.P., Davis, R.E., Fandry, C.B., (1976). A technique for objective analysis and design of oceanographic experiment applied to MODE-73. Deep-Sea Research 23, 559–582.
4. Carrière, O., Hermand, J.-P., Le Gac, J.-C. and Rixen, M., Full field tomography and Kalman tracking of the range-dependent sound speed field in a coastal water environment, Journal of Marine Systems, this issue.
5. Coelho, E., Peggion G., Rowley C., Jacobs, G., Allard, R. and Rodriguez, E., A note on NCOM temperature error calibration using the ensemble transform, Journal of Marine Systems, this issue.
6. Collins, M.D. (1989), A higher-order parabolic equation for wave propagation in an ocean overlying an elastic bottom, J.Acous.Soc.Am. 86, 1459-1464.
7. Dosso, S.E., Morley, M.G., Giles, .M., Brooke, G.H., McCammon, D.F., Pecknold, S., Hines, P.C.(2007), Spatial field shifts in Ocean acoustic environmental sensitivity analysis, J.Acous.Soc.Am. 122(5),pp.2560-2570.
8. Evensen, G. (2006), Data Assimilation: The Ensemble Kalman Filter, Springer, 279 pp.
9. Fofonoff, P. and Millard, R.C. Jr. (1983). Algorithms for computation of fundamental properties of seawater. UNESCO Tech. Pap. in Mar. Sci., No. 44, 53pp.

10. Galmarini S. et al. (2001), Forecasting the consequences of accidental releases of radionuclides in the atmosphere from ensemble dispersion modelling, Journal of Environmental Radioactivity, 57, 3, 203-219.
11. Galmarini S. et al., (2004). Ensemble dispersion forecasting, Part II: application and evaluation, Atmospheric Environment, 38, 28, 4619-4632.
12. Heaney K.D., G. Gawarkiewicz, T.F. Duda and P.F.J. Lermusiaux, 2007. Non-linear Optimization of Autonomous Undersea Vehicle Sampling Strategies for Oceanographic Data-Assimilation. Special issue on Underwater Robotics, Journal of Field Robotics, Vol. 24(6), 437448.
13. Hermand, J.-P.(1999), Broadband geoacoustic inversion in shallow water from waveguide impulse response measurements on a single hydrophone: Theory and experimental results, IEEE J. Ocean. Eng. 24 (1), pp.41-66.
14. Hermand, J.-P., Gerstoft, P.(1996), Inversion of broadband multi-tone acoustic data from the Yellow Shark Summer Experiments, IEEE J. Ocean. Eng. 21 (4), pp.324-346.
15. Hermand, J.-P., Le Gac, J.-C. (2008). Subseafloor geoacoustic characterization in the kilohertz regime with a broadband source and a 4-element receiver array, in Proceedings of OCEANS '08 MTS / IEEE QUEBEC Oceans, Poles & Climate: Technological Challenges, IEEE, Sept. 2008 ISBN 978-1-4244-2620-1
16. Kalman, R. E. (1960), A new approach to linear filtering and prediction problems, Transactions of the ASME - Journal of Basic Engineering Vol. 82: pp. 35-45.
17. Kalnay, E., Ham, M., (1989). Forecasting forecast skill in the southern hemisphere. In: Preprints of the 3rd International Conference on Southern Hemisphere Meteorology and Oceanography, Buenos Aires, 13-17 November 1989.
18. Krishnamurti, T., Kishtawal, C., LaRow, T. E., Bachiochi, D. R., Zhang, Z., Williford, C. E., Gadgil, S., and Surendran, S. S. (1999), Improved weather and seasonal climate forecasts from multimodel superensemble. Science, 285(5433):1548-1550. DOI: 10.1126/science.285.5433.1548.
19. Krishnamurti, T., Kishtawal, C., Shin, D., and Williford, E. (2000), Improving tropical precipitation forecasts from a multianalysis superensemble. Journal of Climate, 13:4217-4227.
20. Krishnamurti, T., Kishtawal, C., Zhang, Z., Larow, T., Bachiochi, D., and Williford, E. (2000), Multimodel ensemble forecasts for weather and seasonal climate. Journal of Climate, 13:4196-4216
21. Kumar, T. V., Krishnamurti, T., Fiorino, M., and Nagata, M (2003), Multimodel superensemble forecasting of tropical cyclones in the Pacific, Monthly Weather Review, 131:574-583.
22. Lam F.-P., Haley P. Jr, Janmaat J., Lermusiaux P.F.J., Leslie, W.G. and Schouten M.W., Real-time coupled four-dimensional oceanographic and acoustic forecasts during Battlespace Preparation 2007, Journal of Marine Systems, this issue.
23. Le Gac, J.-C., Hermand, J.-P.(2007), MREA/BP07 cruise report. Tech. Rep. Technical document NURC-CR-2007-04-1D1, NATO Undersea Research Centre, La Spezia, Italy.

24. Lermusiaux P.F.J., C.-S. Chiu and A.R. Robinson, 2002. Modeling Uncertainties in the Prediction of the Acoustic Wavefield in a Shelfbreak Environment. Proceedings of the 5th International conference on theoretical and computational acoustics, May 21-25, 2001. (Eds: E.-C. Shang, Q. Li and T.F. Gao), World Scientific Publishing Co., 191200.
25. Lermusiaux P.F.J. and C.-S. Chiu, 2002. Four-dimensional data assimilation for coupled physical-acoustical fields. In Acoustic Variability, 2002. N.G. Pace and F.B. Jensen (Eds.), Saclantcen. Kluwer Academic Press, 417424.
26. Lermusiaux P.F.J., Chiu, C.-S., Gawarkiewicz, G.G., Abbot, P., Robinson, A.R., Miller, R.N., Haley, P.J., Leslie, W.G., Majumdar, S.J., Pang A., and Lekien, F. (2006), Quantifying Uncertainities in Ocean Predictions. Oceanography, Special issue on ``Advances in Computational Oceanography", T. Paluszkiewicz and S. Harper, Eds., Vol. 19, 1, 92-105.
27. Logutov, O. G., Robinson, A. R. (2005), Multi-model fusion and error parameter estimation, Quarterly Journal of the Royal Meteorological Society, 131 (613), pp 3397-3408 DOI: 10.1256/qj.05.99.
28. Lorenz, E. N. (1963), Deterministic nonperiodic flow, Journal of the Atmospheric Sciences, 20:130-141.
29. Meyer, M, Hermand, J.-P., Berrada, M. and Asch, M, Remote sensing of Tyrrhenian shallow waters using the adjoint of a full-field acoustic propagation model, Journal of Marine Systems, Mar. 2008.
30. Mutemi, J. N., Ogallo, L. A., Krishnamurti, T. N., Mishra A. K., Kumar, T.and Vijaya S. V.(2007), Multimodel based superensemble forecasts for short and medium range NWP over various regions of Africa, Meteorology and Atmospheric Physics, Volume 95, Numbers 1-2, 10.1007/s00703-006-0187-6, 87-113.
31. Palmer, T., et al.(2004), Development of a European multimodel ensemble system for seasonal-to-interannual prediction (DEMETER). Bulletin of the American Meteorological Society, 85(6):853-872.
32. Pham, D. T., Verron, J., Roubaud, M. C., (1998). A singular evolutive extended Kalman filter for data assimilation in oceanography. Journal of Marine Systems 16 (3-4), 323-340.
33. Rajagopalan, B., Lall, U., and Zebiak, S. E.(2002), Categorical climate forecasts through regularization and optimal combination of multiple GCM ensembles. Monthly Weather Review, 130:1792-1811.
34. Rixen, M. and Ferreira-Coelho, E. (2005), Operational prediction of acoustic properties in the ocean using multi-model statistics. Ocean Modeling, 11(3-4):428-440. doi:10.1016/j.ocemod.2005.02.002.
35. Rixen, M. and Ferreira-Coelho, E. (2007), Operational surface drift prediction using linear and non-linear hyper-ensemble statistics on atmospheric and ocean models. Journal of Marine Systems, 65:105-121.
36. Rixen, M., Beckers, J.-M., Brankart, J.-M., Brasseur, P., (2001). A numerically efficient data analysis method with error map generation. Ocean Model. 2 (1– 2), 45–60.
37. Rixen, M., Book, J., Carta, A., Grandi, V., Gualdesi, L., Stoner, R., Ranelli, P., Cavanna, A., Zanasca, P., Baldasserini, G., Trangeled, A., Lewis, C., Trees, C.,

Grasso, R., Giannecchini, S., Fabiani, A., Merani, D., Berni, A., Leonard, M., Martin, P., Rowley, C., Hulbert, M., Quaid, A., Goode, W., Preller, R., Pinardi, N., Oddo, P., Guarnieri, A., Chiggiato, J., Carniel, S., Russo, A., Tudor, M., Lenartz, F., Vandenbulcke, L. (2008). Improved ocean prediction skill and reduced uncertainty in the coastal region from multi-model super-ensembles. J. Geophys. Res.Submitted.

38. Rixen, M., Ferreira-Coelho, E., Signell, R., (2008). Surface drift prediction in the Adriatic Sea using hyper-ensemble statistics on atmospheric, ocean and wave models: Uncertainties and probability distribution areas. Journal of Marine Systems 69, 86
39. Robinson, A.R. and P.F.J. Lermusiaux, 2004. Prediction Systems with Data Assimilation for Coupled Ocean Science and Ocean Acoustics, Proceedings of the Sixth International Conference on Theoretical and Computational Acoustics (A. Tolstoy, et al., editors), World Scientific Publishing, 325-342. Keynote Manuscript.
40. Shin, D. and Krishnamurti, T.(2003a), Short- to medium-range superensemble precipitation forecasts using satellite products: 1. Deterministic forecasting. Journal of Geophysical Research, 108(8). 8383, DOI 10.1029/2001JD001510.
41. Shin, D. and Krishnamurti, T.(2003b), Short- to medium-range superensemble precipitation forecasts using satellite products: 2. Probabilistic forecasting. Journal of Geophysical Research, 108(8). 8384, DOI 10.1029/2001JD001511
42. Taylor, Karl E. (2001), Summarizing multiple aspects of model performance in single diagram}, J. Geophys. Research, 106, D7, 7183—7192.
43. Tolstoy, A. (1993), Matched field processing for Underwater Acoustics, World Scientific, Singapore-New Jersey-London-Hong Kong, 212 p.
44. Wang D., P.F.J. Lermusiaux, P.J. Haley, D. Eickstedt, W.G. Leslie and H. Schmidt, 2008. Acoustically Focused Adaptive Sampling and On-board Routing for Marine Rapid Environmental Assessment. Special issue of Journal of Marine Systems on "MREA and Coastal processes: challenges for monitoring and prediction", Drs. J.W. Book, Prof. M. Orlic and Michel Rixen (Guest Eds), Submitted.
45. Williford, C. E., Krishnamurti, T., Torres, R. C., and Cocke, S.(2003), Real-time multi-model superensemble forecasts of Atlantic tropical systems of 1999. Monthly Weather Review, 131:1878-1894.
46. Wunsch C (1996) The Ocean Circulation Inverse Problem. Cambridge: Cambridge University Press.
47. Yilmaz N.K., C. Evangelinos, P.F.J. Lermusiaux and N. Patrikalakis, 2008. Path Planning of Autonomous Underwater Vehicles for Adaptive Sampling Using Mixed Integer Linear Programming. IEEE Ocean Engineering. In Press.
48. Yun, W., Stefanova, L., A.K., M., Kumar, T., Dewar, W., and Krishnamurti, T. (2005), A multi-model superensemble algorithm for seasonal climate prediction using DEMETER forecasts. Tellus, 57(3):280-289. DOI: 10.1111/j.1600-0870.2005.00131.x.
49. Yun, W., Stefanova, L., and Krishnamurti, T. (2003), Improvement of the multimodel superensemble technique for seasonal forecasts. J. Climate, 16(22):3834-3840.